TECHNETIUM FROM TWO PERSPECTIVES: SULFIDE REMEDIATION AND SCHIFF BASE CHEMISTRY

A Dissertation

presented to

the Faculty of the Graduate School

at the University of Missouri-Columbia

In Partial Fulfillment

of the Requirements for the Degree

Doctor of Philosophy

---

by

KIMBERLY MARIE REINIG

Professors Silvia S. Jurisson and Carol A. Deakyne, Dissertation Supervisors

DECEMBER 2015

The undersigned, appointed by the dean of the graduate School, have examined the dissertation entitled

TECHNETIUM FROM TWO PERSPECTIVES: SULFIDE REMEDIATION AND SCHIFF BASE CHEMISTRY

presented by Kimberly Marie Reinig,

a candidate for the degree of doctor of philosophy of chemistry,

and hereby certify that, in their opinion, it is worthy of acceptance.

Professor Silvia S. Jurisson

Professor Carol A. Deakyne

Professor Michael Lewis

Professor Justin Walenksy

ACKNOWLEDGMENTS

My graduate career and the work presented here would not have been possible without the help and guidance of many people over the years.

First, I would like to express my deepest gratitude to my graduate advisors, Dr. Silvia Jurisson and Dr. Carol Deakyne. Their support has been a cornerstone in my graduate career; and without their mentorship and patience this work would not have been completed.

Dr. Wei Wycoff was extremely helpful with all the NMR experiments. Dr. Jeff Terry and Rachel Seibert provided support and knowledge with the XAS experiments. Dr. Charles Barnes provided crystal structure analysis and data for the structures in this thesis. Dr. Nathan Leigh obtained the mass spectral data in Chapter 5.

Thank you to Dr. Dave Rotsch and Dr. Eric Weis for helping with several of the Schiff base reactions and giving advice on several different laboratory techniques. Anna Taylor and Nicole Moore assisted with the data collection for the batch studies run in Chapter 3. Tim Phelps helped with electron microscope studies performed on the iron minerals. Dr. Dustin Demoin and Lauren Radford were always there to lend a hand or give advice, especially on the days when nothing seemed to work.

I would like to thank the National Science Foundation, U.S. Department of Energy, and University of Missouri Department of Chemistry for providing financial support for the projects in this dissertation.

Finally, I would like to give a special thanks to my husband, Michael Reinig, for all his encouragement and support. Thank you for keeping me motivated throughout my graduate studies.

TABLE OF CONTENTS

ACKNOWLEDGMENTS ..... **II**

TABLE OF CONTENTS ..... **III**

LIST OF ILLUSTRATIONS ..... **VII**

List of Figures vii

List of Tables x

ABSTRACT ..... **XI**

CHAPTER 1: INTRODUCTION TO TECHNETIUM IN THE ENVIRONMENT **1**

1.1 Sources of Technetium-99 in the Environment 1

1.2 Technetium in Water 3

1.3 Technetium in Soils and Sediments 4

1.4 Technetium in Plants 5

1.5 Technetium in Animals 6

1.6 Remediation Techniques for Technetium-99 7

1.6.1 Bioremediation of Technetium-99 8

1.6.2 Chemical Reduction of Technetium-99 9

CHAPTER 2: CHARACTERIZATION OF SMALL OLEFINIC ACIDS REACTING WITH PERTECHNETATE IN THE PRESENCE OF SODIUM SULFIDE **11**

2.1 Introduction 11

2.2 Experimental Section 13

2.2.1 Materials 13

2.2.2 Interference Reactions 14

2.2.2.1 Aerobic Conditions 14

2.2.2.2 Anaerobic Conditions 15

2.2.3 Control Reactions 15

2.2.4 Synthesis of $[Tc^{V}O(MSA)_2]^{3-}$ 15

2.2.4.1 Method 1 (reference MSA complex $[(Tc^{V}O(MSA)_2]^{3-}$) 15

2.2.4.2 Method 2 (FUM4) 16

2.2.4.3 Method 3 (MAL4) 17

2.2.5 Synthesis of $[TcO(DMSA)_2]^{5-}$ 17

2.2.5.1 Method 1 (reference DMSA complex, [TcO(*meso*-DMSA)]$^{5-}$) 17

2.2.5.2 Method 2 (FUM9) 18

2.2.5.3 Method 3 (MAL9) 18

2.2.6 Characterization 18

2.2.6.1 X-Ray Absorption Spectroscopy 19
2.2.7 Computational Methods 19
2.3 Results and Discussion 23
2.3.1 NMR Analysis 26
2.3.1.1 Tc-Fumaric Acid and Tc-Maleic Acid Reactions 26
2.3.1.3 Tc-Crotonic Acid Reactions 32
2.3.1.4 Tc-Citraconic Acid Reactions 39
2.3.2 XAS Analysis 40
2.3.3 Computational Studies 42
2.4 Conclusion and Future Studies 46
CHAPTER 3: PERTECHNETATE IMMOBILIZATION ON GOETHITE, HEMATITE, AND MAGNETITE 48
3.1 Introduction 48
3.2 Experimental Section 49
3.2.1 Materials 49
3.2.2 Study Preparation 50
3.2.2.1 Control-$^{99m}TcO_4^-$ Samples 50
3.2.2.2 Sulfide treatment of mineral at pH 8-$^{99m}TcO_4^-$ Studies 50
3.2.2.3 Acid pretreatment of mineral-$^{99m}TcO_4^-$ Studies 51
3.2.2.4 Sulfide treatment-$^{99}TcO_4^-$ Studies 51
3.3 Results and Discussion 52
3.3.1 Goethite studies 53
3.3.2 Hematite studies 56
3.3.3 Magnetite studies 58
3.3.4 ^{99}Tc-Mineral Studies 60
3.4 Conclusions and Future Studies 62
CHAPTER 4: INTRODUCTION TO TECHNETIUM AND RHENIUM RADIOPHARMACEUTICALS 63
4.1 Radiopharmaceuticals 63
4.1.1 Nuclear Properties for Radiopharmaceutical Purposes 63
4.1.1.1 Imaging Specific Properties 63
4.1.1.2 Therapy Specific Properties 65
4.1.2 Production and Availability of Radionuclides 66
4.2 Technetium-99m and Rhenium-186/188 68
4.2.1 Technetium-99m Properties 68
4.2.2 Rhenium-186 and Rhenium-188 Properties 69
4.2.3 Technetium and Rhenium Schiff Base Chemistry 69
CHAPTER 5: RHENIUM SCHIFF BASE CHEMISTRY 74

5.1 Introduction 74
5.2 Experimental Section 78
5.2.1 Materials 78
5.2.2 Preparation of *cis*-[$Re^{V}OCl(sal_2ibn)$] · 3 $CHCl_3$ (1) 79
5.2.3 Preparation of *trans*-[μ-$O(Re^{V}O(sal_2ibn))_2$] · 4 $CHCl_3$ (2) 79
5.2.4 Preparation of cis-[$Re^{V}O(NCS)(sal_2ibn)$] (3) 80
5.2.5 Preparation of *trans*-[$Re^{III}(NCS)(PPh_3)(sal_2ibn)$] (4) 81
5.2.6 Preparation of *trans*-[μ-$O(Re^{IV}(NCS)(sal_2ibn))_2$] · 2 CH_3CN (5) 82
5.2.7 X-Ray Characterization 83
5.3 Results and Discussion 83
5.3.1 Synthesis of Re(V) Mono- and Dinuclear Complexes 1, 2, and 3 83
5.3.2 Synthesis of the Mononuclear Re(III) Complex 4 and Novel Dinuclear Re(IV) Complex 5 84
5.3.3 General Characterization 86
5.3.3 NMR Analyses 87
5.3.4 X-Ray Crystal Structures 89
5.3.4.1 *cis*-[$ReOCl(sal_2ibn)$] · 3 $CHCl_3$ (1) 91
5.3.4.2 *trans*-[μ-$O(ReO(sal_2ibn))_2$] · 4 $CHCl_3$ (2) 92
5.3.4.3 *cis*-[$ReO(NCS)(sal_2ibn)$] (3) 94
5.3.4.4 *trans*-[$Re(NCS)(PPh_3)(sal_2ibn)$] (4) 95
5.3.4.5 *trans*-[μ-$O(Re(NCS)(sal_2ibn))_2$] · 2 CH_3CN (5) 96
5.4 Conclusions and Future Studies 97
CHAPTER 6: TECHNETIUM SCHIFF BASE CHEMISTRY 99
6.1 Introduction 99
6.2 Experimental Section 100
6.2.1 Materials 100
6.2.2 Preparation of [*trans*-(μ-$O(Tc^{IV}Cl(sal_2ibn))_2$)] · 3 $(CH_3)_2CO$ (1) 101
6.2.3 Preparation of [*cis*-$(TcO(NCS)sal_2ibn)$] (2) 102
6.2.4 Preparation of (n-$Bu_4N)_2$[*trans*-((TcClsal$_2$ibn)μ-$O(Tc(NCS)_5)$)] · $(CH_3)_2CO$ (3) 102
6.2.5 Preparation of [^{99m}TcOX(sal_2ibn)] 103
6.2.6 Preparation of *trans*-$TcOX(tmf_2en)$ 104
6.2.7 X-Ray Characterization 104
6.3 Results and Discussion 105
6.3.1 Synthesis of Tc(IV) dinuclear complex 105
6.3.2 Synthesis of Tc(V) mononuclear and dinuclear Tc complexes with thiocyanate 105
6.3.3 Synthesis of Tc-tmf_2en product 106
6.3.4 General Characterization 106

6.3.5 X-Ray Crystal Structures 107
6.3.5.1 *trans*-[μ-O(Tc^{IV}Cl(sal_2ibn))$_2$] · 3 $(CH_3)_2CO$ (1) 107
6.3.5.2 *cis*-[TcO(NCS)sal_2ibn] (2) 108
6.3.5.3 $(Bu_4N)_2$[*trans*-((TcCl(sal_2ibn))μ-O(Tc$(NCS)_5$))] · $(CH_3)_2CO$ (3) 109
6.3.6 Translation to tracer level 113
6.4 Conclusion and Future Studies 115
COMBINED REFERENCES 116
VITA.....127

LIST OF ILLUSTRATIONS

List of Figures

Figure 1-1. Process of microbial reduction of Tc(VII) to Tc(IV); (a) direct reduction of metal and (b) indirect reduction of metal via Fe(III) or SO_4^{2-} reduction. Adapted from Roh et al.[18] 9

Figure 2-1. Structures of the bidentate ligands and Tc-complexes optimized for computational studies. 21

Figure 2-2. Examples of different starting geometries optimized for the bidentate ligands, where X = O or S and Y = O or S. 21

Figure 2-3. Geometries optimized for the metal complexes, where X = O or S and Y = O or S. 22

Figure 2-4. Scheme showing the predicted reaction involving the olefinic acid interference with Tc_2S_7 formation. 24

Figure 2-5. Reaction scheme for mono-mercapto products formed in the fumaric or maleic acid reactions. 27

Figure 2-6. Reaction scheme for di-mercapto products formed in the fumaric and maleic reactions. 28

Figure 2-7. ^{13}C DEPT135 NMR spectrum of FUM4. Solvent is D_2O. 29

Figure 2-8. ^{1}H NMR of (a) FUM4, (b) MSA + Sn^{2+} + TcO_4^-, and (c) MSA ligand. All NMR spectra were run in D_2O. 30

Figure 2-9. Structure of $[Tc^{V}O(MSA)_2]^{3-}$ in 5-membered ring formation. 30

Figure 2-10. ^{13}C-DEPT135 for FUM9 (top, blue) and FUM4 (bottom, red). 31

Figure 2-11. Reaction scheme for mono-mercapto products formed in the crotonic acid reactions. 33

Figure 2-12. Reaction scheme for di-mercapto products formed in the crotonic acid reactions. 34

Figure 2-13. Structures of the mono-mercapto products from the crotonic acid reaction. 35

Figure 2-14. COSY NMR of CRO4, ^{1}H NMR on both left and top axis. 35

Figure 2-15. ^{1}H NMR spectrum for CRO7 showing aliphatic region. 36

Figure 2-16. Structure of crotonic acid. 36

Figure 2-17. HMBC NMR spectrum of CRO7 showing the carbon signals corresponding to the aliphatic proton signals. ^{1}H NMR of CRO7 on top axis, internal HMBC NMR on left axis. 37

Figure 2-18. Comparison of CRO7 (top) and CRO9 (bottom) ^{1}H NMR. 38

Figure 2-19. COSY NMR spectrum of CRO9 showing the coupling signals of neighboring protons. ^{1}H NMR of CRO9 on top and left axis. 38

Figure 2-20. Reaction scheme for di-mercapto products formed in the citraconic acid reactions. 40

Figure 2-21. Tc K-edge k^2 weighted EXAFS spectra for MAL9. 41

Figure 2-22. Tc K-edge $\chi(R)$ function for MAL9. 42

Figure 2-23. Lowest energy structures of ligands L1, L2, and L3. Color scheme: H-white, C-grey, O-red, and S-yellow. 43

Figure 2-24. Lowest energy structures found for complexes C1, C2, C3, C5, and C6. Color scheme: H-white, C-grey, O-red, S-yellow and Tc-turquoise. 44

Figure 3-1. Immobilization of $^{99m}TcO_4^-$ on FeS_{am} at pH 4 (x), pH 7 (+), and pH 9 (●) where n=3. 53

Figure 3-2. Immobilization of $^{99m}TcO_4^-$ on goethite at pH 4 (x), pH 7 (+), and pH 9 (●) where n=3. 54

Figure 3-3. Immobilization of $^{99m}TcO_4^-$ on "reduced" goethite at pH 4 (x), pH 7 (+), and pH 9 (●) where n=3. 54

Figure 3-4. Immobilization of $^{99m}TcO_4^-$ on acid-washed, "reduced" goethite. Goethite was washed with pH 1 HCl (x), pH 1 HNO_3 (+), or no acid (●); then reduced with Na_2S solution where n=3. 55

Figure 3-5. Immobilization of $^{99m}TcO_4^-$ on hematite at pH 4 (x), pH 7 (+), and pH 9 (●) where n=3. 56

Figure 3-6. Immobilization of $^{99m}TcO_4^-$ on "reduced" hematite at pH 4 (x), pH 7 (+), and pH 9 (●) where n=3. 57

Figure 3-7. Immobilization of $^{99m}TcO_4^-$ on acid-washed, "reduced" hematite. Hematite was washed with pH 1 HCl (x), pH 1 HNO3 (+), or no acid (●); then reduced with Na_2S solution where n=3. 58

Figure 3-8. Immobilization of $^{99m}TcO_4^-$- on magnetite at pH 4 (x), pH 7 (+), and pH 9 (●) where n=3. 58

Figure 3-9. Immobilization of $^{99m}TcO_4^-$ on "reduced" magnetite at pH 4 (x), pH 7 (+), and pH 9 (●) where n=3. 59

Figure 3-10. Immobilization of $^{99m}TcO_4^-$ on acid-washed, "reduced" magnetite. Magnetite was washed with pH 1 HCl (x), pH 1 HNO3 (+), or no acid (●); then reduced with Na_2S solution where n=3. 60

Figure 3-11. Immobilization of $^{99}TcO_4^-$ on "reduced" goethite at pH 4 (x), pH 7 (+), and pH 9 (●) where n=3. 61

Figure 3-12. Immobilization of $^{99}TcO_4^-$ on "reduced" hematite at pH 4 (x), pH 7 (+), and pH 9 (●)where n=3. 61

Figure 3-13. Immobilization of $^{99}TcO_4^-$ on "reduced" magnetite at pH 4 (x), pH 7 (+), and pH 9 (●) where n=3. 62

Figure 4-1. Illustration showing the use of a collimation system for SPECT imaging. ... 64

Figure 4-2. Scheme of a $^{99m}Tc/^{99}Mo$ generator. ... 68

Figure 4-3. Structures of (A) ^{99m}Tc-tetrofosmin, (B) ^{99m}Tc-sestamibi, and (C) ^{99m}Tc-Q12. ... 70

Figure 4-4. Structures of acac- and sal- based Schiff base ligands. ... 71

Figure 4-5. Structures of *trans*-$Re^{V}OCl(acac_2en)$, *cis*-$Re^{V}O(NCS)(acac_2en)$, *trans*-$Re^{V}OCl(acac_2pn)$, and *cis*-$Re^{V}O(NCS)(acac_2pn)$. ... 72

Figure 5-1. Complete reaction scheme of compounds 1-5. ... 77

Figure 5-2. Thermal ellipsoid plot[70] of *cis*-[$ReO(sal_2ibn)Cl$] (1) with 50% probability ellipsoids (CCDC 933550). Hydrogens and solvent molecules are omitted for clarity. ... 92

Figure 5-3. Thermal ellipsoid plot[70] of *trans*-[μ-$O(ReO(sal_2ibn))_2$] (2) with 50% probability ellipsoids (CCDC 933551). Hydrogens and solvent molecules are omitted for clarity. ... 94

Figure 5-4. Thermal ellipsoid plot[70] of *cis*-[$ReO(NCS)(sal_2ibn)$] (3) with 50% probability ellipsoids (CCDC 933552). Hydrogens are omitted for clarity. ... 95

Figure 5-5. Thermal ellipsoid plot[70] of *trans*-[$Re(NCS)(PPh_3)sal_2ibn$] (4) with 50% probability ellipsoids (CCDC 933553). Hydrogens are omitted for clarity. ... 96

Figure 5-6. Thermal ellipsoid plot[70] of *trans*-[μ-$O(Re(NCS)sal_2ibn)_2$] (5) with 50% probability ellipsoids (CCDC 933554). Hydrogens are omitted for clarity. O3 is labeled as O4 in Table 4 to simplify the table. ... 97

Figure 6-1. Structures of sal_2ibnH_2 and tmf_2enH_2. ... 101

Figure 6-2. ORTEP representation of trans-[μ-$O(TcCl(sal_2ibn))_2$] (1). Thermal ellipsoids are shown with 50% probability. Hydrogens have been removed for clarity. ... 108

Figure 6-3. ORTEP representation of cis-[$(TcO(NCS)sal_2ibn)$] (2). Thermal ellipsoids are shown with 50% probability. Hydrogens have been removed. ... 109

Figure 6-4. ORTEP representation of *trans*-[$(TcClsal_2ibn)\mu$-$O(Tc(NCS)_5)$] (3). Thermal ellipsoids are shown with 50% probability. Hydrogens have been removed for clarity. ... 111

Figure 6-5. Overlaying HPLC chromatograms of ReO(sal2ibn)(NCS) (red line) and TcO(sal2ibn) with NCS-(blue line) ... 114

Figure 6-6. HPLC chromatograms of NCS^- stability studies. (A) Rad-HPLC of $TcO(sal_2ibn)$ w/ NCS^- at 4 hours; (B) Rad-HPLC of $TcO(sal_2ibn)$ w/ NCS^- at 24 hours; (C) Rad-HPLC of $TcO(sal_2ibn)$ w/o NCS^-- at 4 hours; (D) Rad-HPLC of $TcO(sal_2ibn)$ w/o NCS^- at 24 hours. ... 114

List of Tables

Table 1-1. ^{99}Tc concentrations in selected samples. 3

Table 2-1. Interference reactions including pH conditions and abbreviations. 25

Table 2-2. XAS data for $[TcO(DMSA)_2]^{5-}$ standard and MAL9 sample. 41

Table 2-3. Structures and RMSD values of $Tc^{V}O$ complexes used to validate computational model. 45

Table 2-4. ΔG_{rxn} at each level of theory (kcal/mol). 46

Table 5-1. ^{1}H NMR Chemical Shifts. 88

Table 5-2. X-ray crystal data, data collection parameters, and refinement parameters. ... 90

Table 5-3. Selected bond lengths (Å) and angles (deg) for compounds 1-5 91

Table 6-1. X-ray Crystal Data, Data Collection Parameters, and Refinement parameters. 111

Table 6-2. Selected bond lengths (Å) and angles (deg) for compounds 1-3 112

ABSTRACT

Part I: Sulfide Remediation

Technetium-99 is an environmental concern at nuclear waste storage facilities. Hanford, WA is one of the largest waste storage facilities, and unfortunately some of the nuclear waste contained at this site has leaked into the ground. Technetium is most stable as the pertechnetate anion in aqueous, aerobic environments, which is mobile in water. Due to this high mobility and its long half-life, studies have been done to understand the environmental impact of technetium and to prevent further contamination issues.

The H_2S gaseous diffusion method has shown potential in immobilizing technetium by forming reduced Tc solids in the ground. In past work, it has been shown that olefinic low molecular weight organic acids (LMWOAs) can inhibit immobilization. Therefore, one objective for this project was to identify the complexes formed in these reactions. Additionally, work has been done to investigate the interaction of sulfide and pertechnetate with common Fe-containing minerals.

Part II: Schiff Base Chemistry

Technetium-99m Schiff base complexes have been studied for use as single photon emission computed tomography (SPECT) imaging agents. Rhenium is often considered a structural analog to technetium and has isotopes ideal for radiotherapy and imaging.

Many Tc and Re N_2O_2 Schiff base complexes have been investigated. Reaction with π-backbonding ligands may lead to complexes that are more kinetically inert. In previous work, addition of thiocyanate (NCS^-) to *trans*-[ReO(X)($acac_2$en/pn)] (X = OH_2 or Cl^-) led to the formation of *cis*-[ReO(NCS)$acac_2$en/pn]. Efforts to understand and

develop suitable Tc/Re radiopharmaceuticals have led to unusually aqueous-stable $M^{V}O(NCS)$ Schiff base complexes.

CHAPTER 1: INTRODUCTION TO TECHNETIUM IN THE ENVIRONMENT

Technetium was first discovered by Perrier and Segre in 1937 after they analyzed a sample of molybdenum that had been bombarded with deuterons. It is the lightest element with no stable isotope. Most isotopes of Tc are very short-lived, with only ^{97}Tc ($t_{1/2}$ = 2.6 x 10^6 y), ^{98}Tc ($t_{1/2}$ = 4.2. x 10^6 y), and ^{99}Tc ($t_{1/2}$ = 2.1 x 10^5 y) having significantly long half-lives. Technetium-97 and technetium-98 have been formed in nuclear reactions, but only in very small amounts; the environmental contributions from these two isotopes are negligible. On the other hand, ^{99}Tc has a high yield of 6.06% from the fission of ^{235}U and ^{239}Pu. Consequently, the majority of ^{99}Tc in the environment is due to uranium fuel reprocessing at nuclear facilities.[1]

In its elemental form, technetium is a silvery-gray metal, similar to platinum. However, in the environment, technetium is usually found as Tc(IV) or Tc(VII). In an oxidizing environment, the predominant species is pertechnetate (TcO_4^-), which is mobile in aqueous conditions. Pertechnetate is stable over a wide pH range when no reducing agent is present. When in a reductive environment, technetium is most stable as Tc(IV), commonly seen as technetium (IV) oxide (TcO_2). Technetium oxide is not soluble in water, but once in the presence of water, it can readily hydrolyze.

1.1 Sources of Technetium-99 in the Environment

It has been shown that ^{99}Tc can be formed by the fission of uranium. Spontaneous fission of ^{238}U can yield ^{99}Tc, and neutron induced fission of ^{235}U can also produce ^{99}Tc.[2,3] Aside from being a fission product, ^{99}Tc can be generated by cosmic ray interactions with molybdenum, ruthenium, and niobium.[4,5] The amount of technetium made by these pathways is about 60 PBq, which is distributed throughout the earth's

crust.[1] Taking into consideration the long half-life of ^{99}Tc, this concentration of natural-occurring technetium-99 is undetectable in the environment.[1]

The major contribution of technetium-99 in the environment comes from anthropogenic sources. It is estimated that about 140 TBq of ^{99}Tc was introduced to the environment from nuclear testing fallout. The amount contributed from nuclear power plants is much less. Even though the production of ^{99}Tc is about 5.8 TBq/y (9 kg Tc/y),[6] it is estimated that less than 10 GBq (15 g Tc) has been released due to small leakages, up to 2010.[1] In addition to this leakage, major accidents at nuclear power plants have contributed an estimated 1 TBq (1.5 kg Tc) to the environment. This amount does not include the waste water that was distributed into the sea during the Fukushima accident. Another source is from the widely used ^{99}Mo/^{99m}Tc generators used for medical imaging. This source only produces a maximum of 0.78 GBq/y (1.2 g Tc/y) that would be found in the environment. From 1970-2010, an estimated total of about 20 GBq (30 g Tc) was released from medical imaging.[1] These sources, nuclear weapons testing, power plants, and medical generators, account for less than 10% of the ^{99}Tc released into the environment. The major impact comes from nuclear fuel reprocessing plants, such as Sellafield (UK) and Hanford (USA). Table 1-1 shows ^{99}Tc concentrations in selected samples from contaminated areas.

Table 1-1. ^{99}Tc concentrations in selected samples.

Sample	Location	^{99}Tc conc. (Bq/g)	Reference
EPA drinking water limit		0.078	
Sediment	Irish Sea	0.014-0.45	[7,8]
Soil	Chernobyl	0.001-0.015	[9]
Soil	Sellafield	0.82	[7]
flounder	Irish Sea	0.0056	[8]
mussel	Irish Sea	0.075	[8]
lobster	Sellafield	0.14	[8]
potatoes	Sellafield	0.00025	[8]
seaweed	Capenhurst	1.6	[8]
seaweed	Greenland Sea	0.04	[8]

1.2 Technetium in Water

Technetium-99 concentrations are typically very low in the environment unless direct contamination has taken place. Precipitation concentrations can vary from 20-60 μBq/L, whereas seawater samples only show a few μBq/L.[10,11] Reprocessing plants at Sellafield and La Hague deposit ^{99}Tc waste directly into the Irish Sea and the English Channel, which leads to ^{99}Tc traveling north to the North Sea, Norwegian Sea, Greenland Sea, and the Arctic. Together these plants have discharged more than 1870 TBq into the Irish Sea and the English Channel.[7] These bodies of water have shown concentrations up to 75 mBq/L and 21 mBq/L, respectively.[7] Concentrations further north have reached 0.3 mBq/L for the Greenland Sea and 0.07 mBq/L for Arctic seawater.[7]

1.3 Technetium in Soils and Sediments

Technetium typically enters soils and sediments through discharge or leakage from nuclear reprocessing plants or from fallout due to nuclear weapons or reactor accidents. Due to the high water solubility of pertechnetate, once technetium is deposited into soil, it will easily migrate when water is present. This migration can eventually lead to pertechnetate in groundwater. Also, technetium species adsorbing to sediment can easily be taken up into marine plant life and then consumed by marine animals, thus entering the food cycle.

Due to the continual migration of technetium species in aqueous environments and the resulting dilution, it can be difficult to quantify the amount of technetium present and to identify the dominant species present. In reductive environments, several oxidation states are achievable. Technetium (IV) is commonly seen due to its stability. In areas when organic matter content is high, technetium(IV) can be complexed in the organic material.[12] Where organic content is low, Tc(IV) will form TcO_2 or carbonate species.[12] Due to the complexity of the chemistry, it is difficult to predict speciation; but in non-reducing conditions, technetium's mobility is higher due to the stability of pertechnetate, and absorption into plant life is more likely.

Sediment samples from areas of no direct contamination show less than 10 μBq/g (1.5 fg Tc/g soil).[1] In the Irish Sea, sediment activities have continued to decline as less and less waste is being discharged. In 2009, a range of 18-450 mBq/g (17-690 pg Tc/g soil) was observed.[7] A more recent sampling, in 2012, shows a lower range of 14-55 mBq/g (21-84 pg Tc/g soil), which shows an eight-fold decrease over three years.[8]

In a 30-km zone around Chernobyl, a concentration range of 1-15 mBq/g (1.5-23 pg Tc/g soil) has been reported.[9] The areas surrounding the Fukushima power plant will likely have an elevated level of ^{99}Tc in the soil, but most likely lower concentration on average due to the lower amount of radiation released during the accident. It is estimated that 30 PBq of ^{137}Cs was released to the atmosphere during Fukushima, which is approximately one-third of the ^{137}Cs activity released during Chernobyl.[1] Based on this ratio, the ^{99}Tc amount released would be about 0.25 TBq. Since waste water was discharged into the Pacific Ocean during the Fukushima accident, sediment contamination is more difficult to predict.

Several studies have also been done observing the impact of nuclear weapons on the environment. Regions in Japan show a technetium concentration range from 4-88 μBq/g (6-135 fg Tc/g soil).[13] Due to the larger contribution from nuclear reprocessing plants, the influence of nuclear weapons detonation is many times overshadowed.

1.4 Technetium in Plants

As mentioned above, technetium is generally introduced to plants through the soil or in aqueous conditions. Although it is not clear which pathways allow for pertechnetate to be absorbed by the plant, the high solubility of the anion in water allows for competition with other biologically available ions. One possible mechanism for the uptake of technetium in plants is from the absorption of pertechnetate into the plant, and then reduction by chloroplast and chelation with intercellular molecules.[14,15] Both the type of plant and the growth rate will affect the amount of radioactivity accumulated.

Marine life has been studied in areas such as Sellafield due to the contamination deposited directly into the Irish Sea. Many seaweeds have been found to incorporate

high levels of technetium in relation to other plants. It has been seen that aquatic plants do not uptake reduced Tc species; therefore, the high uptake is attributed to foliar absorption of pertechnetate.[16] Measurements as high as 0.4 mBq/g (0.6 pg Tc/g seaweed) have been seen in *Fucus vesiculosus* off the coast of Spain; this is explained as fallout background.[17] Seaweed taken from the Irish Sea has shown up to 1600 mBq/g (2.4 ng Tc/g seaweed), and seaweed from the coast of Greenland (Greenland Sea) shows concentrations up to 40 mBq/g (61 pg Tc/g seaweed).[7]

Several other types of plants have been evaluated on land in the Sellafield area in order to monitor the transfer of radioactivity from sea to land. The majority of these concentrations is very low, and the numbers have been decreasing over the years. For example, in 2009 onions showed an uptake of 880 μBq/g (1.35 pg Tc/g onion), and in 2012, the concentration dropped to less than 81 μBq/g (0.12 pg Tc/g onion).[7,8] For potatoes, the technetium level stayed consistent at 250 μBq/g (0.38 pg Tc/g potato).[7,8]

1.5 Technetium in Animals

Marine animals will be more likely to be affected by technetium in the environment, especially in areas like Sellafield, where waste is deposited into the water. In particular shellfish have an overall higher accumulation. Crabs off the coast of Sellafield in 2009 were found to have 11 mBq/g (16.9 pg Tc/g crab) and lobsters averaged 250 mBq/g (380 pg Tc/g lobster).[7] Cod had an accumulation of less than 0.5 mBq/g (0.7 pg Tc/g cod).[7] Similarly to other trends, all the levels have since gone down in activity with 8.7 mBq/g (13 pg Tc/g crab) for crabs, 140 mBq/g (210 pg Tc/g lobster) for lobsters, and 0.17 mBq/g (0.26 pg Tc/g cod) for cod.[8]

Land animals in the Sellafield area have also been investigated. Most of these activities are very low because the main pathway to ingest technetium-99 is by eating plant life or fishmeal (made for livestock). Over the years of 2008-2012, activity levels in land animals, including cows, sheep, rabbits, pheasants, and deer, stayed in the range of 21-41 μBq/g (32-63 fg Tc/g meat).[7,8] The amount shown to transfer to cow's milk is even lower at 5 μBq/g (7 fg Tc/g milk).[8]

1.6 Remediation Techniques for Technetium-99

As mentioned above, under aqueous, non-reducing conditions, technetium can remain highly stable as the pertechnetate anion. Pertechnetate migrates very easily through the environment due to its high water solubility and poor interactions with soil. Once pertechnetate is introduced into the soil, its pathway will be to diffuse through the vadose zone and eventually into the groundwater. Briefly, the vadose zone is the area between the land surface and the water table. Groundwater is typically recharged naturally and becomes surface water. For example, groundwater near the Hanford site will flow towards the Columbia River, consequently dispersing radioactive waste into the Columbia River. Downstream from Hanford, the Columbia River is used as drinking water; therefore, if waste does reach the Columbia River, it could potentially impact the cities nearby.

Several techniques have been developed to remove $^{99}TcO_4^-$ from water sources that involve the anion interacting with different chromatographic materials and adsorbing to the surface. Some of these show high selectivity for pertechnetate over other common ions found in the environment. These methods, however, are not suitable for

contamination in the vadose zone. A National Research Council has reported that the contamination at Department of Energy sites (Hanford, Oakridge National Laboratory, Savannah River Site, etc.) will not be removed in remediation efforts because cost and technological necessities are too limiting.

Therefore, research exploring potential *in situ* methods of immobilization has been of interest. This approach would mean introducing some chemical or biological species into the environment, inducing the contaminant to form an insoluble, stable species that is preferably adsorbed to the surface of the soil. This adsorption would prevent the contaminant from migrating farther, effectively immobilizing the species in the vadose zone. With technetium, the most common immobilization techniques revolve around reducing the technetium to Tc(IV) because Tc(IV) species are less water soluble and would have a slower diffusion rate. The two main ways of achieving this *in situ* are bioreduction and chemical reduction.

1.6.1 Bioremediation of Technetium-99

Bioremediation involves the use of reducing bacteria to change the oxidation state of the metal directly or indirectly. Common bacteria studied for the immobilization of technetium are *Geobacter metallireducens*, *Shewanella putrefaciens*, *Rhodobacter sphaeroides*, *Paracoccus denitrificans*, and *Escherichia coli*.[18] The bacteria can either reduce Tc(VII) directly to Tc(IV) (Figure 1-1a) or reduce Fe(III) or sulfate, which will then reduce Tc(VII) (Figure 1-1b). *E. coli* was able to reduce Tc(VII) directly to Tc(II), but only in anaerobic cultures. It is generally assumed that the vadose zone is well-aerated at several meters depth, but there is evidence of low oxygen level regions.

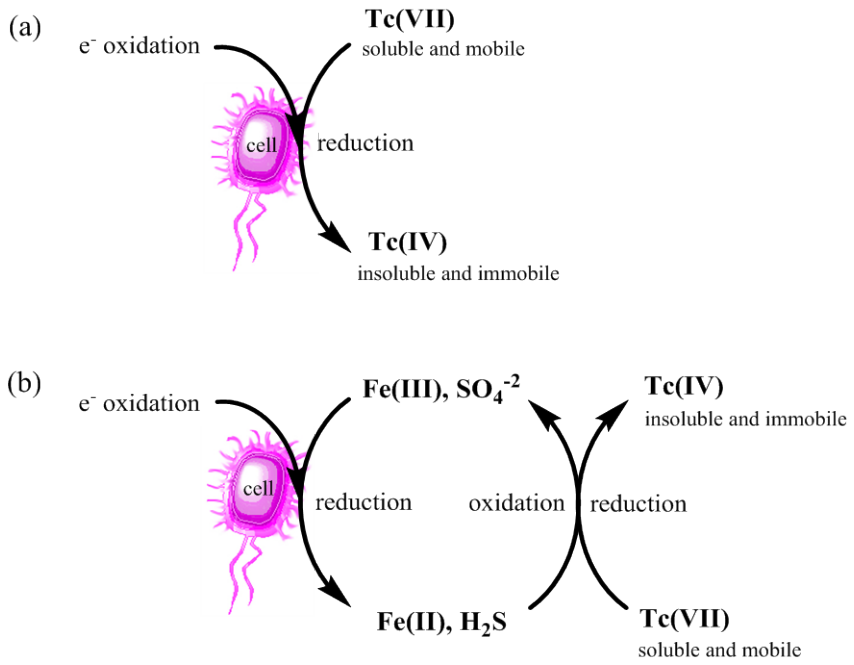

Figure 1-1. Process of microbial reduction of Tc(VII) to Tc(IV); (a) direct reduction of metal and (b) indirect reduction of metal via Fe(III) or SO_4^{2-} reduction. Adapted from Roh et al.[18]

McBeth et al. investigated the effect of oxidative conditions on "post reduction" systems.[19] These systems, prior to re-oxidation, contained Fe(II), Tc(IV), and sulfide. After the addition of air, Fe(II), sulfide, and Tc(IV) re-oxidized, and about 60% of the technetium was re-mobilized in solution after 60 days. Interestingly, when nitrate was used as an oxidant, only small amounts of technetium were re-oxidized. After 20 days, nearly all of the Fe(II) present was re-oxidized to Fe(III), and the sulfide was re-oxidized to sulfate. The amount of technetium present in solution remained low, reaching about 8% after 60 days.

1.6.2 Chemical Reduction of Technetium-99

There have been several methods investigated in a laboratory setting to probe potential technetium immobilization by chemical reduction. Some of the reductants include zero-valent iron[20–22], Fe(II)[23], and sulfide[20,24]. Hydrogen sulfide has been used in the field to immobilize Cr(VI) by using a method called *in situ* gas reduction (ISGR).[25]

Similar to immobilization of Tc by sulfide, Cr(VI) is immobilized by forming a reduced Cr(III) species that has limited solubility and toxicity.[26] At White Sands, Cr(VI) contamination was treated by ISGR of hydrogen sulfide to test the field effectiveness of the method.[25] The site had about a 15 ft radius with an injection well of dilute hydrogen gas at the center. To limit hydrogen sulfide released into the atmosphere, six extraction wells were installed that extracted gas from the wellfield and used a sodium hydroxide scrubber to remove excess hydrogen sulfide before releasing the gas back into the atmosphere. Overall, the field test was successful at immobilizing 70% of the Cr(VI) in the vadose zone. Immobilization was limited to areas of good permeability and high Fe-mineral concentrations. This method could be very useful for pertechnetate immobilization as well.

Studies have been done investigating the effectiveness of immobilization of pertechnetate by sulfide.[24] In areas of technetium contamination, however, there are a wide variety of other components that may interfere with sulfide immobilization.[27] Understanding possible interference interactions is important in pursuing this method of immobilization further.

CHAPTER 2: CHARACTERIZATION OF SMALL OLEFINIC ACIDS REACTING WITH PERTECHNETATE IN THE PRESENCE OF SODIUM SULFIDE

2.1 Introduction

Technetium is a group 7 element on the periodic table. It has a complex redox chemistry with oxidation states ranging from -1 to +7. The most well-known isotope of technetium is ^{99m}Tc because of its use in radiopharmaceuticals, where the most useful oxidation states are +1, +3, and +5. From an environmental perspective, the isotope of concern is ^{99}Tc due to its long half-life ($t_{1/2}$ = 2.1x10^5 years). In the environment, technetium exists predominantly as one of two species: pertechnetate (TcO_4^-) or technetium (IV) oxide (TcO_2). In oxic conditions, pertechnetate is the most stable species and is mobile in water.

Technetium-99 is mainly produced as a fission product from the thermal neutron fission of ^{235}U and ^{239}Pu. Hanford, Washington was one of the larger sites used for nuclear weapons development for the Manhattan Project. Several tons of nuclear fuel were reprocessed in order to isolate plutonium-239. Underground storage tanks were used that ranged in size from 55,000 gallons to 1,000,000 gallons in order to contain the 54 million gallons of radioactive waste produced during reprocessing. Unfortunately, some of the 149 single-shelled tanks have leaked, resulting in more than 1 million gallons of radioactive waste seeping into the vadose zone. Technetium-99 is an environmental concern, especially in the case of the Hanford site because the site is in close proximity to the Columbia River. There have been many studies involved in remediating pertechnetate in the vadose zone by stabilizing the technetium *in situ*.[18,20,22–24,28] It has been generally accepted that many Tc(IV) species are sparingly soluble or insoluble in aqueous media. Several techniques have been based on the idea of immobilizing

technetium by adding a reducing agent, that would react with technetium to form these insoluble Tc(IV) species.

In order to form insoluble Tc species *in situ*, a reductant can be used to interact with the Tc(VII) directly or it can reduce surface Fe(III) in minerals common in soils (e.g., goethite, hematite), which would then reduce the Tc. One potential method involves sulfide reduction. Sulfides, such as sodium sulfide and hydrogen sulfide, will react with pertechnetate in solution and precipitate technetium (IV) oxide or insoluble technetium sulfides, namely TcS_2 and Tc_2S_7.[24]

$$TcO_4^- + 3e^- + (n+2)H_2O \leftrightarrow TcO_2 \cdot nH_2O \quad (2\text{-}1)$$

$$TcO_4^- + 7HS^- + H_2O \leftrightarrow Tc_2S_7 + 9OH^- \quad (2\text{-}2)$$

Liu et al. demonstrated the effectiveness of using Na_2S as a reducing agent to precipitate technetium from aqueous solutions.[24] Lui found that pertechnetate precipitated as Tc_2S_7 when in an aqueous solution with Na_2S. These experiments were done under oxic and anoxic conditions, and over a wide pH range. In oxic conditions, Tc_2S_7 only formed under acidic conditions. The best result from the aerobic experiments was an immobilization yield of about 80% at pH 1 with a sulfide concentration of 6 mM and pertechnetate concentration of 0.6 mM. As the pH increased, the immobilization yield decreased; above pH 7 yields were below 5%.[24] In anaerobic environments, the Tc_2S_7 yields were comparable to the aerobic results at pH levels below 7. In the alkaline solutions, the anoxic experiments had very high immobilization yields (near 80%), while the oxic experiments showed very low immobilization yields (<5%).

Along with varying the reaction conditions, Liu et al. also demonstrated the effects of several competing agents, including minerals, chelating agents, low molecular

weight organic acids (LMWOAs), and anions.[27] LMWOAs are used as humic acid mimics, which is the majority of organic material found in soils. The majority of these showed little or no effect on Tc_2S_7 precipitation. An interesting occurrence resulted on the addition of olefinic LMWOAs. Even with low concentrations of the LMWOA, maleic and fumaric acid form water-soluble Tc complexes on reaction with pertechnetate in the presence of sodium sulfide, (i.e., no precipitate (Tc_2S_7) formed).[27]

To further probe this chemistry, an investigation of the sulfide reduction of pertechnetate in the presence of the olefinic acids mentioned and similar acids (crotonic and citraconic) was pursued to better understand this chemistry and to identify the soluble ^{99}Tc compounds that formed.

2.2 Experimental Section

2.2.1 Materials

Caution! Technetium-99 is a weak β^- emitter (E_{max} = 0.294 MeV, 100% abundance). All operations were carried out in a radiochemical laboratory equipped for handling this radionuclide. Solid ammonium pertechnetate was obtained from Oak Ridge National Laboratory. This material, which should be white, was black indicating it had undergone radiolytic autoreduction to TcO_2. This mostly black solid was purified by refluxing with hydrogen peroxide for one hour to regenerate pertechnetate and destroy excess H_2O_2 and quantified by liquid scintillation counting (LSC).

All water used was 18-MΩ water and was degassed with Ar prior to use. Except where noted, chemicals were reagent grade, obtained from either Aldrich Chemical Co. or Fisher Scientific, and used without further purification. Sodium sulfide in solution was used in place of hydrogen sulfide gas and was prepared by adding the crystalline solid to

water or buffer that had been purged with Ar for at least 2 hours prior to use. C_{18}-reversed phase silica gel (230-400 mesh) was purchased from Aldrich Chemical Co. TLC saturation pads were purchased from Aldrich Chemical Co.

2.2.2 Interference Reactions

All reactions were performed at room temperature. Degassed phosphate buffers (100 mM) were used to adjust pH. Both aerobic and anaerobic conditions were studied.

2.2.2.1 Aerobic Conditions

Aerobic reactions were run in 20 mL scintillation vials. Each acid (0.41 mmol) was dissolved in 2.5 mL of phosphate buffer. In a separate vial, sodium sulfide nonahydrate (0.97 mmol) was dissolved in 2.5 mL of phosphate buffer. Both solutions were combined in a single reaction vial, followed by the addition of ammonium pertechnetate, NH_4TcO_4 (0.14 mmol); the reaction was allowed to sit for 24 hours. Acids used for these experiments were fumaric acid, maleic acid, crotonic acid, and citraconic acid. Phosphate buffers were prepared at pH 4, 7, and 9.

TLC saturation pads were run on crude solutions, with mobile phases of acetone, water, and acetone-water (50:50, v/v). Each crude reaction mixture was filtered to eliminate any solids. These solids likely contained TcO_2 and/or Tc_2S_7. The resultant filtrate was run on a C-18 column with acetonitrile, and then increasing concentrations of water until the product eluted. Desired products eluted from the column at between 25-30% v/v water in acetonitrile.

For example, the fumaric acid reaction run at pH 4 was performed by first dissolving 0.41 mmol of fumaric acid in 2.5 mL of pH 4 phosphate buffer (100 mM). Then 0.97 mmol of $Na_2S{\cdot}9H_2O$ was dissolved in 2.5 mL of phosphate buffer in a separate

vial. Once the solid dissolved, the sodium sulfide solution was added to the fumaric acid solution. To this vial, an aliquot of ammonium pertechnetate (0.14 mmol) in water was added.

2.2.2.2 Anaerobic Conditions

For the anaerobic experiments, 10 mL crimp seal vials were dried, evacuated, and purged with argon gas. Amounts of each reagent were the same as specified in the aerobic set up, but the solutions were transferred to the reaction vial via cannula or syringe to maintain the air-free environment.

2.2.3 Control Reactions

All control experiments were run in both aerobic and anaerobic conditions. The control experiments included the reactions (1) without an acid present, (2) without pertechnetate present, and (3) without sulfide present. Each reaction was performed using the same quantities as detailed previously. Each reaction was run in a total of 5 mL of phosphate buffer to maintain the same concentrations as the interference reactions.

2.2.4 Synthesis of $[Tc^{V}O(MSA)_2]^{3-}$

2.2.4.1 Method 1 (reference MSA complex $[(Tc^{V}O(MSA)_2]^{3-}$)

Mercaptosuccinic acid (MSA; 104 mg) was dissolved in 2 mL of H_2O. In a separate vial, 31 mg of stannous chloride dihydrate was dissolved in 1 mL of H_2O. The stannous chloride solution was added to the mercaptosuccinic acid solution. Sodium bicarbonate (0.1 M solution) was added dropwise until the pH reached 7-8. Ammonium pertechnetate (0.14 mmol) was added as an aqueous solution to the reaction vial. The reaction was stirred at room temperature for 30 minutes and then was filtered to remove any solids. The resultant brown solution was dried by Centrifan and washed with cold

acetone (5 mL x 3). Yield 56%. ^{1}H NMR [500 MHz, D_2O, 27ºC, δ (ppm)]: 3.97 (2H, ddd, J = 8, 8, 15 Hz, -SC**H**-); 2.97-3.05 (2H, m, -C**H**$_2$-); 2.80-2.90 (2H, m, -C**H**$_2$-). ^{13}C NMR [500 MHz, D_2O, 27ºC, δ (ppm)]: 179.4(-CH_2**C**OO); 177.8 (-SC**C**OO); 48.1 (-S**C**H-); 47.3 (-S**C**H-); 41.2 (-C**H**$_2$-). FT-IR (oil mull, ν/cm^{-1}): 941 (Tc≡O st).

2.2.4.2 Method 2 (FUM4)

Fumaric acid (48 mg; 0.41 mmol) was weighed into a 20 mL scintillation vial and dissolved in 2.5 mL of pH 4 phosphate buffer (100 mM). Sodium sulfide (200 mg) was dissolved in 1 mL of H_2O in a 20 mL scintillation vial. 1.5 mL of pH 4 phosphate buffer was slowly added to the sulfide solution to avoid forming H_2S and elemental sulfur. The sulfide solution was added to the fumaric acid solution. Any pH adjustments were made with 0.1 M HCl or NaOH to bring the reaction to pH 4. To this vial, an aliquot of ammonium pertechnetate (0.14 mmol) in water was added. The reaction was allowed to stir for 24 hours. The crude reaction mixture was filtered to remove any solids. $[Tc^{V}O(MSA)_2]^{3-}$ was purified by one of two methods: (1) C_{18} silica gel column separation or (2) liquid-liquid extraction.

For the column separation, the crude reaction was loaded onto a C_{18} silica gel column equilibrated in acetonitrile. The column was washed with 20 mL of acetonitrile. After washing, increasing amounts of H_2O were added to the mobile phase, starting at 5% v/v water in acetonitrile and increasing by 5% until the product eluted. The desired product eluted as a brown-orange solution with 25% H_2O in acetonitrile.

For liquid-liquid extraction, 2 mL of the filtered crude reaction was added to a 20 mL scintillation vial. Two mL of acetonitrile was added to the vial. An orange species, $[Tc^{V}O(MSA)_2]^{-}$, separated into the organic layer. Yield 47%. ^{1}H NMR [500 MHz, D_2O,

27ºC, δ (ppm)]: 3.95 (2H, ddd, J = 24, 8.5, 6 Hz, -SC**H**-); 3.08-2.97 (2H, m, -C**H**$_2$-); 2.93-2.83 (2H, m, -C**H**$_2$-). ^{13}C NMR [500 MHz, D_2O, 27ºC, δ (ppm)]: 175.07(-**C**OO); 174.4 (-**C**OO); 42.6 (-S**C**H-); 41.9 (-S**C**H-); 36.5 (-C**H**$_2$-); 37.0 (-C**H**$_2$-). FT-IR (oil mull, ν/cm^{-1}): 945 (Tc≡O st).

2.2.4.3 Method 3 (MAL4)

This reaction was run similarly to FUM4, with the substitution of maleic acid for fumaric acid. Yield 35%. ^{1}H NMR [500 MHz, D_2O, 27ºC, δ (ppm)]: 3.94 (2H, ddd, J = 27, 8.5, 6 Hz, -SC**H**-); 3.08-2.97 (2H, m, -C**H**$_2$-); 2.94-2.85 (2H, m, -C**H**$_2$-). ^{13}C NMR [500 MHz, D_2O, 27ºC, δ (ppm)]: 175.74(-**C**OO); 174.84 (-**C**OO); 43.48 (-S**C**H-); 42.80 (-S**C**H-); 36.97 (-C**H**$_2$-); 36.88 (-C**H**$_2$-). FT-IR (oil mull, ν/cm^{-1}): 944 (Tc≡O st).

2.2.5 Synthesis of $[TcO(DMSA)_2]^{5-}$

2.2.5.1 Method 1 (reference DMSA complex, [TcO(*meso*-DMSA)]$^{5-}$)

This procedure was adapted from Blower et al.[29] Stannous chloride ($SnCl_2$•$2H_2O$; 31 mg) was dissolved in 1 mL of H_2O in a 20 mL scintillation vial. *meso*-2,3-Dimercaptosuccinic acid (DMSA; 51 mg) was dissolved in 2 mL of H_2O. The stannous solution and the DMSA solution were combined. Sodium bicarbonate solution ($NaHCO_3$; 0.1 M) was added dropwise until the pH of the solution was between 7 and 8. An aliquot of ammonium pertechnetate (0.14 mmol) in H_2O was added to the reaction vial. The reaction was allowed to stir at room temperature for 30 minutes. A white precipitate was filtered from the solution and the orange filtrate was collected and dried by Centrifan. The solid was washed with acetone (5 mL x 3). Yield 83%. ^{1}H NMR [500 MHz, D_2O, 27ºC, δ (ppm)]: 4.18 (s, -SC**H**-); 4.23 (s, -SC**H**-); 4.29 (s, -SC**H**-**)**. FT-IR (oil mull, ν/cm^{-1}): 951 (Tc≡O st).

2.2.5.2 Method 2 (FUM9)

The reaction was performed similarly to FUM4 using pH 9 phosphate buffer. The column separation was performed by the same procedure as FUM4. The orange band that eluted at 30% H_2O in acetonitrile was the desired product. Extraction was performed as described in FUM4. Yield 29%. ^{1}H NMR [500 MHz, D_2O, 27ºC, δ (ppm)]: 4.48 (1H, d, J = 10 Hz, -SC**H**-); 4.36 (1H, d, J = 12 Hz, -SC**H**-); 4.04 (1H, d, J = 10 Hz, -SC**H**-); 3.92 (1H, d, J = 12 Hz, -SC**H**-). ^{13}C NMR [500 MHz, D_2O, 27ºC, δ (ppm)]: 63.12 (-S**C**H-); 62.32 (-S**C**H-); 58.84 (-S**C**H-); 58.25 (-S**C**H-). FT-IR (oil mull, ν/cm^{-1}): 949 (Tc≡O st).

2.2.5.3 Method 3 (MAL9)

The reaction was run similarly to FUM4, with the following changes made. Maleic acid was used instead of fumaric acid, and pH 9 phosphate buffer was used instead of pH 4 phosphate buffer. Separation methods were the same as described for FUM9. Yield 21%. ^{1}H NMR [500 MHz, D_2O, 27ºC, δ (ppm)]: 4.48 (1H, d, J = 10.5 Hz, -SC**H**-); 4.37 (1H, d, J = 12 Hz, -SC**H**-); 4.05 (1H, d, J = 10.5 Hz, -SC**H**-); 3.92 (1H, d, J = 12 Hz, -SC**H**-). ^{13}C NMR [500 MHz, D_2O, 27ºC, δ (ppm)]: 63.12 (-S**C**H-); 62.32 (-S**C**H-); 58.84 (-S**C**H-); 58.25 (-S**C**H-). FT-IR (oil mull, ν/cm^{-1}): 948 (Tc≡O st).

2.2.6 Characterization

Nuclear magnetic resonance (NMR) spectroscopy was run on a Bruker DRX500 or a Bruker DRX600 at 25º C in D_2O. 4,4-dimethyl-4-silapentane-1-sulfonic acid (DSS) was used as an internal reference. Infrared (IR) spectra were obtained as oil mulls on a Thermo Nicolet Nexus 670 FT-IR instrument. All yields were determined by ^{99}Tc radio-TLC using an acetone-water (50:50 v/v) mobile phase.

2.2.6.1 X-Ray Absorption Spectroscopy

X-ray absorption spectroscopy (XAS) was used for characterization of solid products obtained from the reactions. The solids were prepared in triply-encapsulated aluminum holders. The solids analyzed were $[(Tc^{V}O(DMSA)_2]^{5-}$, FUM7, and MAL9. The samples were analyzed at the 10-BM beamline at the Advanced Photon Source at Argonne National Laboratory (APS, Argonne, IL).

2.2.7 Computational Methods

Quantum chemical calculations were performed using the Gaussian09 program package[30]. Ligands and complexes were fully optimized in the gas phase using a mixed basis set model. Normal mode vibrational frequency calculations were performed to confirm structures were minima. The PBE0 DFT method was employed for these calculations. For all non-metal atoms, the 6-31G** basis set was used; for Tc atoms, the LANL2TZ basis set was used (MBS1). Gas-phase and solvent-phase single-point energy calculations were performed on each structure within 10 kcal/mol of the lowest energy equilibrium structure. Structures were not re-optimized at the single-point energy level. The single-point energy calculations were performed using the PBE0 method in conjunction with the 6-311+G* (non-metals) and LANL2TZ(f) (Tc atoms) basis sets (MBS2).

The solvent-phase calculations were carried out using polarizable continuum model (PCM) methods, both IEF-PCM and SMD, with water as the model solvent. Since adding several separate solvent molecules to determine a solvent effect is computationally expensive, methods have been developed to implicitly mimic a solvent environment. In the PCM methods, the solute is placed in a cavity in a uniform

polarizable field with a dielectric constant particular to the solvent of interest. The cavity for PCM is designed from the van der Waals (vdW) radius of each atom of the molecule, typically extending slightly past the radius (~1.2 vdW radius).

The quantum chemical calculations were used to compare the stability of possible complexes formed in the reaction of pertechnetate and sulfide in the presence of an olefinic acid. All ligands investigated were bidentate with sulfur and/or oxygen donors. Technetium complexes had a $Tc^{V}O$ core and two bidentate ligands chelating the technetium atom, giving the complex an overall -1 charge. The bidentate ligands and complexes optimized are shown in Figure 2-1. The bidentate ligands were optimized at several different starting geometries to find the lowest energy structure. Figure 2-2 gives an example of the angles that were used in the bidentate ligand optimization. The hydrogen positions for the bidentate ligands were altered for both X and Y; the bottom structures in Figure 2-2 are showing only a representation of the possibilities when the Y-H bond is held constant. Several starting arrangements were considered for the metal complexes as well. The geometry around the metal center for the metal complexes was either square pyramidal or trigonal bipyramdal (Figure 2-3).

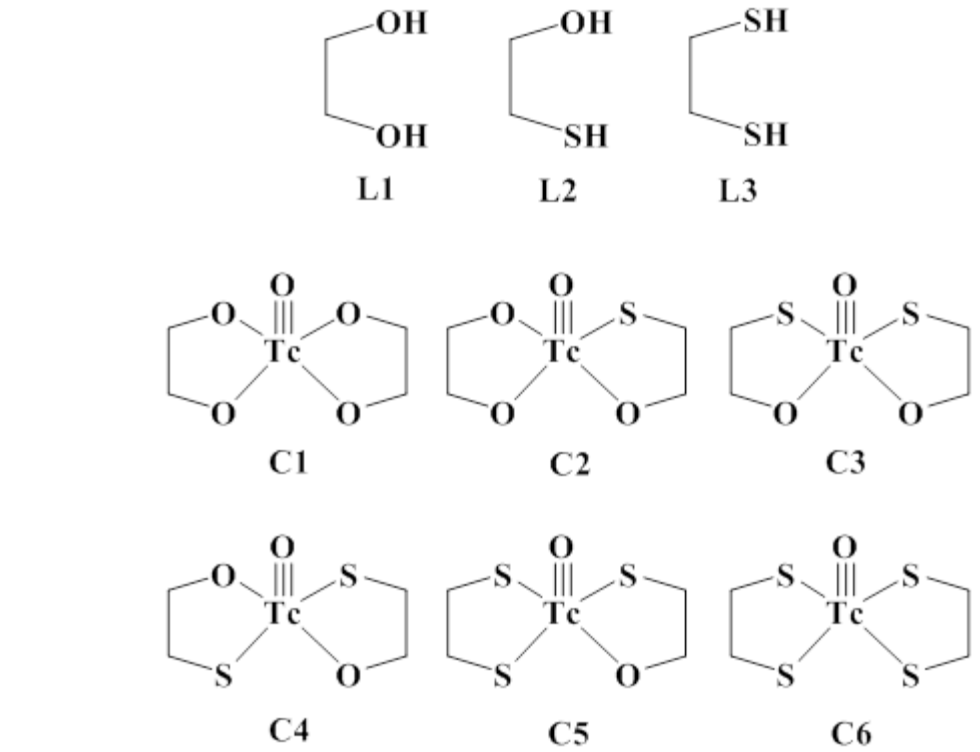

Figure 2-1. Structures of the bidentate ligands and Tc-complexes optimized for computational studies.

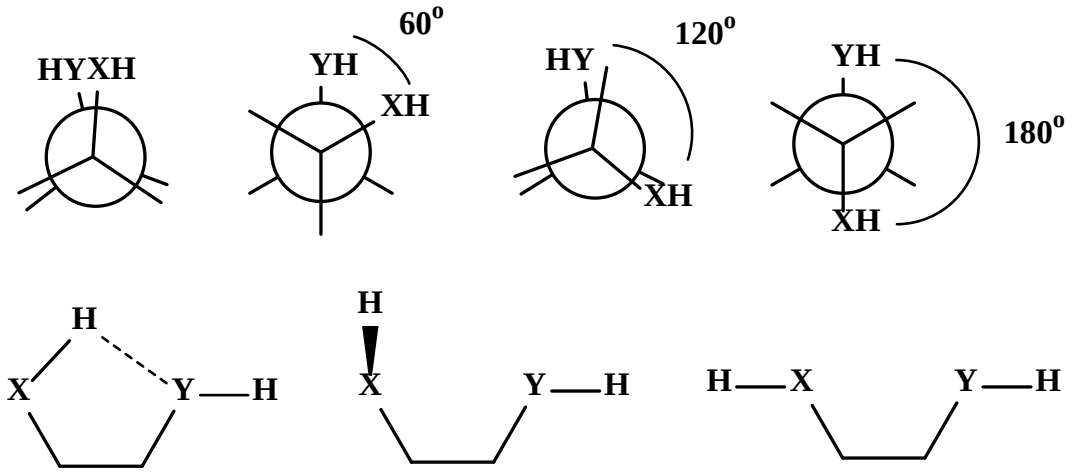

Figure 2-2. Examples of different starting geometries optimized for the bidentate ligands, where X = O or S and Y = O or S.

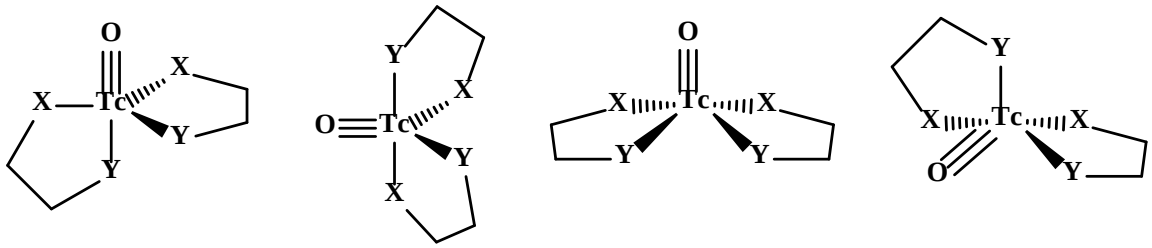

Figure 2-3. Geometries optimized for the metal complexes, where X = O or S and Y = O or S.

In order to compare complexes (C1-C6) to each other, a homodesmotic equation was developed. A homodesmotic equation must have the same number and types of bonds, the same hybridization around each atom, and an equal number of groups containing the same number of hydrogens.[31] This allows for optimal cancellation of errors. To balance the equations, optimizations of CH_3OH, CH_3SH, $[TcO(OCH_3)_4]^-$, $[TcO(OCH_3)_3(SCH_3)]^-$, $[TcO(OCH_3)_2(SCH_3)_2]^-$, $[TcO(OCH_3)(SCH_3)_3]^-$, and $[TcO(SCH_3)_4]^-$ were included. These species were optimized using the same computational model as the ligands and complexes. The homodesmotic equation used to investigate the stability between C1 and C6 is shown in Equation 2-1.

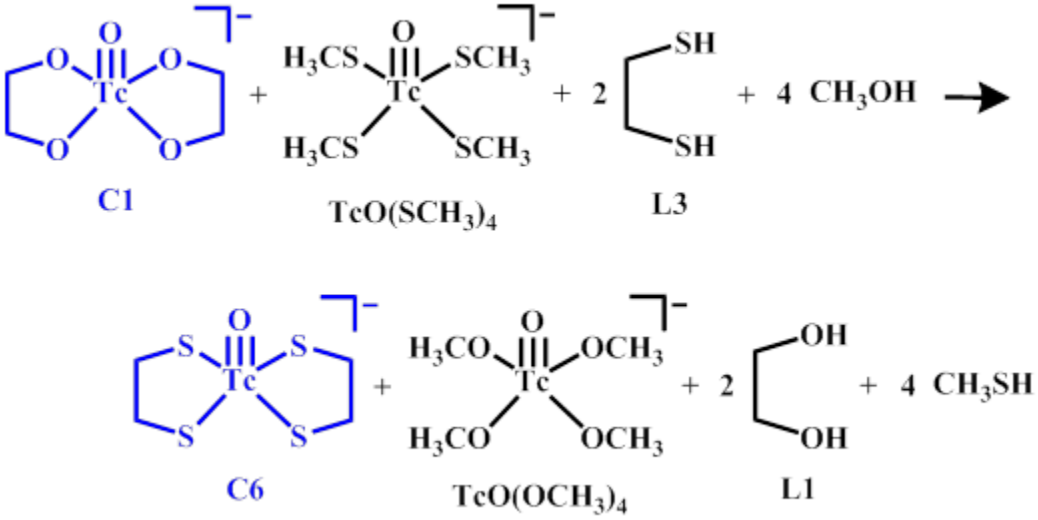

Equation 2-1. Homodesmotic equation used to compare C1 to C6.

2.3 Results and Discussion

Humic and fulvic substances account for a large amount of the organic material present in soils. These acids are complex structures that form as a result of the degradation of dead organic matter. Since humic and fulvic acids contain carboxylate groups, as well as other potentially reactive sites, they pose a risk to remediation methods used to immobilize radioactivity in the environment due to their ability to potentially chelate metals.[32,33] To model this possible interference, low molecular weight organic acids (LMWOA) have been used to investigate any potential reactions.[27] Past work has shown that certain olefinic acids interfere with the use of sulfide to immobilize pertechnetate.[27] When adding a solution of sodium sulfide to a solution with a LMWOA, alkenes specifically, no reaction occurs. However, when pertechnetate is added to this solution, a dark brown-black mixture forms. Colloids appear to be present in the mixture, but they do not separate from the solution as they do when no LMWOA is present.[24] In the absence of the LMWOA, pertechnetate reacts with the sulfide to form Tc_2S_7 (Equation 2-2).[24] The Tc_2S_7 precipitates and is easily separated from solution.

$$TcO_4^- + 7HS^- + H_2O \leftrightarrow Tc_2S_7 + 9OH^- \quad \textbf{(2-2)}$$

One possible interaction that could occur is bisulfide (SH^-) reacts across the double bond of the olefinic LMWOA present. This would result in the reduction of the alkene double bond and the addition of one or two mercaptan groups. Also, with SH^- present, Tc(VII) can easily be reduced to Tc(V) and chelated by the mercapto-acid ligands. A scheme for this process is shown in Figure 2-4.

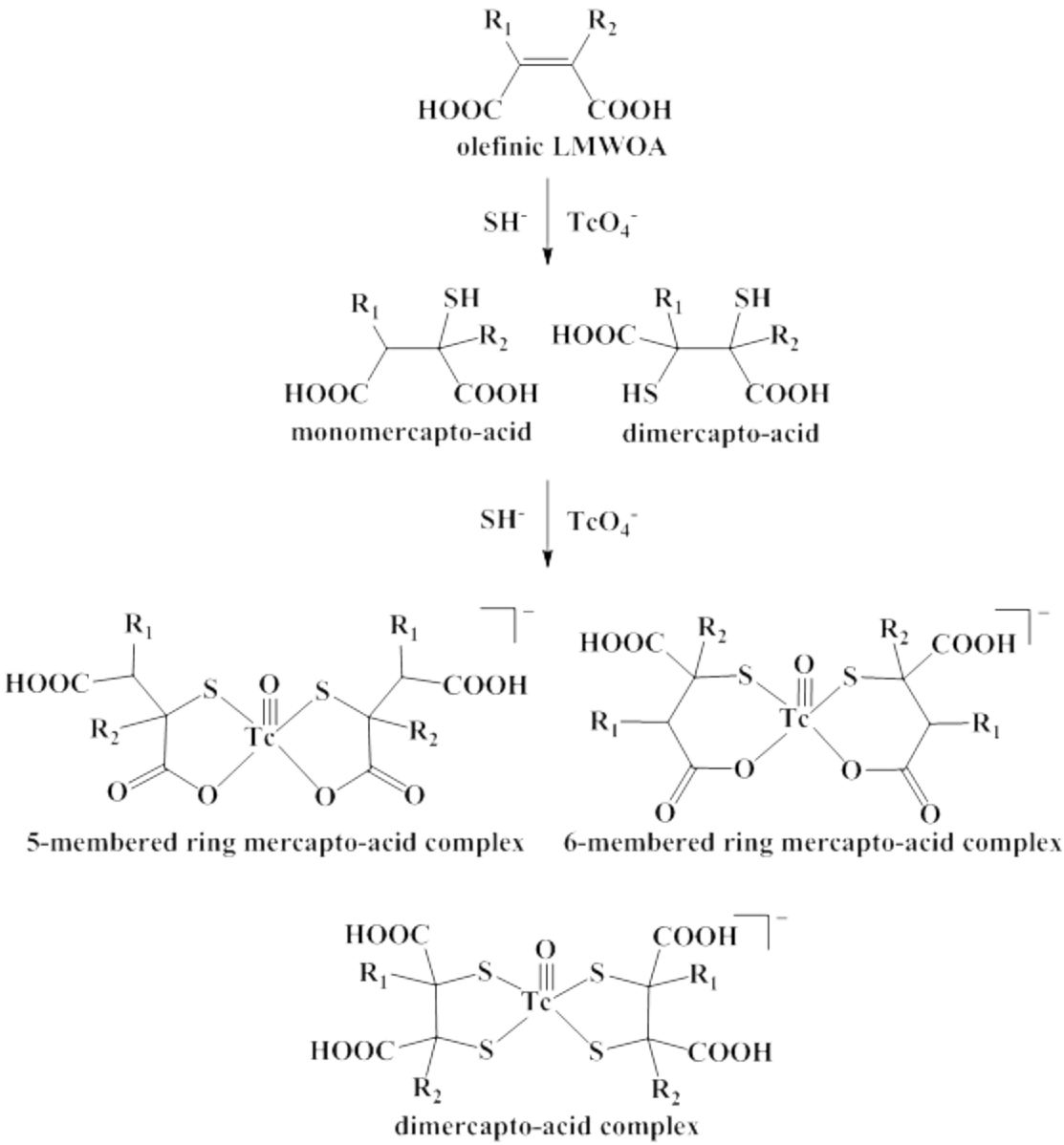

Figure 2-4. Scheme showing the predicted reaction involving the olefinic acid interference with Tc_2S_7 formation.

Reactions for this work were run with maleic, fumaric, crotonic and citraconic acid. Each olefinic LMWOA was evaluated at pH 4, 7, and 9 under both aerobic and anaerobic conditions. Table 2-1 depicts each experiment along with the abbreviation used to distinguish each set of conditions. No significant differences were observed when comparing the aerobic and anaerobic experiments, indicating the reactions proceeded in both the presence and absence of oxygen. All the LMWOA reactions

formed brown solutions under all pH conditions except citraconic acid, which only interfered with Tc_2S_7 formation at pH 4.

Table 2-1. Interference reactions including pH conditions and abbreviations.

Basic Experiment	Acid Structure	pH	Abbreviated Name
Fumaric + TcO_4^- + SH^-	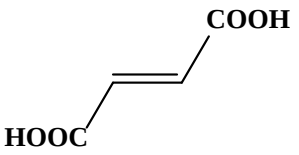	4	FUM4
		7	FUM7
		9	FUM9
Maleic + TcO_4^- + SH^-	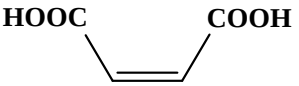	4	MAL4
		7	MAL7
		9	MAL9
Crotonic + TcO_4^- + SH^-	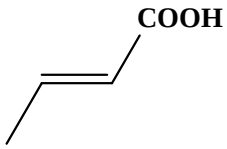	4	CRO4
		7	CRO7
		9	CRO9
Citraconic + TcO_4^- + SH^-	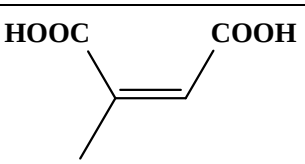	4	CIT4
		7	CIT7
		9	CIT9

When the reactions were run with maleic, fumaric, crotonic acid, or CIT4, an orange or brown compound was isolated by C_{18} silica gel column chromatography. The orange species was also isolated by adding an equal volume of acetone to the crude reaction mixture, with the orange/brown species extracted into the organic layer. TLC saturation pads with 50% H_2O in acetone were used to identify species by comparison to the reference Tc-mercaptan products. In this mobile phase, Tc colloids remained at the origin, pertechnetate had an R_f of 1, and the Tc-mercaptan complexes had an R_f between 0.3 and 0.8. Monomercapto-acid complexes had R_f values around 0.7-0.8, and the dimercapto-acid complexes had R_f values around 0.25-0.35.

2.3.1 NMR Analysis

Several NMR spectroscopic methods were used to identify the products formed in these reactions. The various experiments included: ^{1}H and ^{13}C NMR, ^{13}C DEPT 90, ^{13}C DEPT 135, HSQC, HMBC, and COSY. DEPT (**d**istortionless **e**nhancement by **p**olarization **t**ransfer) NMR is used to distinguish between CH, CH_2, and CH_3. HSQC (**h**eteronuclear **s**ingle **q**uantum **c**oherence) and HMBC (**h**eteronuclear **m**ultiple-**b**ond **c**orrelation) are 2D NMR experiments that show correlations between the protons and carbons on the complex. Lastly, COSY (**co**rrelation **s**pectroscop**y**) NMR demonstrates proton-proton interactions between three bonds.

2.3.1.1 Tc-Fumaric Acid and Tc-Maleic Acid Reactions

The reaction schemes for these products are shown in Figures 2-5 and 2-6. Figure 2-5 shows the likely complexes produced if the monomercapto acid is formed, and Figure 2-6 shows the complexes formed if a dimercapto acid is formed. The monomercapto acid ligand formed from fumaric or maleic acid is mercaptosuccinic acid (H_3MSA), and the dimercapto acid is dimercaptosuccinic acid (H_4DMSA). H_4DMSA has two stereocenters resulting in the possibility of three stereoisomers. Two of the stereoisomers, *2R,3R*-H_4DMSA and *2S,3S*-H_4DMSA, are enantiomers and would form identical Tc-complexes, therefore only one is shown in the Figure 2-6 (*dl*- H_4DMSA), but both forms are likely to form in the reaction. The third stereoisomer is the *meso* form.

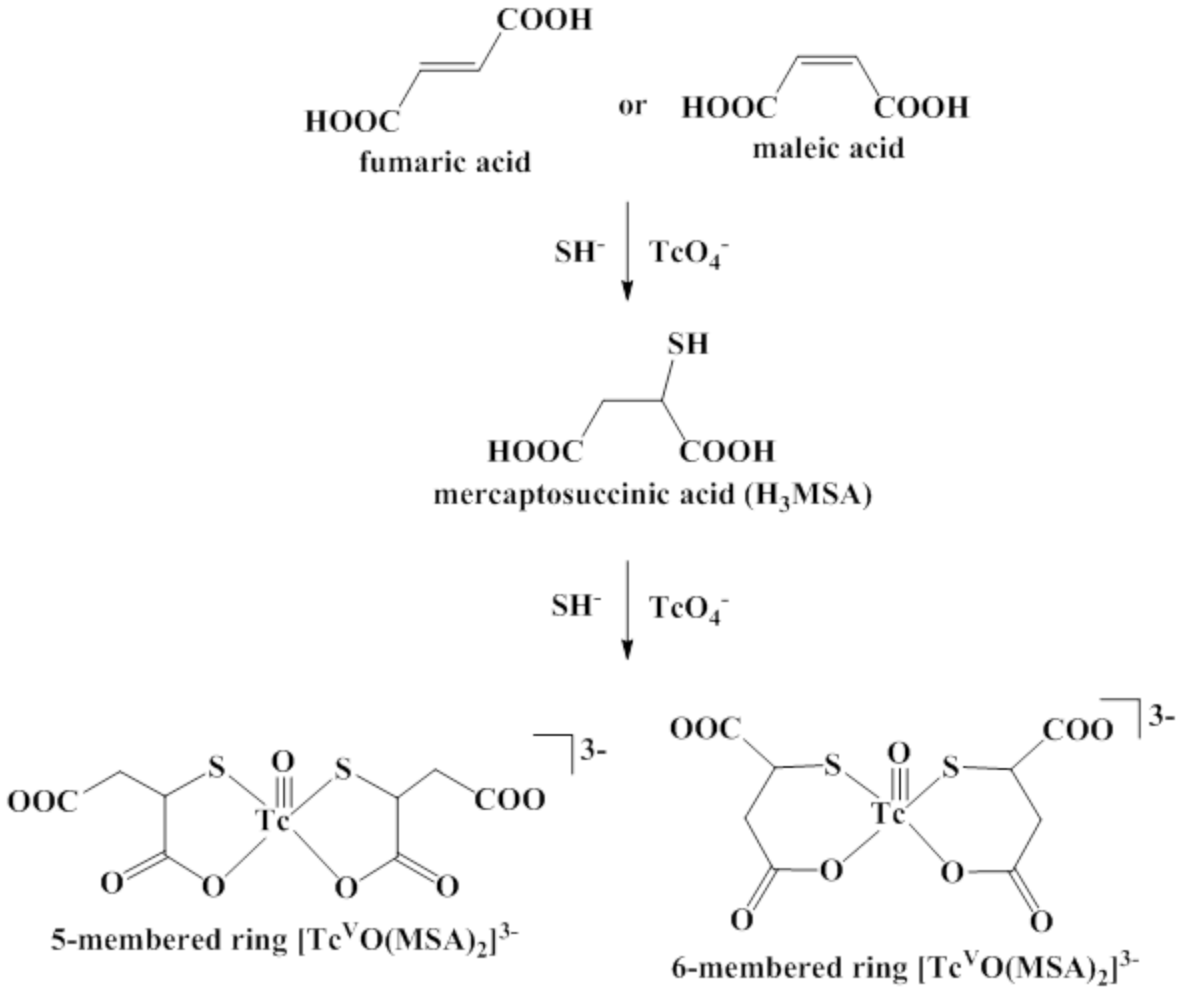

Figure 2-5. Reaction scheme for mono-mercapto products formed in the fumaric or maleic acid reactions.

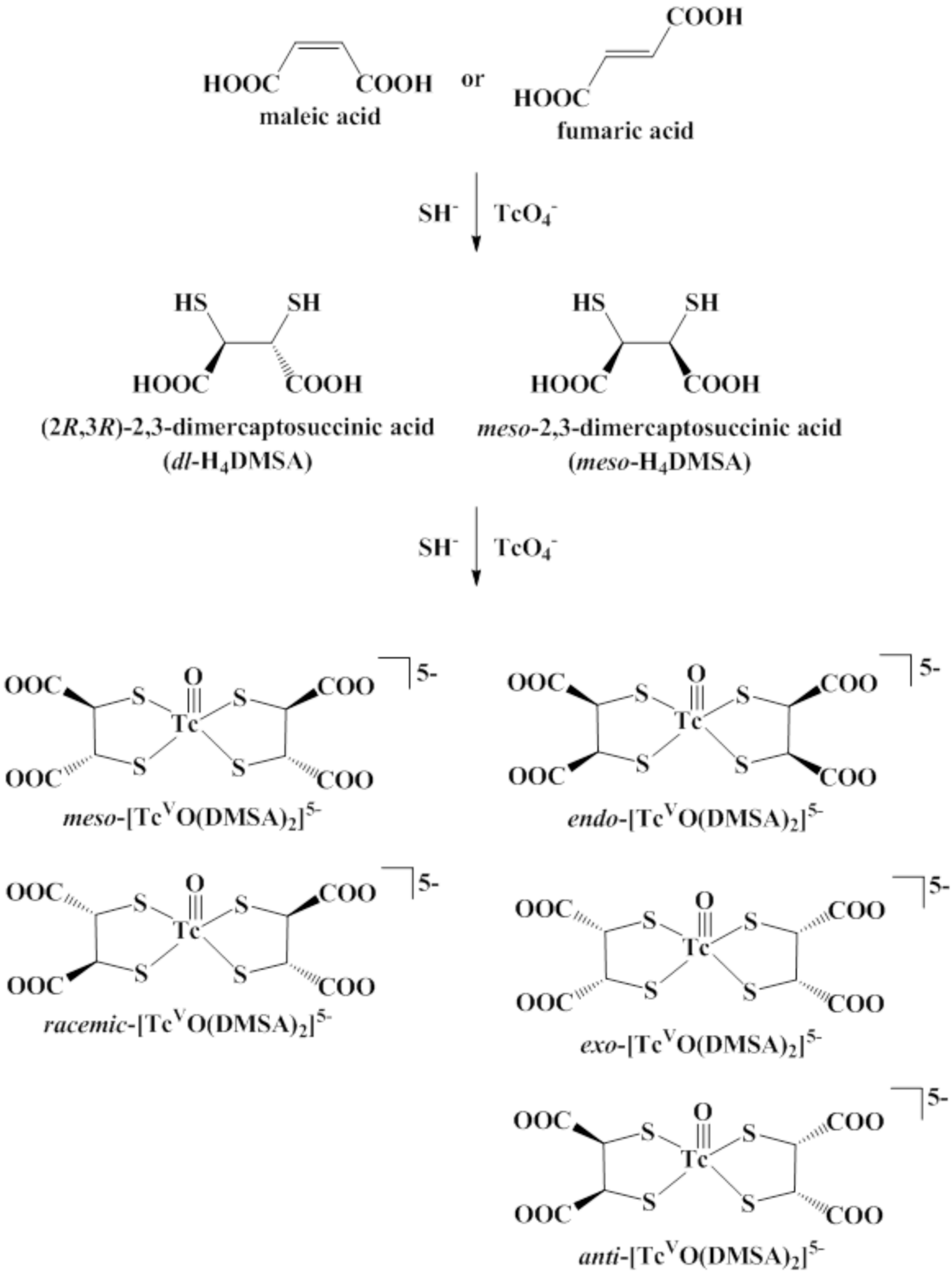

Figure 2-6. Reaction scheme for di-mercapto products formed in the fumaric and maleic reactions.

For the fumaric and maleic acid reactions, NMR spectra show that $[Tc^{V}O(DMSA)_2]^{5-}$ is favored at pH 9, and $[Tc^{V}O(MSA)_2]^{3-}$ is favored at pH 4. The NMR spectra of FUM4 and MAL4 (Table 2-1) show the formation of $[Tc^{V}O(MSA)_2]^{3-}$. The ^{13}C DEPT 135 shows two CH carbons and two CH_2 carbons, indicating that the MSA is coordinated in such a way that places the carbons in slightly different environments (Figure 2-7). Figure 2-8 shows the comparison between ^{1}H NMR of the FUM4 reaction to the standard Tc-MSA reaction (briefly, $TcO_4^- + H_3MSA + Sn^{2+}$) and H_3MSA.

Interestingly, the $[Tc^{V}O(MSA)_2]^{3-}$ complex was formed at both pH 4 and pH 7, but the structures were slightly different by NMR analysis. FUM4 showed a much more complicated splitting pattern for both the -CH- and the $-CH_2-$ protons, indicating that the methylene group was most likely locked in a more rigid structure with its protons experiencing two distinctly different environments. In order for this to occur the MSA molecule would likely coordinate through the mercapto group and the carboxylate group furthest from it (C_4 carboxylate), forming a 6-membered ring with the Tc.

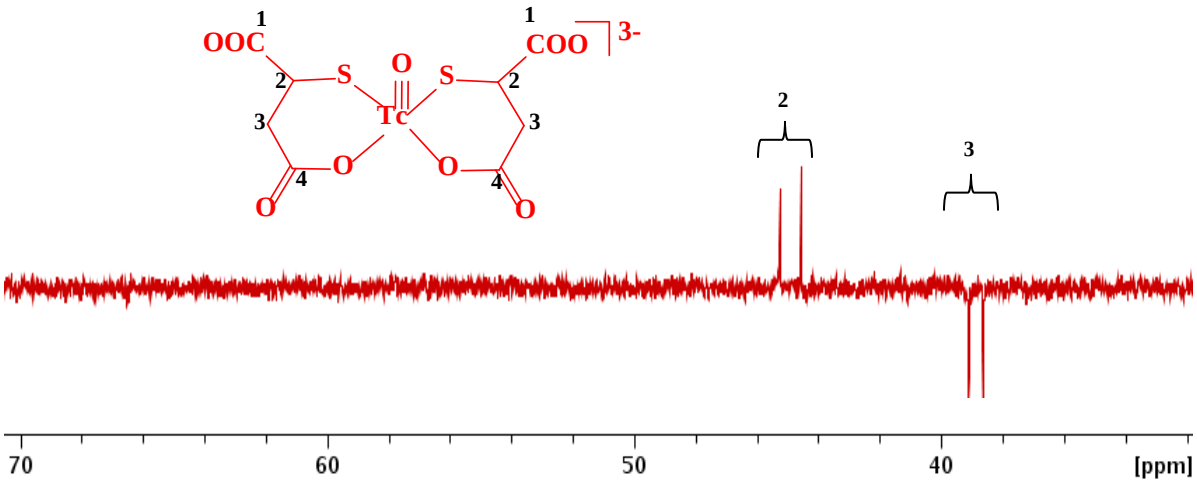

Figure 2-7. ^{13}C DEPT135 NMR spectrum of FUM4. Solvent is D_2O.

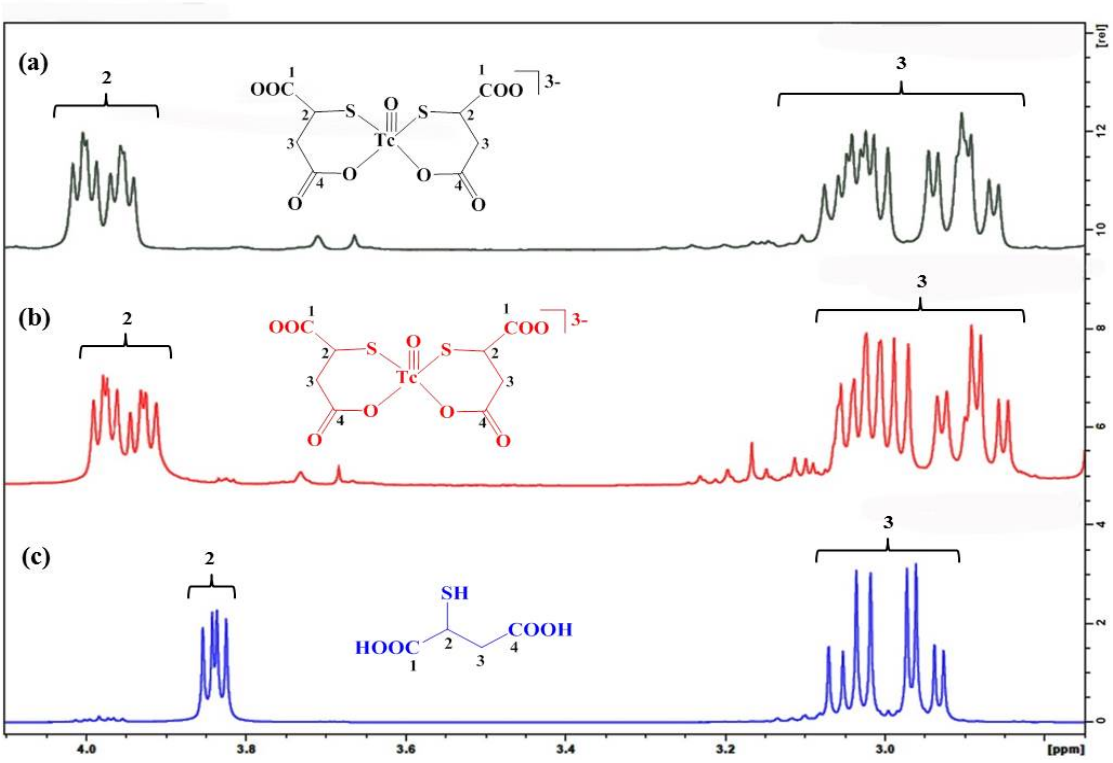

Figure 2-8. ^{1}H NMR of (a) FUM4, (b) MSA + Sn^{2+} + TcO_4^-, and (c) MSA ligand. All NMR spectra were run in D_2O.

FUM4, but the chemical shifts are in similar regions just slightly shifted upfield. This could indicate that the ligand has more free rotation, which can be achieved by forming a 5-membered ring with Tc (Figure 2-9).

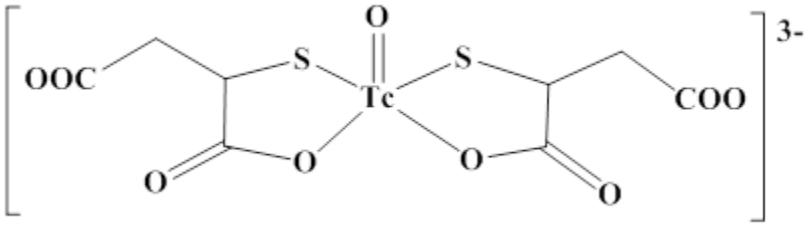

Figure 2-9. Structure of $[Tc^{V}O(MSA)_2]^{3-}$ in 5-membered ring formation.

FUM9 formed the $[Tc^{V}O(DMSA)_2]^{5-}$ complex. Any MSA formed in the reaction was not coordinated to Tc. The Tc-DMSA complexes can form several different isomers because the DMSA ligand can be in either the *meso* or *dl* form. Figure 2-6 shows the possible options. The ^{1}H NMR spectra of these complexes show splitting patterns

indicating that the protons are not equivalent. The coupling constants of these signals are also similar to those reported in the literature.[34] The ^{13}C DEPT 90 shows that all the carbons for the complex are CHs. Figure 2-10 compares the ^{13}C DEPT 135 of FUM4 and FUM9.

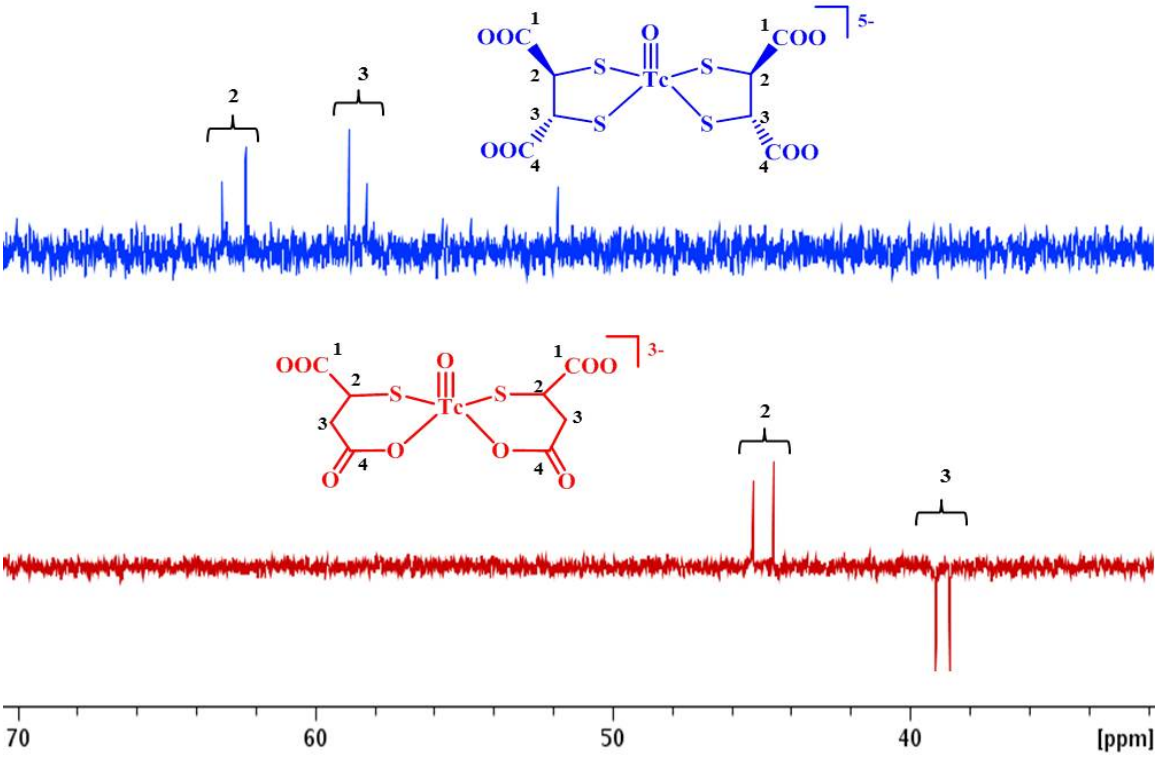

Figure 2-10. ^{13}C-DEPT135 for FUM9 (top, blue) and FUM4 (bottom, red).

The maleic acid reactions presented very similar results to the fumaric acid reactions. Similarly to FUM4 and FUM7, the NMR spectra of MAL4 and MAL7 indicated the presence of the bound MSA product, $[Tc^{V}O(MSA)_2]^{3-}$. Both the ^{1}H and ^{13}C NMR spectra show similar chemical shifts and splitting patterns to those observed for FUM4 and FUM7. The pH 9 reactions gave similar results as well when comparing FUM9 and MAL9.

2.3.1.3 Tc-Crotonic Acid Reactions

The crotonic acid reactions had more complicated NMR spectra. With maleic and fumaric acid, the di-carboxylic acids offered more symmetry throughout the reaction, limiting the possible structures. In Figure 2-11, a scheme is shown for the mono-mercapto products of the crotonic acid reaction. This scheme ignores the stereochemistry of the chiral atom, which would increase the structure possibilities.

For the di-mercapto products (Figure 2-12), the stereochemistry becomes even more important. With the maleic and fumaric acid reactions, there were two stereocenters, but the substituents on each chiral carbon were the same. The crotonic acid reactions do not have this same ligand symmetry creating more possibilities when complexed to Tc. More specifically, for the maleic and fumaric reaction ligands (MSA and DMSA), the only substituents that could be *syn* or *anti* to the Tc≡O bond were carboxylate groups. With the crotonic acid reactions, the complexes will have a carboxylate and a methyl group, either of which can be *syn* or *anti* to the Tc≡O.

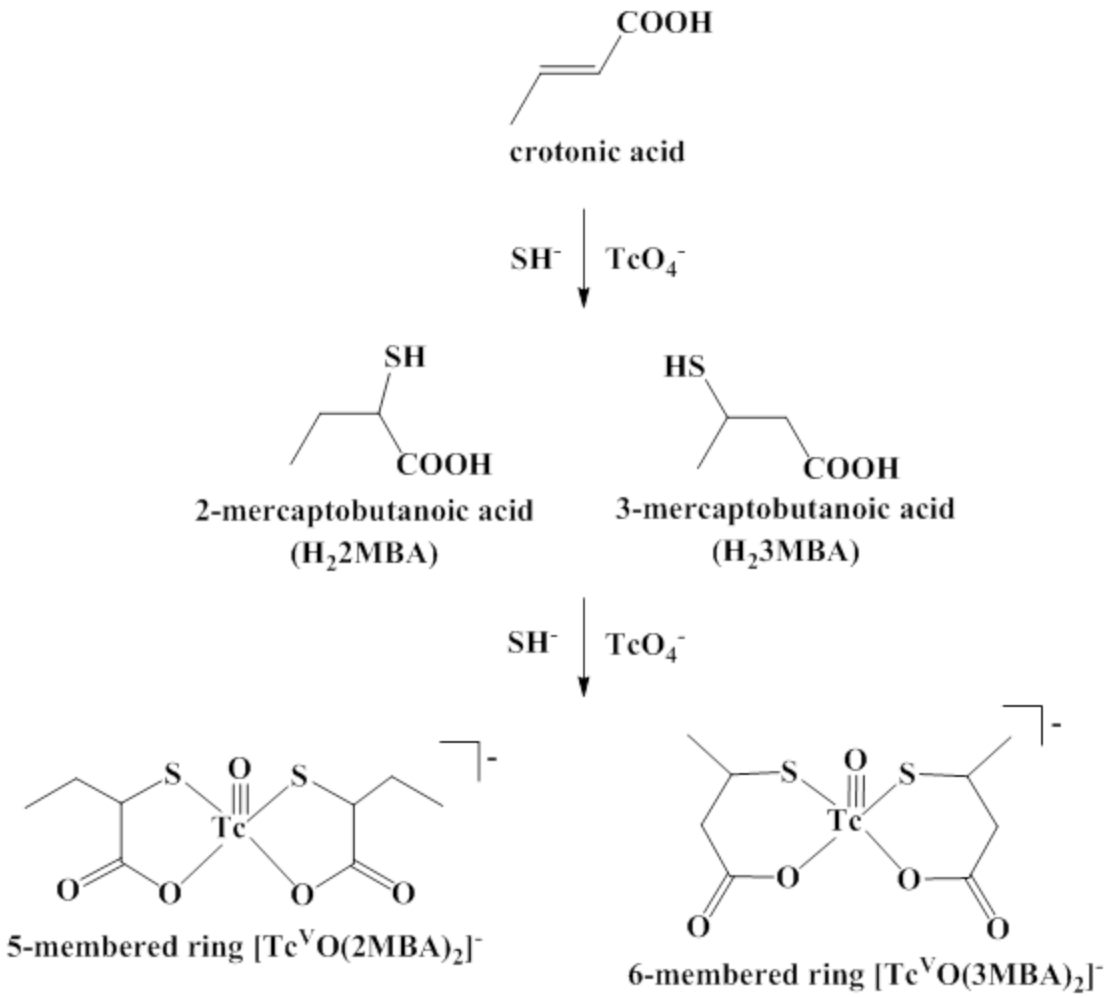

Figure 2-11. Reaction scheme for mono-mercapto products formed in the crotonic acid reactions.

The CRO4 reaction showed one major product. The ^{1}H NMR spectrum showed a doublet in the aliphatic region at 1.3 ppm for the methyl group (C_4 in Figure 2-13) . The signal is shifted upfield of the starting material (crotonic acid, 1.7 ppm in D_2O) indicating that the double bond has been reduced. Also, since the signal is split into a doublet (Figure 2-14, left axis). This indicates that C_4 is only interacting with one other neighboring proton, as shown in the 6-membered ring $[Tc^{V}O(3MBA)_2]^-$ (Figure 2-13 right). The COSY NMR spectrum (Figure 2-14) shows this proton is coupled with the proton corresponding to the 4.2 ppm signal. This 4.2 ppm signal, a multiplet, accounts for two separate proton signals (i.e., overlapping signals). The carbon signals for the 4.2

ppm proton signals are at 68 and 74 ppm. These peak positions are also indicative of double bond reduction.

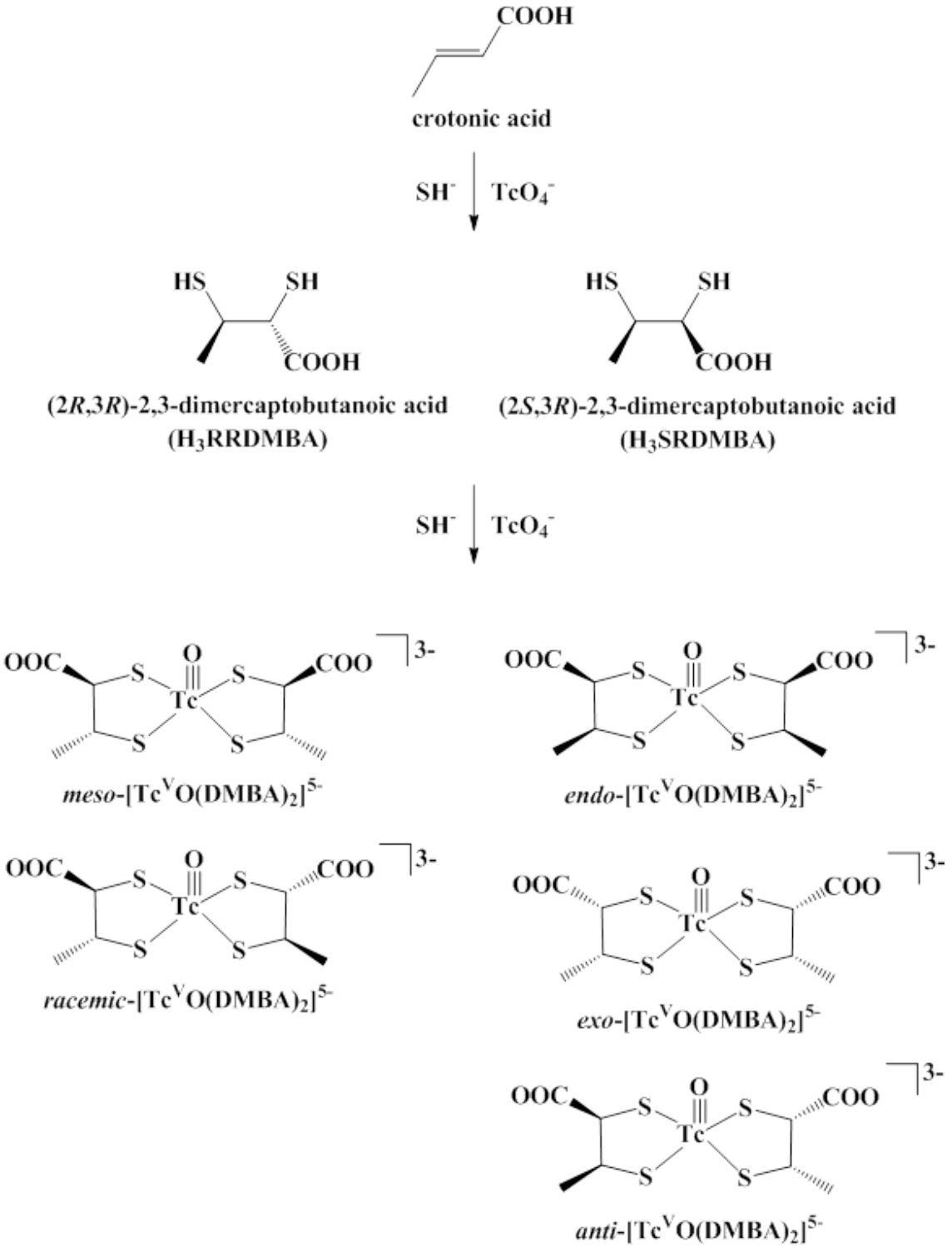

Figure 2-12. Reaction scheme for di-mercapto products formed in the crotonic acid reactions.

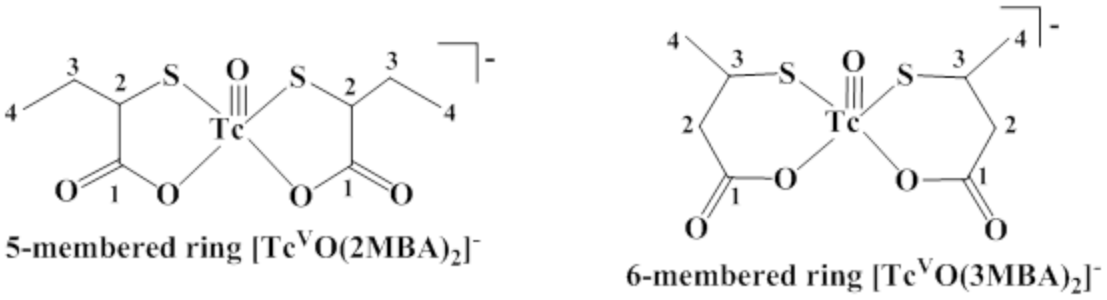

Figure 2-13. Structures of the mono-mercapto products from the crotonic acid reaction.

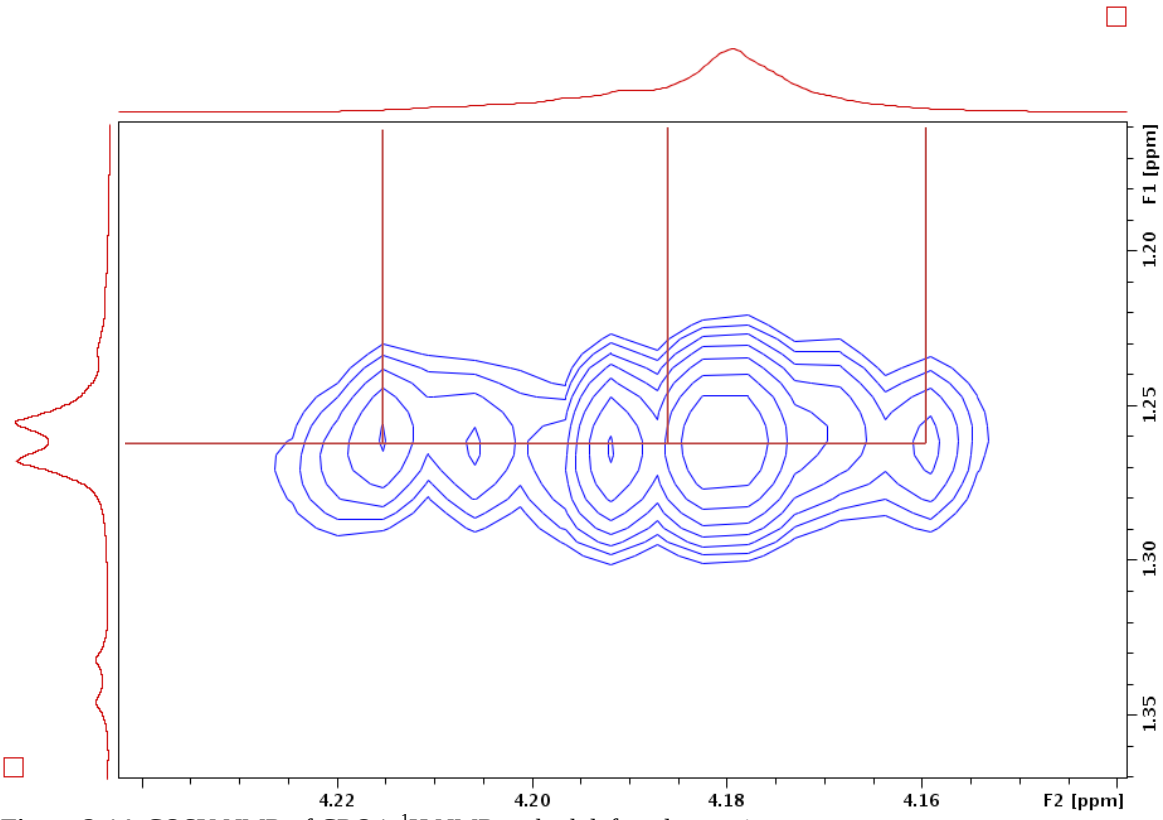

Figure 2-14. COSY NMR of CRO4, ^{1}H NMR on both left and top axis.

The CRO7 reaction showed more products than the CRO4 reaction. The aliphatic region of the ^{1}H NMR spectrum of CRO7 is shown in Figure 2-15. This section shows several different doublets. The methyl group protons of crotonic acid (C_4 protons of Figure 2-16) form a doublet as well, but the signal is observed downfield at ~1.7 ppm (in D_2O) due to the double bound. Additionally, the neighboring carbon to the methyl group of crotonic acid (C_3 of Figure 2-16) has a ^{13}C signal at 128 ppm. The signals shown in

Figure 2-15 from the CRO7 reaction correspond to carbon signals in the 40-60 ppm range, which can be seen in the HMBC NMR spectrum shown in Figure 2-17.

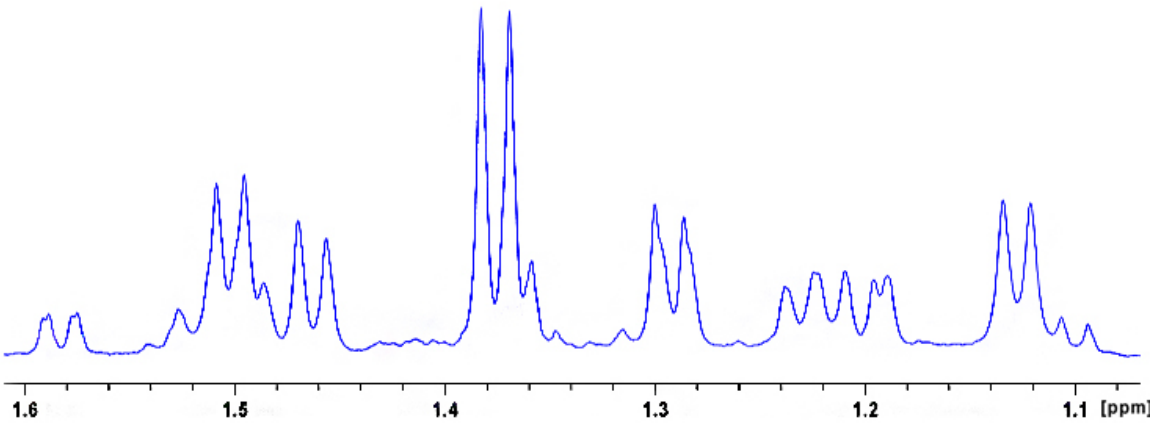

Figure 2-15. ^{1}H NMR spectrum for CRO7 showing aliphatic region.

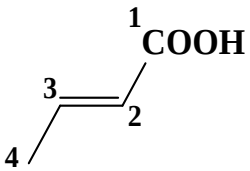

Figure 2-16. Structure of crotonic acid.

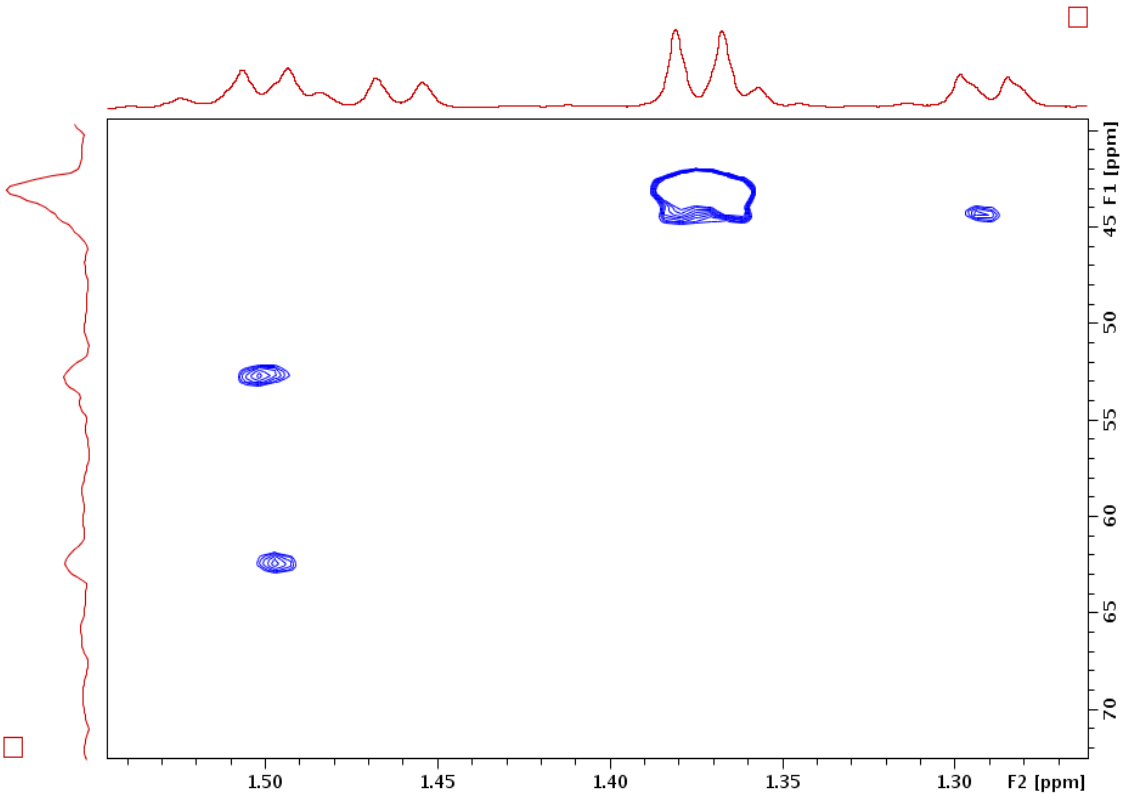

Figure 2-17. HMBC NMR spectrum of CRO7 showing the carbon signals corresponding to the aliphatic proton signals. ^{1}H NMR of CRO7 on top axis, internal HMBC NMR on left axis.

Like CRO7, CRO9 showed several methyl signals, some of which are seen in both the CRO7 and CRO9 spectra (Figure 2-18). Comparing the ^{1}H NMR spectra of CRO7 and CRO9, we can see that there are at least five methyl peaks in common in both. Each spectrum has different intensities of these peaks indicating that different complexes are favored under the different pH conditions. The COSY NMR spectrum of CRO9 (Figure 2-19) shows that these methyl protons are coupling with neighboring protons (C**H** or C**H**$_2$) with chemical shifts in the 3.5-4 ppm range. This is comparable to the fumaric/maleic acid reactions.

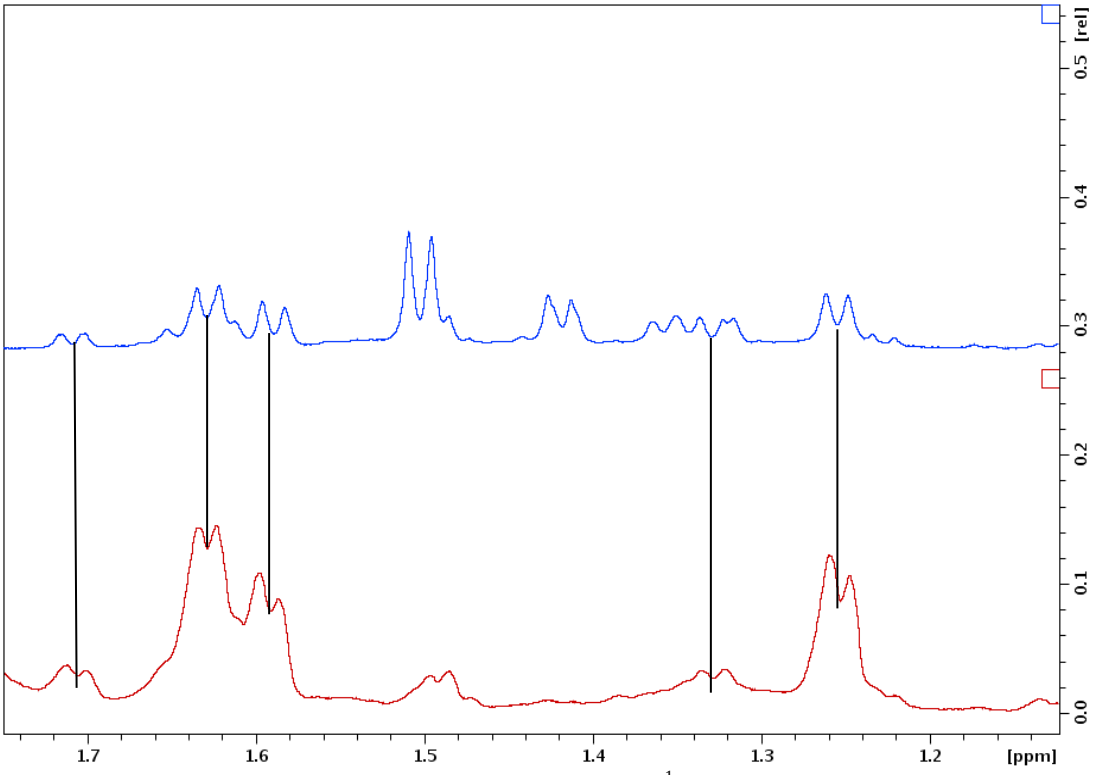

Figure 2-18. Comparison of CRO7 (top) and CRO9 (bottom) ^{1}H NMR.

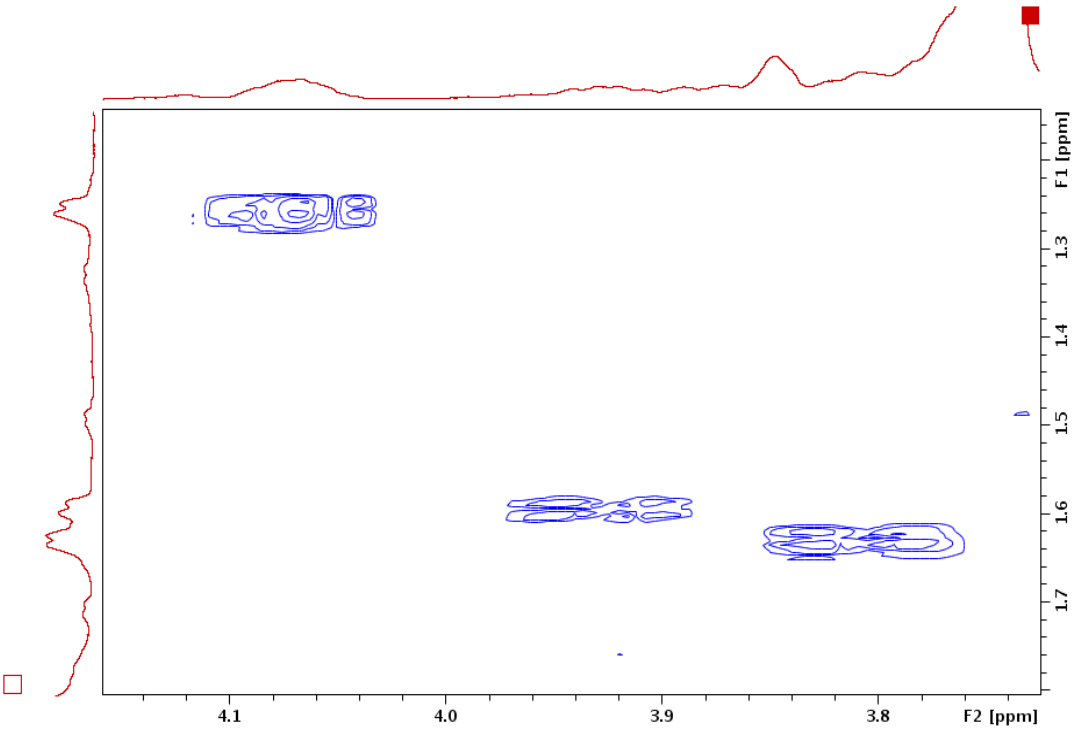

Figure 2-19. COSY NMR spectrum of CRO9 showing the coupling signals of neighboring protons. ^{1}H NMR of CRO9 on top and left axis.

2.3.1.4 Tc-Citraconic Acid Reactions

CIT7 and CIT9 did not yield enough material after separation to obtain an NMR spectrum. The majority of the product with these reactions was reduced Tc, most likely Tc_2S_7 or TcO_2, and was not soluble in water.

The CIT4 NMR spectrum showed evidence of a dithiol complex, where 2,3-dimercapto-2-methylsuccinic acid (DMMS) chelated Tc; the reaction scheme for these products is shown in Figure 2-20. The ^{1}H NMR spectrum showed two singlets at 1.34 ppm (CH_3) and 4.46 ppm (CH). The ^{13}C NMR signals corresponding to these proton signals are observed at 22.3 ppm and 73.5 ppm, respectively. The HMBC NMR spectrum shows two distinct carboxylate groups. The carboxylate bound to the same carbon as the methyl group is observed at a chemical shift of 178.5 ppm, while the other carboxylate group is observed at 173.4 ppm.

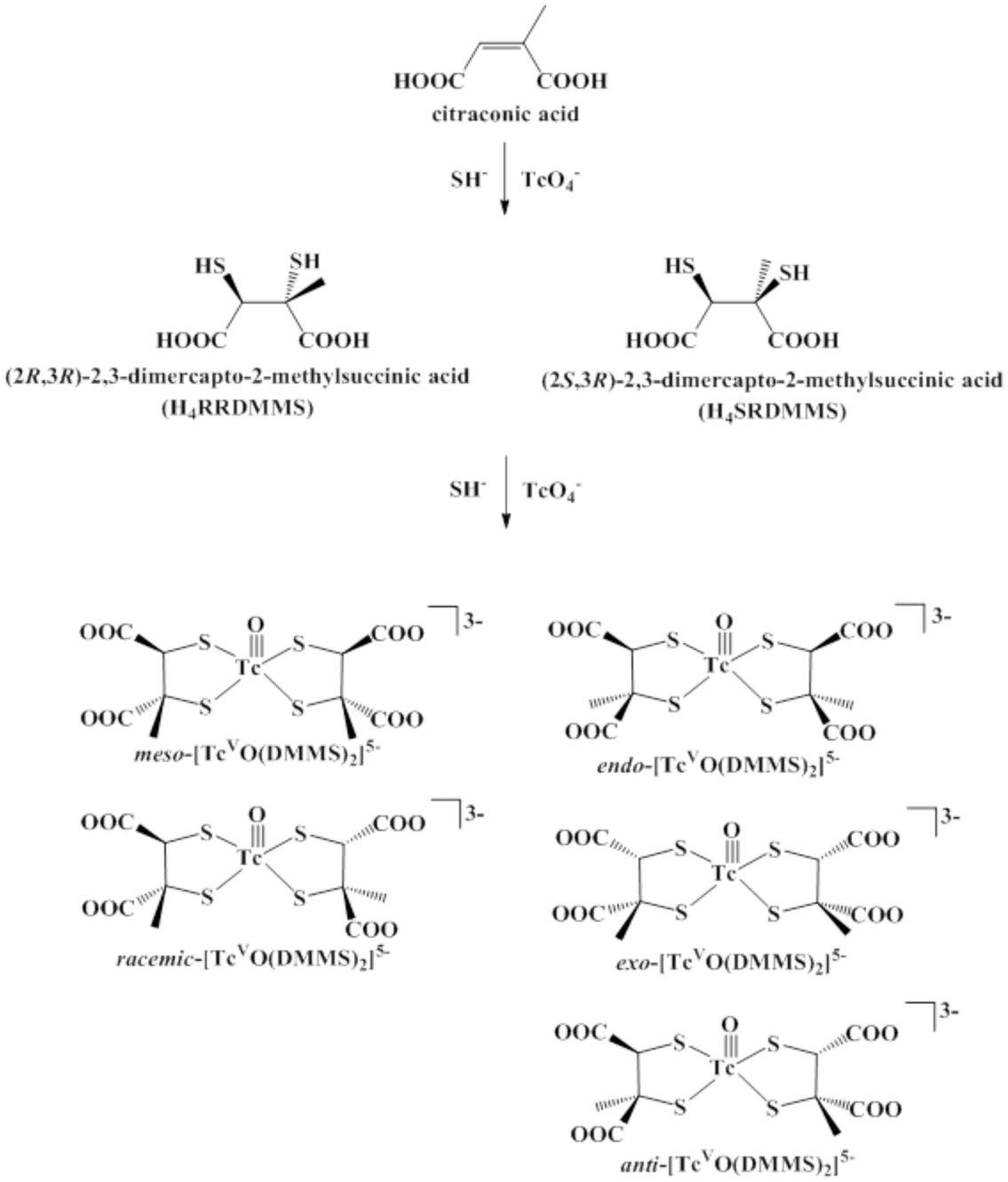

Figure 2-20. Reaction scheme for di-mercapto products formed in the citraconic acid reactions.

2.3.2 XAS Analysis

X-ray absorption spectroscopy (XAS) can be very useful in identifying nearest neighbor atoms and bond lengths. XAS was used to characterize some of the water soluble products generated from the Tc-sulfide-LMWOA reactions. These reactions were compared to a standard of $[TcO(DMSA)_2]^{5-}$. The $[TcO(DMSA)_2]^{5-}$ complex was made as

detailed in the experimental section and verified by NMR. In addition to the standard DMSA complex, both MAL9 and FUM7 reactions were analyzed.

MAL9 shows characteristics similar to the $[TcO(DMSA)_2]^{5-}$ standard that was run. Both show a Tc≡O length of 1.7 Å, as well as four Tc-S bonds with lengths at 2.3 Å. These lengths are consistent with the bond lengths observed computationally, with lengths of 1.67 Å (Tc≡O) and 2.33 Å (Tc-S). Bond lengths and their associated errors are depicted in Table 2-2. Figure 2-21 shows the k^2-weighted χ(k) data for MAL9 compared to the expected fit. Figure 2-22 shows the corresponding, uncorrected χ(R) data for MAL9.

Table 2-2. XAS data for $[TcO(DMSA)_2]^{5-}$ standard and MAL9 sample.

$[TcO(DMSA)_2]^{5-}$					
Path	N	R_{eff}	E_0	ΔR	σ^2
Tc≡O	1	1.7 ± 0.3	2.66 ± 1.1	0.01 ± 0.02	0.004 ± 0.003
Tc-S	4	2.3 ± 0.3	2.66 ± 1.1	0.03 ± 0.02	0.002 ± 0.001
MAL9					
Path	N	R_{eff}	E_0	ΔR	σ^2
Tc≡O	1	1.7 ± 0.2	-1.3 ± 1.5	-1.3 ± 1.5	0.001 ± 0.001
Tc-S	4	2.3 ± 0.4	-1.3 ± 1.5	-1.3 ± 1.5	0.004 ± 0.001

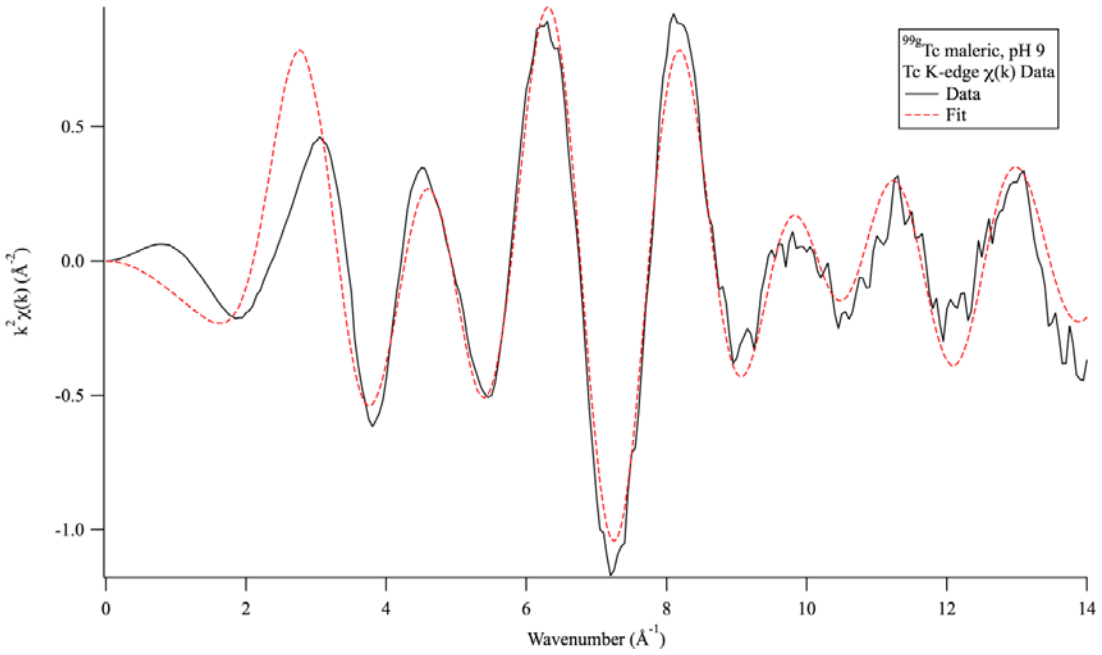

Figure 2-21. Tc K-edge k^2 weighted EXAFS spectra for MAL9.

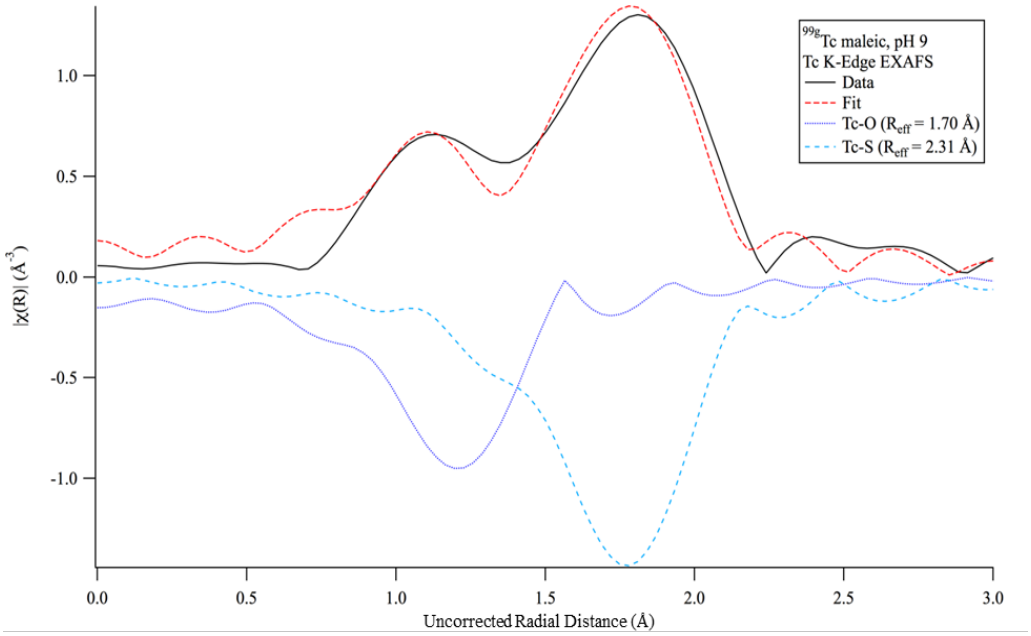

Figure 2-22. Tc K-edge χ(R) function for MAL9.

2.3.3 Computational Studies

Computational studies were performed to investigate which ligand system is more thermodynamically favorable. The computational models used for this study were evaluated extensively for small oxorhenium and oxotechnetium compounds in previous work.[35] To simplify the optimizations, modified ligands, L1, L2, and L3 (shown in Table 2-3), were used. These ligands and the resulting complexes were representative of the experimental work done here.

At the optimization level (MBS1), different starting orientations were attempted for both the ligands and the complexes (Figure 2-2 and 2-3) to find the lowest energy structure. Several starting structures rearranged to more stable geometries. The lowest energy structures for the ligands are shown in Figure 2-23. **L1** has an O-C-C-O dihedral angle of 59º and a hydrogen bond to an oxygen that is 2.2 Å. The lowest energy structure for **L2** varied depending on the phase. In the gas phase calculations, the structure of **L2**

had an O-C-C-S dihedral angle of 59º, similar to the **L1** structure. However, in the solvent phase, the lowest energy structure had an O-C-C-S dihedral angle of 175º, which inhibited any hydrogen bonding. Finally, the **L3** was very similar to the gas phase **L2** structure. The S-C-C-S dihedral angle is slightly larger at 66º.

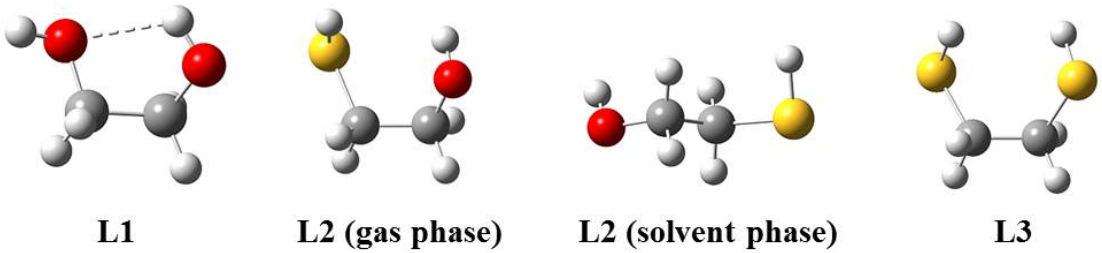

Figure 2-23. Lowest energy structures of ligands **L1**, **L2**, and **L3**. Color scheme: H-white, C-grey, O-red, and S-yellow.

The lowest energy structures for the complexes **C1**, **C2**, **C3**, **C5** and **C6** are shown in Figure 2-24. **C4** has been excluded because it is significantly less stable than **C3**. All of these structures have similar features. Each structure has a square pyramidal geometry around the metal center. This was similar to the results obtained for Re, which is structural analogous to Tc.[36,37] Also, the X-C-C-Y dihedral angles of the coordinating bidentate ligands are similar. The O-C-C-O dihedral ligand is about 41º, the O-C-C-S dihedral angle is about 47º, and the S-C-C-S dihedral angle is about 52º.

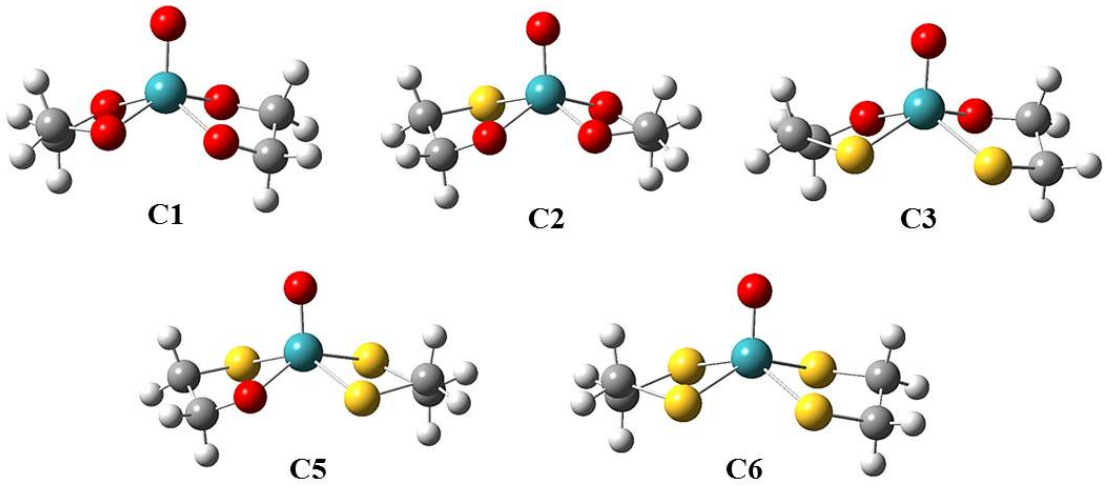

Figure 2-24. Lowest energy structures found for complexes **C1, C2, C3, C5**, and **C6.** Color scheme: H-white, C-grey, O-red, S-yellow and Tc-turquoise.

Crystal structures for $Tc^{V}O$ complexes similar to those used for the computational studies were used to validate the chosen computational model. Root mean square deviation (RMSD) values were generated from the Visual Molecular Dynamics (VMD) program[38] comparing the crystal structure and the optimized computational structure. The RMSD is defined in Equation 2-3, where *N* is the number of atoms whose positions are being compared, $r_{i,calc}$ is the position of atom *i* of the optimized structure and $r_{i,cif}$ is the position of atom *i* of the crystal structure.

$$RMSD = \sqrt{\frac{\sum_{i=1}^{N}(r_{i,calc} - r_{i,cif})^2}{N}} \qquad \textbf{(2-3)}$$

The complexes that were used to calculate RMSD values were C1, C3, C6, and a carbonyl-derivative of C6, abbreviated as C6A. Complexes, structure alignments, and RMSD values are shown in Table 2-3. According to the RMSD calculations, the optimized structures agree well with the published crystal structures. In other words, the computational model chosen for these complexes agrees well with the structural data published in literature.

Table 2-3. Structures and RMSD values of $Tc^{V}O$ complexes used to validate computational model.

	C1	C3	C6	C6A
Structure[a]	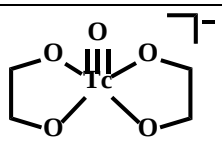	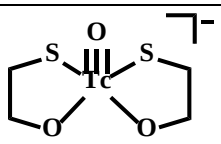	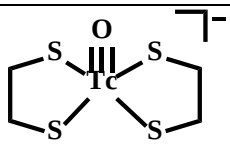	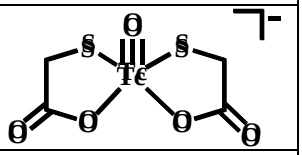
VMD Structure alignment[b]	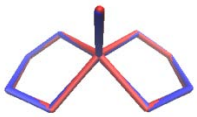	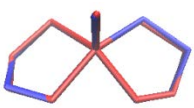	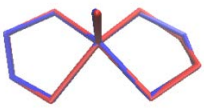	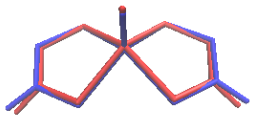
RMSD (Å)	0.047	0.096	0.082	0.195

[a]All complexes have an overall -1 charge.
[b]Crystal structures are in red and computationally optimized structures are in blue. Hydrogens have been removed for clarity.

The change in Gibbs free energy in the homodesmic reactions (ΔG_{rxn}) (example shown in Equation 2-1) was used to determine which ligand systems were favorable. Each ligand system is compared to C1, which has four oxygen donors. Negative ΔG_{rxn} values indicate that the compared ligand system is more favorable than the C1 complex.

The ΔG_{rxn} values were calculated at each level of theory. The results are shown in Table 2-4. The two sets of gas-phase calculations agree very well, indicating that the reaction becomes more favorable as more sulfur donors are added. The solvent phase reactions showed two different results. The energies from the IEF-PCM method showed a similar trend as the gas phase calculations, with the ΔG_{rxn} being slightly less negative for the solvent phase. The SMD model did not show the same trend as the other calculations. For this method, the C1 to C2 reaction showed no significant change in energy. The other reactions (i.e., C1 to C3, C1 to C5, and C1 to C6) strongly favored the sulfur donor ligands and the energies calculated for each reaction were within error of each other.

When looking at the ΔG_{solv} (change in Gibbs free energy of solvation, energy difference between gas phase and solvent phase) for each component, the biggest difference between IEF and SMD occurred for the $[TcO(SCH_3)_x(OCH_3)_{4-x}]^-$ complexes, where x = 2, 3, or 4. Further investigation into this anomaly is underway.

Table 2-4. ΔG_{rxn} at each level of theory (kcal/mol).

	PBE0/MBS1 Gas Phase	PBE0/MBS2//PBE0/MBS1 SPE Gas Phase	PBE0/MBS2//PBE0/MBS1 SPE IEF-PCM water	PBE0/MBS2//PBE0/MBS1 SPE SMD water
C1 to C6	-22.23	-23.74	-14.78	-49.73
C1 to C5	-11.84	-13.52	-7.08	-41.33
C1 to C3	-7.09	-9.54	-5.76	-43.74
C1 to C2	-3.20	-4.57	-2.41	-0.73

[a]PBE0/MBS2 single point energy for PBE0/MBS1 geometry.

2.4 Conclusion and Future Studies

These studies have shown that olefinic acids do interfere with the formation of Tc_2S_7. With these acids present, there are several water soluble Tc species that form. Some of these products show characteristics by TLC, NMR, and XAS to be the thiolated acid Tc complexes, either with one thiol or two. To further characterize these products, it may be useful to esterify the resulting complexes. This would help in making the complexes more organic soluble and facilitate an easier separation, as well as present a better opportunity for crystallization.

Sterically hindered olefinic acids, like citraconic acid, are less likely to form complexes with Tc at higher pH levels, but still cause an interference at low pH. This could give insight into the primary mechanism for the reduction of the double bond. The mechanism for the addition of SH^- across a double bond is not well known, but it has been shown to occur in both acidic conditions and basic conditions.[39]

Humic and fulvic acids make up the majority of the organic matter present in soils. Since these acids can form several different structures and contain reactive

substituent groups, it is important to test the effect of these acids on this method of immobilization.

CHAPTER 3: PERTECHNETATE IMMOBILIZATION ON GOETHITE, HEMATITE, AND MAGNETITE

3.1 Introduction

In the 1940s, three major sites were used for the purpose of designing and building nuclear weapons for the Manhattan Project: Los Alamos National Laboratory (Los Alamos, NM), Clinton Engineer Works (Oakridge, TN), and Hanford, Washington. Hanford, Washington was chosen as a suitable site for plutonium production because it was flat, remote, and close to running water. Production continued at Hanford for over 40 years, and was halted in 1989. Over this span of time, the high level nuclear waste (HLW) that was generated was stored in large underground tanks. These tanks have a 20 year design life, and were never meant for long-term storage. Now, at least 67 of the tanks are assumed to have leaked.[40,41] This leakage has resulted in more than one million gallons of HLW leaking into the environment surrounding the tank farms. A major component of the HLW is the slew of fission products separated from the plutonium-239. Among these isotopes is technetium-99, which has a high fission yield of 6.06% from uranium-235.

Technetium-99 has a long half-life (2.1×10^5 years) and therefore will continue to be an environmental concern. Due to the volume of soil contaminated, removing the contaminated environment is not a feasible option. Therefore, different ways to "trap" or immobilize the radionuclides of concern were considered to keep them from continuing to migrate toward the groundwater and Columbia River.[18,20,42] One method that has been investigated is diffusion of dilute H_2S gas.[24–26] Sulfide reacts with many metals to form insoluble sulfide compounds.

Sulfide reacting with pertechnetate in aqueous solutions has been previously studied by Liu et al.[24] Pertechnetate was used as the technetium starting material because it is the most stable, soluble species in aerobic, aqueous conditions. Liu reported that about 80% of the pertechnetate precipitated as solid Tc_2S_7.[24] When investigating the stability of Tc_2S_7, it was found that in an oxygenated environment, the solid would re-oxidize to TcO_4^-.[24]

Another way that sulfide can immobilize technetium is through an indirect reduction. Sulfide can react with the surface of iron-containing minerals and form FeS. Pertechnetate is known to be reduced and immobilized on the surface of amorphous iron (II) sulfide (FeS_{am}).[43] The current work investigates the immobilization of pertechnetate on the surface of common iron-containing minerals (goethite, hematite, and magnetite) with and without sulfide treatment.

3.2 Experimental Section

3.2.1 Materials

Caution! Technetium-99m emits a 140 keV γ-ray with a half-life of 6.0 hours and ^{99}Tc emits a 0.294 MeV β^- with a half-life of 2.1×10^5 years. All operations were carried out in radiochemical laboratories equipped and approved for handling these radionuclides.

Technetium-99m was eluted as sodium pertechnetate from a ^{99}Mo/^{99m}Tc generator (Covidien) using saline. Technetium-99 was obtained from Oak Ridge National Laboratory as ammonium pertechnetate. The material was black due to the formation of TcO_2. Prior to use, the material was refluxed in hydrogen peroxide for 1 hour to

regenerate pertechnetate and then to destroy excess H_2O_2. The peroxide level was checked with Quantofix peroxide indicator strips.

Chemicals were reagent grade and obtained from Aldrich Chemical Co. or Fisher Scientific. Chemicals were used without further purification. Goethite (α-$Fe^{III}O(OH)$), hematite (Fe_2O_3), and magnetite (Fe_3O_4) were obtained from Aldrich Chemical Co. All water was 18 MΩ water. Water and buffer solutions were degassed prior to use.

3.2.2 Study Preparation

3.2.2.1 Control-$^{99m}TcO_4^-$ Samples

A 50 mg aliquot of mineral was measured into a 2 mL centrifuge tube. Phosphate buffer (700 μL, 100 mM) was added to the centrifuge tube. Any adjustments to pH were made using 0.1 M HCl or 0.1 NaOH. Sodium pertechnetate ($Na^{99m}TcO_4$) was added in saline solution (10-15 μCi, 30-35 μL). Aliquots of 10 μL were sampled at 0.5, 1, 2, 4, 6, and 24 hour time points. Prior to collection, samples were centrifuged to separate any particulate from the solution. The 10 μL aliquots were counted on a NaI(Tl) detector calibrated for ^{99m}Tc. Minerals used were goethite, hematite and magnetite. Phosphate buffer was at pH 4, 7, and 9.

3.2.2.2 Sulfide treatment of mineral at pH 8-$^{99m}TcO_4^-$ Studies

A 200 mg aliquot of mineral was weighed into a 20 mL scintillation vial, followed by the addition of 5 mL of $Na_2S•9H_2O$ solution (6 mM, pH 8). The mixture was set to shake for 18 hours. The mixture was filtered through a fritted filter. The solid was washed with DI H_2O (4 mL x 3) and dried *in vacuo* to remove excess H_2O. A 50 mg sample of this "reduced" solid was weighed into a 1.5 mL centrifuge tube. Phosphate buffer (700 μL; pH 4, 7, or 9) was added to the tube. Last, sodium (^{99m}Tc) pertechnetate

(30-35 μL, 10-15 μCi) in saline solution was added. Aliquots of 10 μL were taken from the solution after centrifuging the tubes at the following time points: 0.5, 1, 2, 4, 6, and 24 hours. Solids were re-suspended following the sampling. The aliquots were counted on the NaI(Tl) detector. Minerals used were goethite, hematite and magnetite.

3.2.2.3 Acid pretreatment of mineral-$^{99m}TcO_4^-$ Studies

A 200 mg sample of mineral was measured into a 20 mL scintillation vial, 5 mL of acid (pH 1) was added to the vial, and the vial was put on a shaker for 1 hour. The mixture was filtered through a fritted filter. The mineral was then collected into a 20 mL scintillation vial and 5 mL of a sodium sulfide solution (6 mM, pH 8) was added, and the vial was placed on the shaker overnight. The mixture was filtered through a fritted filter. The solid was washed with DI H_2O (4 mL x 3), and dried *in vacuo* to remove excess H_2O. A 50 mg sample of this "reduced" solid was weighed into a 1.5 mL centrifuge tube. Phosphate buffer (700 μL; pH 7) was added to the tube. Last, sodium (^{99m}Tc) pertechnetate (30-35 μL, 10-15 μCi) in saline solution was added. After centrifuging the tubes, aliquots (10 μL) were taken from the solution at the following time points: 0.5, 1, 2, 4, 6, and 24 hours. Solids were re-suspended following the sampling. The aliquots were counted on a NaI(Tl) detector. The minerals used were goethite, hematite and magnetite. The acids used were 0.1 M hydrochloric acid and 0.1 M nitric acid.

3.2.2.4 Sulfide treatment-$^{99}TcO_4^-$ Studies

Minerals were treated similarly as in section 3.2.2.2, with the only changes made in the amounts of reagents. A 200 mg sample of mineral was weighed into a 20 mL scintillation vial, followed by the addition of 5 mL of $Na_2S•9H_2O$ solution (6 mM, pH 8). The mixture was shaken for 18 hours, then filtered through a fritted filter and the solid

was washed with 12 mL DI H_2O (4 mL x 3). The solid was dried *in vacuo* and a 50 mg sample of this "reduced" mineral was weighed into a 1.5 mL centrifuge tube. Phosphate buffer (1 mL; 100 mM) and 50 μL of ammonium (^{99}Tc) pertechnetate solution in water were added to the centrifuge tube. The final concentration of ^{99}Tc was 0.1 mM. Aliquots of 10 μL were taken several times over 160 days and counted by LSC to determine the activity remaining in solution. Phosphate buffers used were at pH 4, 7, and 9. Minerals used were goethite, hematite, and magnetite.

3.3 Results and Discussion

Pertechnetate (TcO_4^-) is known to interact with iron (II) sulfide to form insoluble species.[43,44] A recent study investigated the effectiveness of H_2S and NH_3 gases as immobilizing agents for technetium vadose zone sediments.[28] In these studies, sediments from Hanford were used to evaluate the mobility of technetium when treated with H_2S and/or NH_3 gases. Simultaneous injection of the gases was found to significantly reduce the mobility of technetium and limited the re-oxidation of technetium. With H_2S gas alone, about 80% of the Tc was immobilized, but after introduction of air, only about 25% remained immobile.[28] Due to the complexity of these sediments, it was not clear with which mineral the Tc associated upon immobilization.

Um et al. specifically investigated Tc incorporation into goethite samples.[23] In these studies, ferrous chloride was added to a slurry of goethite to act as a reducing agent for Tc(VII). Pertechnetate was added to solution, followed by the addition of $Fe(NO_3)_3$ and NaOH. This approach allowed for the formation of goethite over the precipitated Tc. Up to 100% of the Tc was incorporated and these samples were resistant to leaching and re-oxidation.[23]

In our investigation, we observed the immobilization yield of ^{99m}Tc with amorphous iron sulfide (FeS_{am}) in phosphate buffer at pH 4, 7, and 9. Figure 3-1 shows that at 6 hours about 80% of the $^{99m}TcO_4^-$ was immobilized and after 8 hours about 94-96% of the activity had precipitated from solution, regardless of the pH.

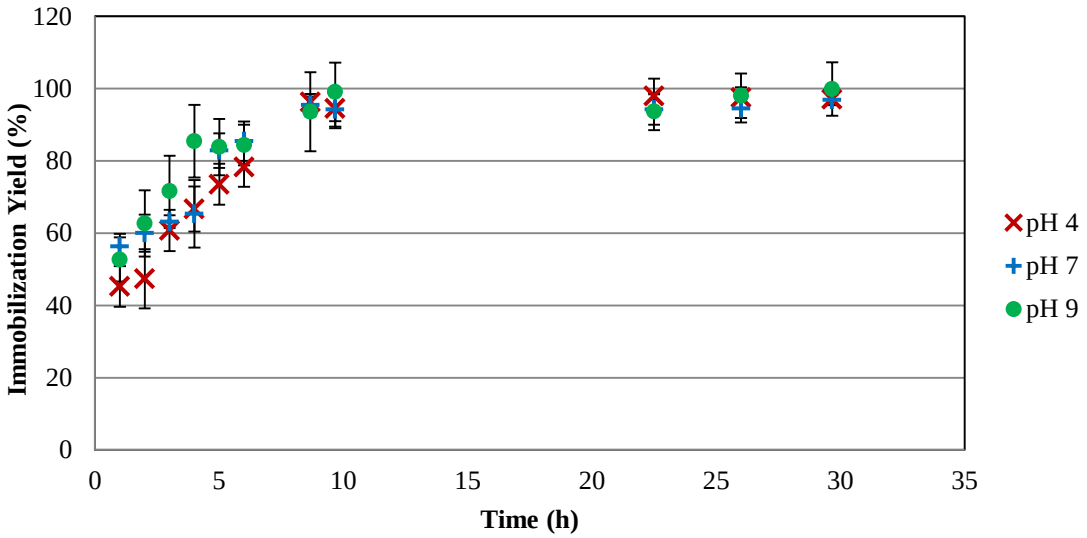

Figure 3-1. Immobilization of $^{99m}TcO_4^-$ on FeS_{am} at pH 4 (x), pH 7 (+), and pH 9 (●) where n=3.

When evaluating the interaction of pertechnetate with Fe-containing minerals, the focus was on goethite (α-$Fe^{III}O(OH)$), hematite (Fe_2O_3), and magnetite (Fe_3O_4).

3.3.1 Goethite studies

Goethite is an iron(III) oxyhydroxide. As a powder, it is yellow in color. Interaction of pertechnetate with untreated goethite at pH 4, 7, and 9 is minimal (Figure 3-2).

"Reduced" goethite was made by treatment with Na_2S. To prevent the formation of H_2S gas, pH adjustment of the sulfide solution was done by slowly adding 0.1 M HCl dropwise while the solution was rapidly stirring. When reacted with Na_2S in aqueous solution, goethite becomes dark green.

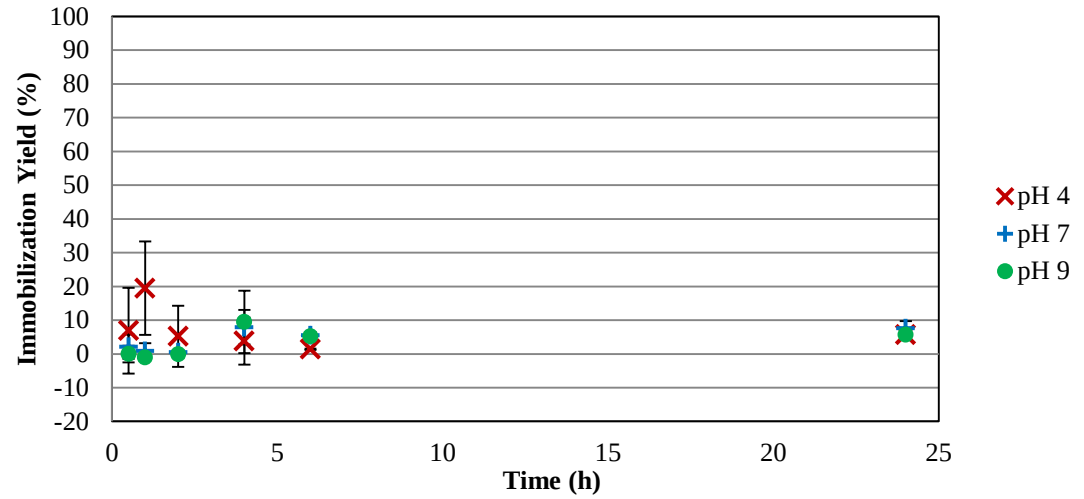

Figure 3-2. Immobilization of $^{99m}TcO_4^-$ on goethite at pH 4 (x), pH 7 (+), and pH 9 (●) where n=3.

Figure 3-3 shows the results for pertechnetate in the presence of "reduced" goethite. At least 71% of ^{99m}Tc was immobilized after 24 hours at pH 4. At pH 7 and pH 9, immobilization yields were 88% or higher after 24 hours.

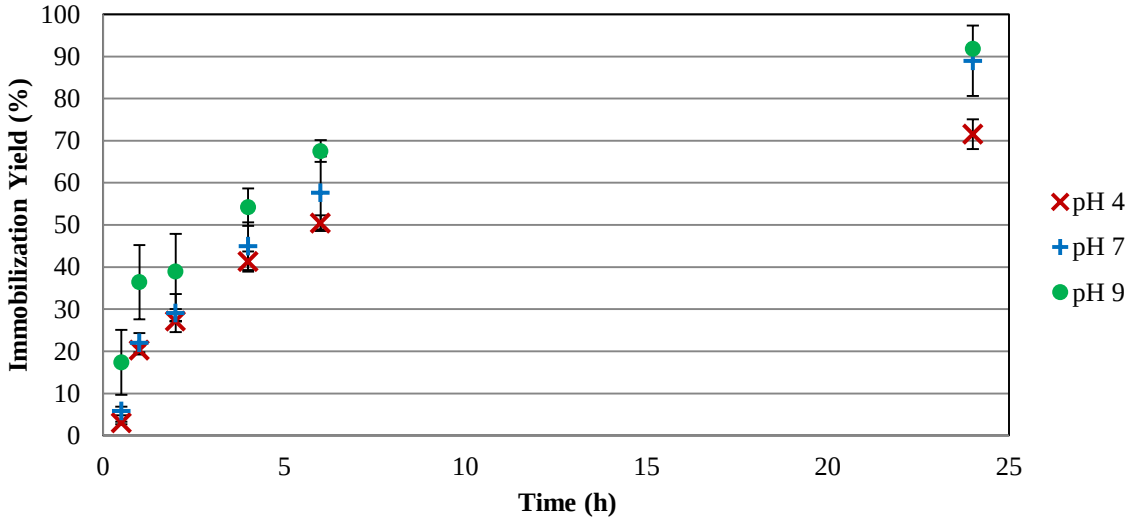

Figure 3-3. Immobilization of $^{99m}TcO_4^-$ on "reduced" goethite at pH 4 (x), pH 7 (+), and pH 9 (●) where n=3.

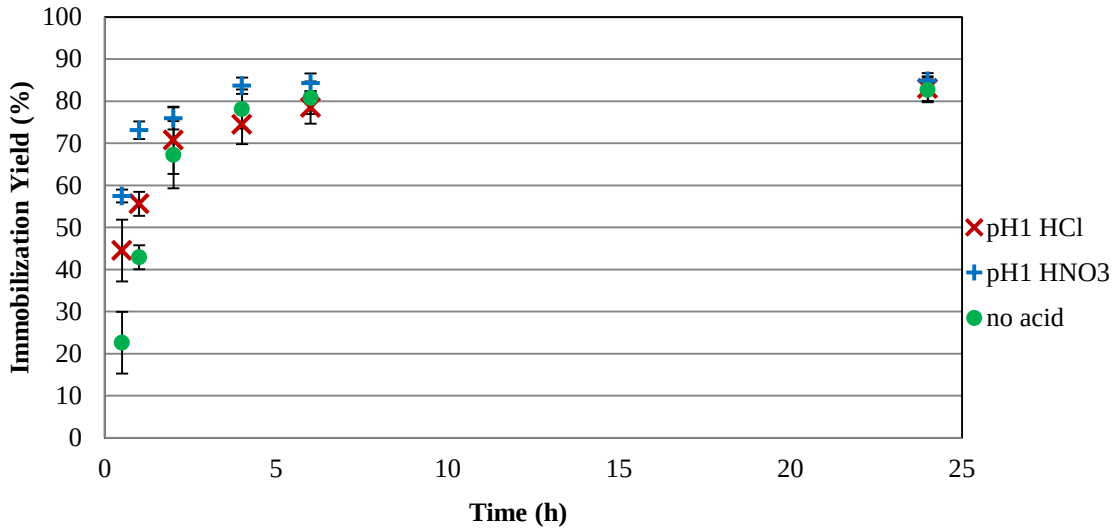

Figure 3-4. Immobilization of $^{99m}TcO_4^-$ on acid-washed, "reduced" goethite. Goethite was washed with pH 1 HCl (x), pH 1 HNO_3 (+), or no acid (●); then reduced with Na_2S solution where n=3.

The effects of acid washing the mineral on the FeS formation were investigated by using both HNO_3 and HCl to pre-treat the mineral before treatment with sulfide. No visible change to the mineral was observed on acid washing. The mineral was then treated with Na_2S, which produced the dark green "reduced" mineral similarly to the study without the acid wash. Figure 3-4 shows the immobilization yield of pertechnetate over 24 hours. Both of the acid washed samples appear to immobilize pertechnetate more rapidly over the first hour. After 1 hour, immobilization yields for all samples were the same within the uncertainty.

The acid-washed samples immobilized the pertechnetate much more rapidly; thus, acid pre-treatment does aid FeS formation for goethite. The FeS is in great excess for both the reduced goethite and the pre-treated, reduced goethite in comparison to the pertechnetate present; consequently, the overall immobilization was similar (≈83%) for both samples after 24 hours.

3.3.2 Hematite studies

Similar studies were performed for hematite. Hematite is an iron (III) oxide mineral that is a dull red powder before treatment with sulfide. Figure 3-5 depicts the interaction between untreated hematite and pertechnetate in phosphate buffer. Similarly to goethite, pertechnetate showed very little interaction with the mineral.

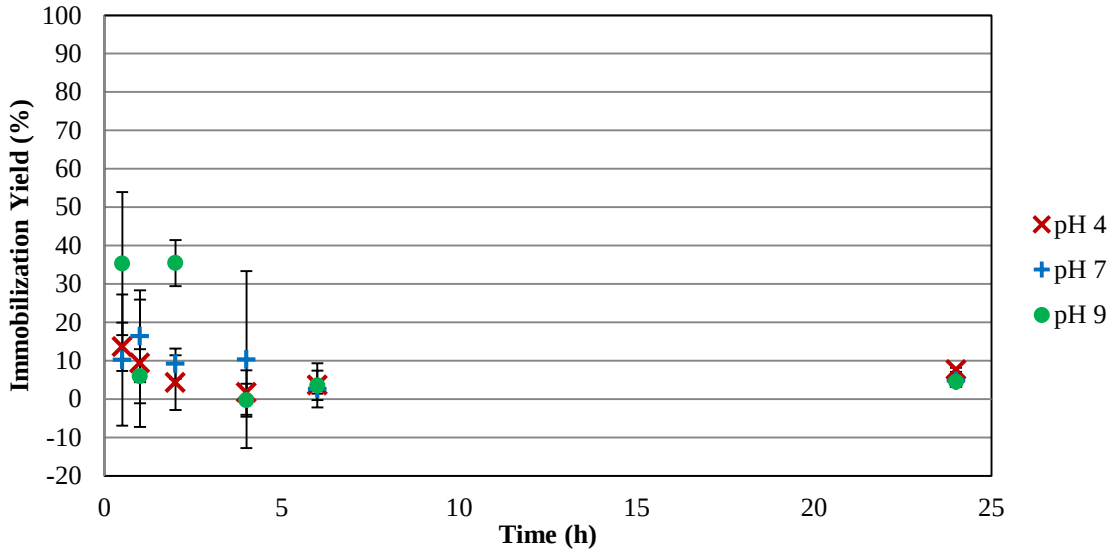

Figure 3-5. Immobilization of $^{99m}TcO_4^-$ on hematite at pH 4 (x), pH 7 (+), and pH 9 (●) where n=3.

The resulting sulfide-hematite mixture gave a dark red solid and a green solution. The green solution is indicative of solubilized Fe(II) species, such as $FeCl_2$. Figure 3-6 shows the immobilization yield of pertechnetate with "reduced" hematite at pH 4, 7, and 9. The "reduced" hematite immobilized at least 65% of the pertechnetate with the pH 4 samples immobilizing up to 74% of the activity. In the goethite samples, the pH 4 experiment showed less immobilization than at the higher pH levels. For the hematite sample, the trend is reversed with the pH 4 experiment showing improved immobilization yield in comparison to the pH 7 and 9 experiments. Also, overall the goethite immobilized more technetium, with a maximum yield of 90%, as compared to 75% with the hematite.

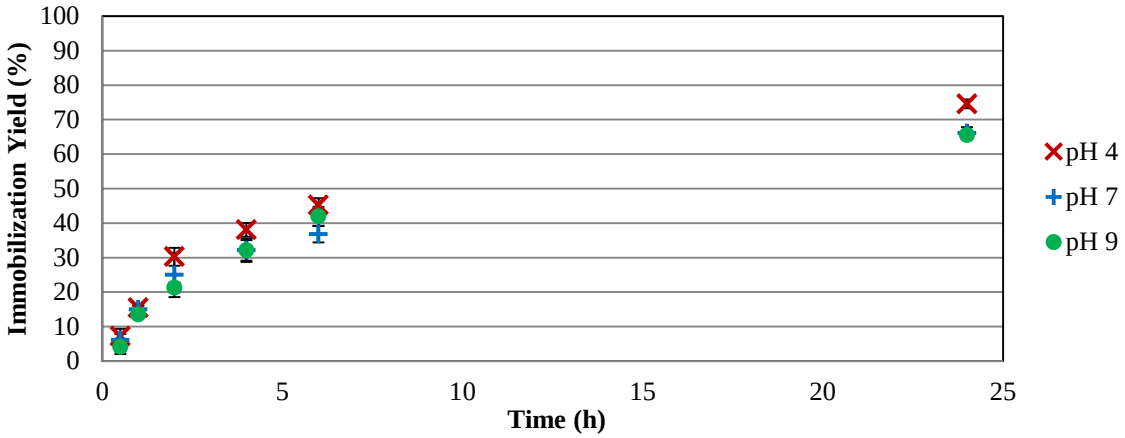

Figure 3-6. Immobilization of $^{99m}TcO_4^-$ on "reduced" hematite at pH 4 (x), pH 7 (+), and pH 9 (●) where n=3.

The hematite experiments shown in Figure 3-7 involved samples pretreated with acid similarly to the goethite samples. These results show that the acid wash improved immobilization yield by about 10%. The HCl samples showed the fastest immobilization over the 24 hours; however, both the HCl and HNO_3 samples had yields close to 75% after 24 hours. The samples without acid pretreatment reached up to only 65% immobilization. The acid-washed hematite also behaved differently from the goethite experiments. With the pre-treated goethite samples, the HNO_3-washed mineral immobilized pertechnetate more rapidly than the HCl-washed mineral. For the hematite samples, the HCl-washed mineral outperformed the HNO_3-washed mineral.

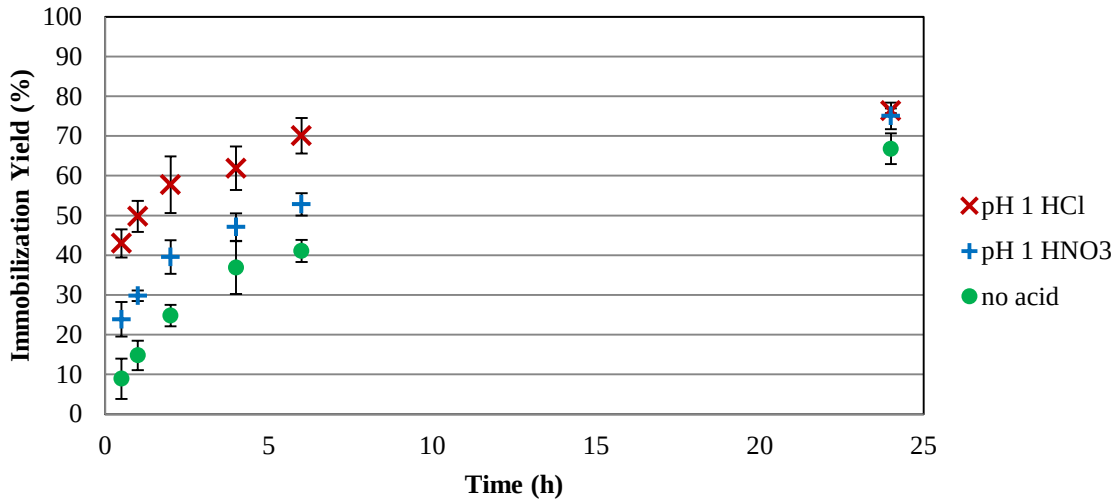

Figure 3-7. Immobilization of $^{99m}TcO_4^-$ on acid-washed, "reduced" hematite. Hematite was washed with pH 1 HCl (x), pH 1 HNO3 (+), or no acid (●); then reduced with Na_2S solution where n=3.

3.3.3 Magnetite studies

Magnetite (Fe_3O_4) is a mixed oxidation state mineral containing iron in the +2 and +3 states. When reacting pertechnetate with magnetite, great variability in the immobilization yield was observed (Figure 3-8) for the first 4 hours in comparison to the other two minerals. The variability could be due to the pertechnetate interacting with the Fe^{2+} on the mineral surface. Pertechnetate can be reduced by Fe^{2+}, but can easily re-oxidize in an oxic environment.

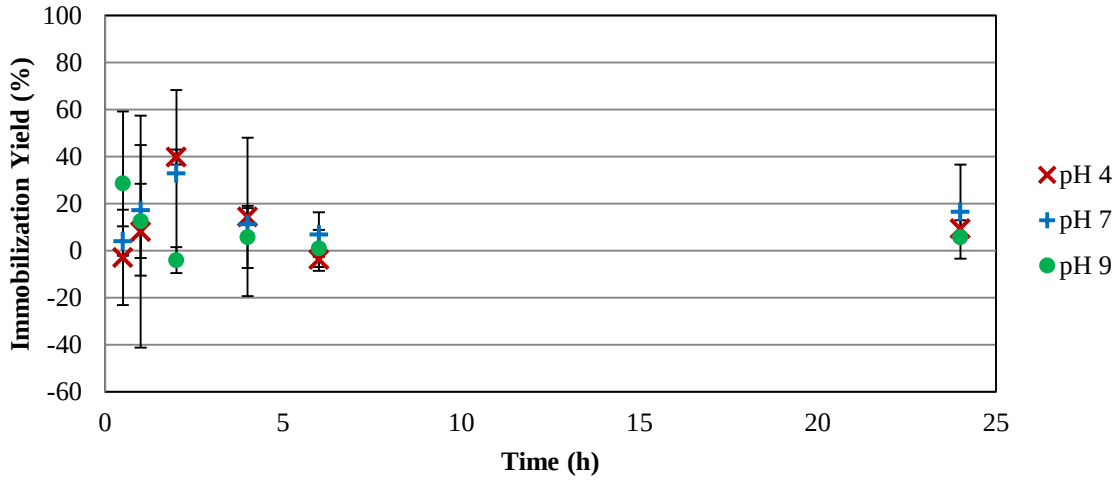

Figure 3-8. Immobilization of $^{99m}TcO_4^-$ on magnetite at pH 4 (x), pH 7 (+), and pH 9 (●) where n=3.

When magnetite is treated with sulfide solution, the solid remains black and the solution becomes green. When the "reduced" magnetite is in the presence of pertechnetate, it can immobilize up to 85% of the Tc at pH 4 (Figure 3-9), whereas less Tc, about 60-70%, was immobilized at higher pH. When magnetite was pretreated with acid (Figure 3-10), the results varied compared to both the goethite and hematite samples. With goethite and hematite, the acid-washed samples immobilized as much or more than the control samples (i.e., pH 7 sulfide treated samples without acid pre-treatment). With magnetite, the control did as well as the HNO_3 acid samples, with both yielding about 65% immobilization after 24 hours; the hydrochloric acid samples immobilized only about 55% of the Tc.

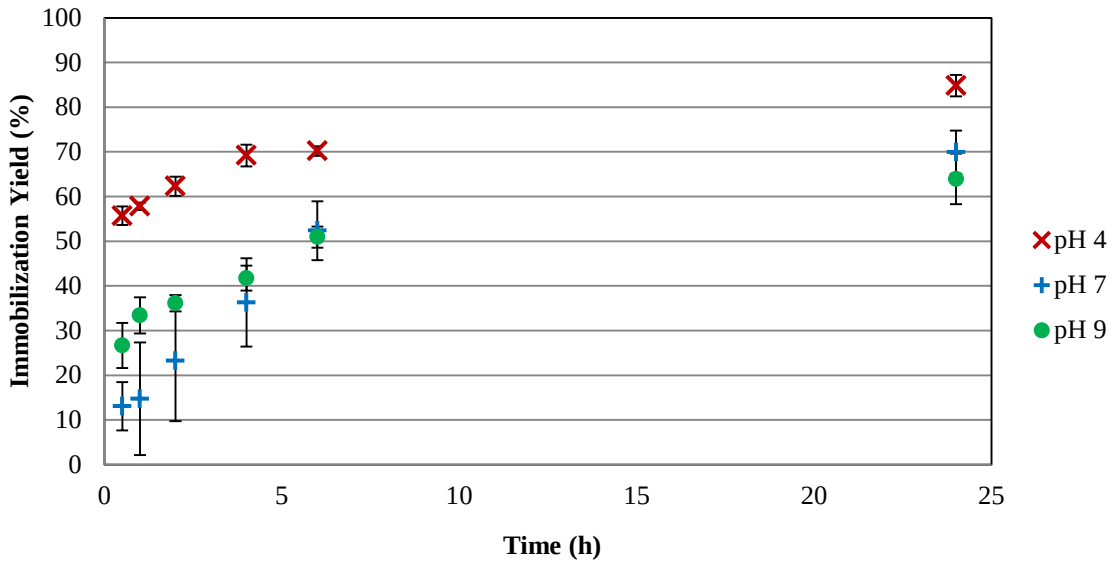

Figure 3-9. Immobilization of $^{99m}TcO_4^-$ on "reduced" magnetite at pH 4 (x), pH 7 (+), and pH 9 (●) where n=3.

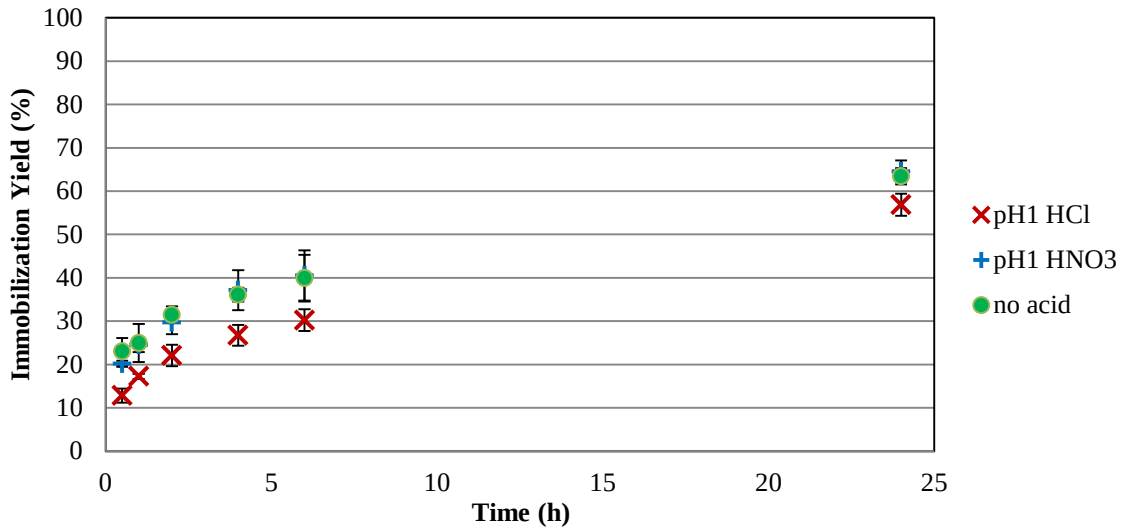

Figure 3-10. Immobilization of $^{99m}TcO_4^-$ on acid-washed, "reduced" magnetite. Magnetite was washed with pH 1 HCl (**x**), pH 1 HNO3 (+), or no acid (●); then reduced with Na_2S solution where n=3.

3.3.4 ^{99}Tc-Mineral Studies

Due to the inconsistencies of the acid pre-treatment effect on the mineral, the studies using the long-lived ^{99}Tc did not include the acid washing step. Nearly 100% of the pertechnetate is immobilized by the reduced minerals (Figures 3-11 to 3-13). The immobilization rate was slowest for the pH 9 experiments with each mineral. Magnetite at pH 9 required close to 40 days to reach maximum Tc immobilization yield, but the pH 4 and 7 samples reached maximum Tc immobilization yield in one week.

After 160 days, most of the ^{99}Tc activity remained associated with the reduced mineral even though the mineral appeared to have re-oxidized. The only samples showing significant re-oxidation of the technetium after 160 days are those from the goethite-pH 4 experiments. After 75 days, the ^{99}Tc activity in solution started to rise slowly, reaching about 7% activity in solution after 160 days.

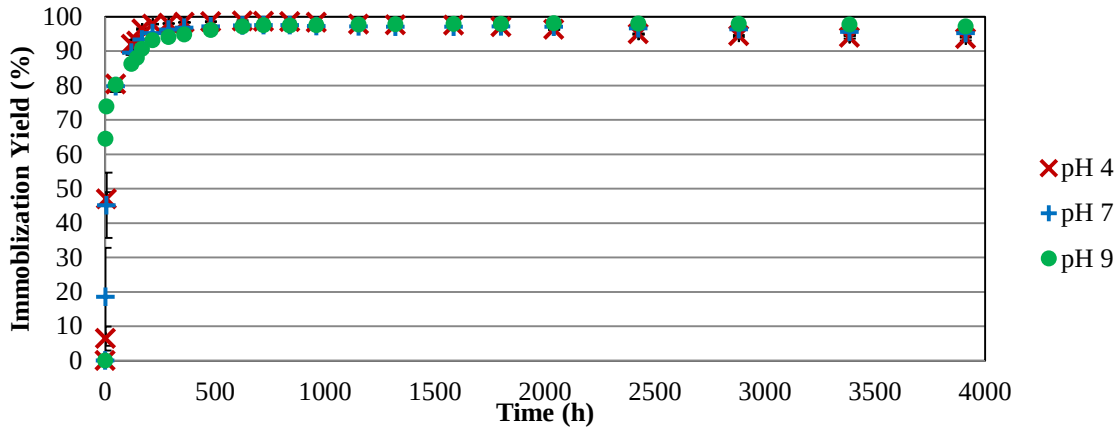

Figure 3-11. Immobilization of $^{99}TcO_4^-$ on "reduced" goethite at pH 4 (x), pH 7 (+), and pH 9 (●) where n=3.

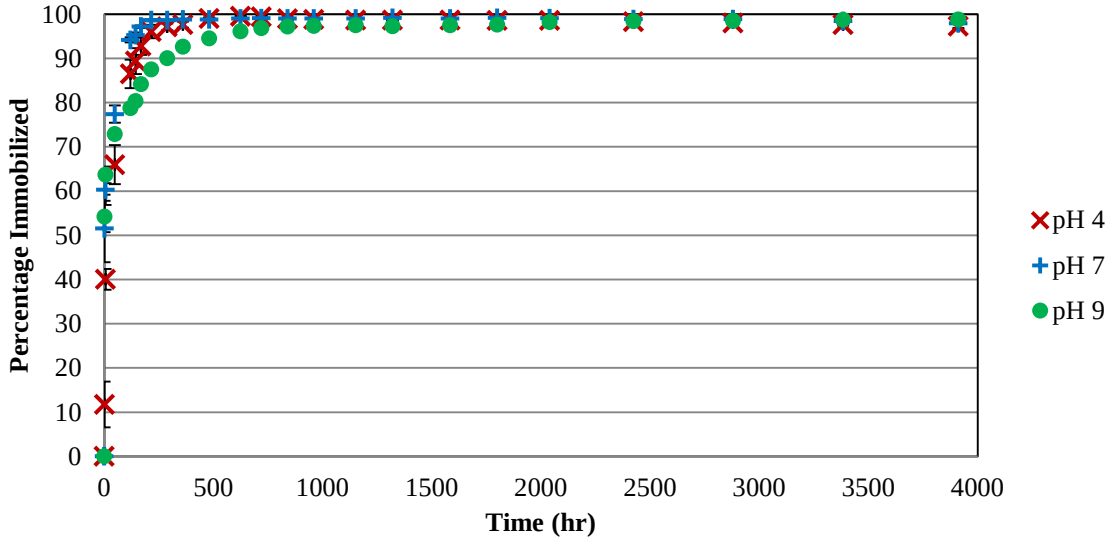

Figure 3-12. Immobilization of $^{99}TcO_4^-$ on "reduced" hematite at pH 4 (x), pH 7 (+), and pH 9 (●)where n=3.

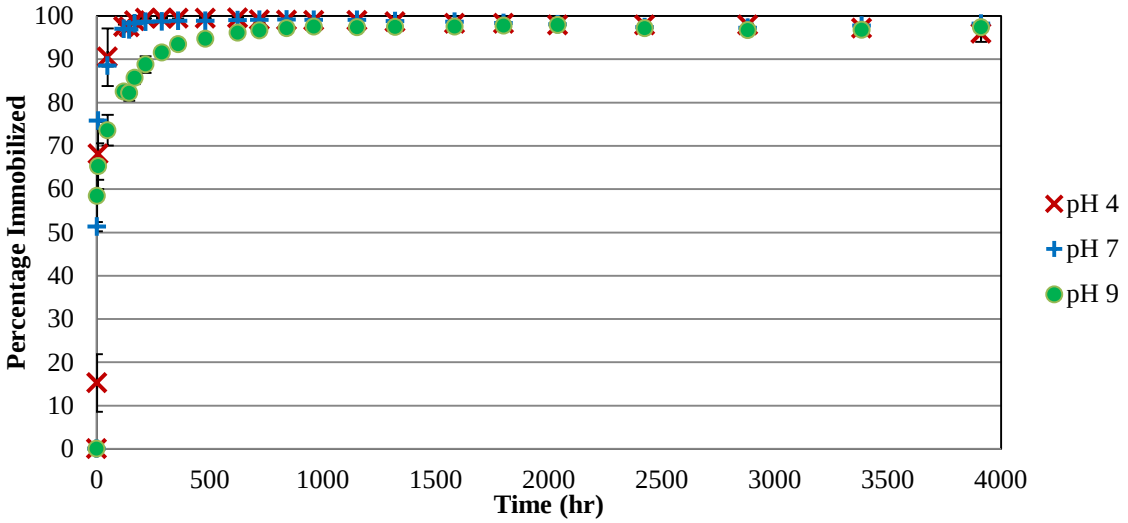

Figure 3-13. Immobilization of $^{99}TcO_4^-$ on "reduced" magnetite at pH 4 (x), pH 7 (+), and pH 9 (●) where n=3.

3.4 Conclusions and Future Studies

Sulfide treatment showed reduction of Fe(III) on the surface of common iron-containing minerals found in soils. This reduced iron was shown to be effective in immobilizing pertechnetate from aqueous solutions. Acid pre-treatment of the mineral prior to sulfide treatment enhances the immobilization rate, but the effect is dependent on the mineral.

When evaluated in a long-term study (160 days), the immobilized pertechnetate showed very little re-oxidation in aerobic, aqueous solutions. Even though the minerals showed re-oxidation over time, more than 95% of the ^{99}Tc activity remained out of solution. To determine if this method would be useful in vadose zone applications, similar studies would need to be done using soils and sediments from the areas of concern. Also, due to the complex environment of DOE nuclear waste sites, possible interferences would need to be addressed to justify the use of *in situ* hydrogen sulfide gas diffusion as an immobilization technique for ^{99}Tc.

CHAPTER 4: INTRODUCTION TO TECHNETIUM AND RHENIUM RADIOPHARMACEUTICALS

4.1 Radiopharmaceuticals

As mentioned in Chapter 1, technetium-99m is widely used in radiopharmaceuticals.[45–53] A radiopharmaceutical is a drug containing a radioactive atom that is used for medical imaging or therapy. Several factors are considered when developing a radiopharmaceutical. Some of these factors include: the nuclear properties of the radioactive atom, the *in vivo* behavior of the drug, the availability of the radionuclide, and the overall cost of the drug.

4.1.1 Nuclear Properties for Radiopharmaceutical Purposes

One important nuclear property to consider is the nuclear half-life of the radionuclide chosen. Nuclear half-lives for radiopharmaceuticals can range from several minutes to several days. The half-life needs to allow enough time for production of the drug, administration of the drug to the patient, and localization to target tissue with enough dose to be effective for its intended purpose. The biological half-life of the drug can play an important role as well. For example, a drug containing an antibody can take several days to localize in the body[54,55]; therefore, the radioactive component of the drug would need a nuclear half-life long enough to allow for localization to occur and still deliver an effective dose.

4.1.1.1 Imaging Specific Properties

Along with the nuclear half-life, the type of emission that a radionuclide undergoes is critical when designing a radiopharmaceutical. The most common types of emission used for imaging agents are isomeric transition (IT), electron capture (ε), and positron (β^+ emission). Radionuclides that decay by isomeric transition or electron

capture generate gamma (γ) photons that are unique to each nuclide. These γ photons can be used for single photon emission computed tomography (SPECT).

SPECT imagers are composed of an array of NaI(Tl) detectors fitted with a collimation system. The collimation system is essential for getting an accurate image. A collimator is usually made from lead and is designed to prevent photons from hitting the detector at an angle (Figure 4-1).[56] By limiting the detector to photons that run parallel to the collimator holes, the resolution of the image can be improved.

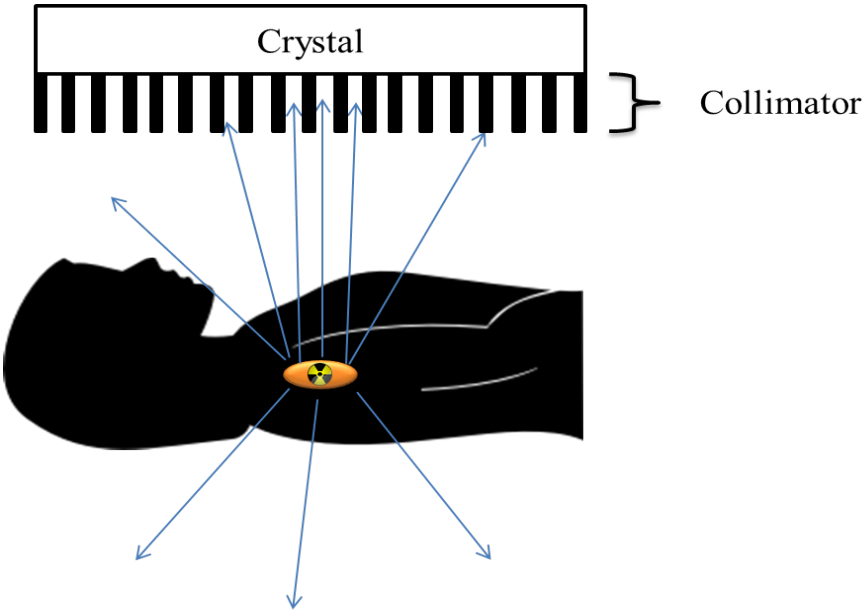

Figure 4-1. Illustration showing the use of a collimation system for SPECT imaging.

Aside from SPECT, another type of imager is positron emission tomography (PET), which is used with positron emitting nuclides. A positron is a positively charged electron that is emitted from the nucleus. The β^+ particle travels a short distance after being emitted, releasing its kinetic energy by interacting with surrounding matter. When most of the kinetic energy is lost, the β^+ annihilates with a nearby electron converting into pure energy.[57] This energy is released as two 511 keV photons that travel in opposite directions (180° apart), commonly referred to as annihilation photons.

These annihilation photons can be detected by a PET imaging system. PET imagers are similar to SPECT imagers in that they both utilize solid scintillation detectors. For PET instruments, several scintillating crystals are arranged in a circle, which allows for coincident events to be detected. Since annihilaton photons are released 180º apart from each other, the point of origin can be traced back when the photons strike two detectors at the same time (i.e., a coincident event). With the use of coincidence circuits, PET instruments do not need a collimator, and can often achieve great resolution in images.

4.1.1.2 Therapy Specific Properties

Whereas nuclides used for imaging release photons in some manner, radionuclides used for therapy are typically particle emitters. The two most commonly used are alpha (α) and beta (β^-) emitters.

Alpha particles are composed of two neutrons and two protons, which amounts to a helium nucleus with an overall positive charge of two. The energy of the alpha particle released from the nucleus is monoenergetic and distinctive for each radionuclide.[58]

Alpha particles are very large in comparison to electrons. Due to their larger mass and charge, α particles will have several interactions with matter over a short path before losing their kinetic energy. These interactions can cause irreparable damage to cells, such as double strand breaks in DNA, causing cell death.[59,60] This damage allows for alpha emitters to be very effective in killing cells, but also indicates that selectivity for cancer cells is highly important in α-emitting drugs.[61,62]

Beta particles are electrons released from the nucleus. Unlike alpha particles, beta particles are not monoenergetic. Beta emitters release a β^- particle and an antineutrino ($\bar{\upsilon}$)

simultaneously. Each beta emitter has a distinctive maximum energy for the beta particle, but the energy released ranges to the maximum beta energy, with the majority of the beta particles being one-third of the maximum energy.[58,63,64] Due to their much smaller size, β^- particles travel much farther from the nucleus than α particles. Also, alpha particles are more likely to interact with DNA strands directly, whereas β^- particles generally interact with DNA indirectly. Beta particles create radicals by interacting with molecules in the body, most commonly water. These radicals then ionize DNA strands, creating the potential for a single strand break, which can result in cell death.[60] As with all radiopharmaceutical drugs, it is imperative to have good target-selectivity for β^- emitters.

4.1.2 Production and Availability of Radionuclides

Commonly, radionuclides are generated by use of an accelerator or a nuclear reactor. Typically, accelerators are used to produce proton-rich nuclides and reactors are used to produce neutron-rich nuclides. An accelerator will use an electromagnetic field to accelerate charged particles (most often protons or deuterons) to high speeds and channel them into controlled beams. These beams are then directed toward a stable target and used to create medically useful radionuclides. For example, rhenium-186 is of interest for therapeutic radiopharmaceuticals, and it can be produced by bombarding tungsten with protons (Equation 4-1)

$$^{186}_{74}\mathrm{W} + {}^{1}_{1}\mathrm{p} \rightarrow {}^{186}_{75}\mathrm{Re} + {}^{1}_{0}\mathrm{n} \qquad \textbf{(4-1)}$$

Reactors use neutrons to produce radionuclides. In accelerators, the starting target material is placed in front of a beam, whereas, with nuclear reactor production, the target is placed in a field of neutrons. One drawback to some reactor generated nuclides

is the desired nuclide cannot be separated from the target material if they are the same element. For example, when using ^{185}Re to produce ^{186}Re (Equation 4-2), these cannot be separated because they will have the same chemical properties. In some situations the parent nuclide is produced and allowed to decay into the desired product. Equation 4-3 shows the production equation for rhenium-188. Rhenium-188 can be separated from ^{188}W, making high specific activity (activity per total mass of element) ^{188}Re. The half-lives of the parent and daughter nuclides also make a generator system feasible.

$$^{185}_{75}\mathrm{Re} + {}^{1}_{0}\mathrm{n} \rightarrow {}^{186}_{75}\mathrm{Re} + \gamma \qquad \textbf{(4-2)}$$

$$^{186}_{74}\mathrm{W} + 2{}^{1}_{0}\mathrm{n} \rightarrow {}^{188}_{74}\mathrm{W} \xrightarrow{69.8\ \mathrm{d}} {}^{188}_{75}\mathrm{Re} + {}^{0}_{-1}\beta + \bar{\nu} + \gamma \qquad \textbf{(4-3)}$$

Generators can be employed when the parent nuclide has a half-life sufficiently higher than the daughter nuclide. Generator systems allow the parent nuclide to continue to decay into the daughter while loaded on a column of chromatographic material. Then, when desired, the generator can be eluted to separate the daughter nuclide from the parent.

The most common type of generator is the ^{99}Mo/^{99m}Tc generator (Figure 4-2), which is used in hospitals worldwide. [^{99}Mo]-molybdate is adsorbed onto an acidic alumina column.[65] As the ^{99}Mo decays, the activity of ^{99m}Tc increases. When needed, the ^{99m}Tc can be eluted from the generator using saline solution. Molybdate is more negatively charged than pertechnetate, therefore the [^{99m}Tc]-pertechnetate easily separates off the alumina column.

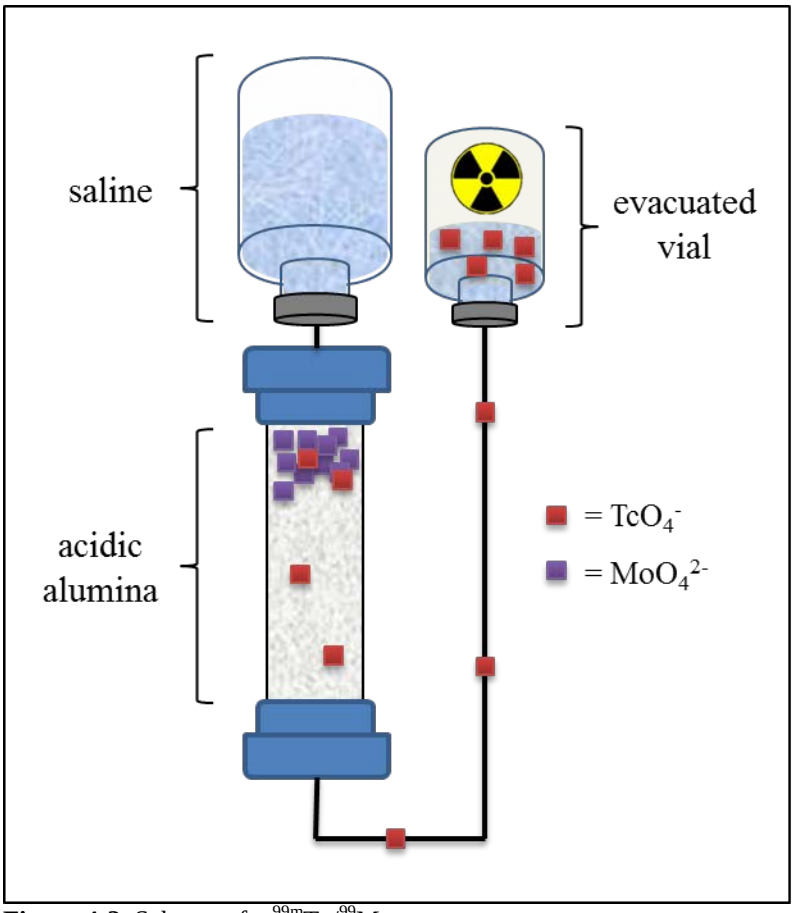

Figure 4-2. Scheme of a $^{99m}Tc/^{99}Mo$ generator.

4.2 Technetium-99m and Rhenium-186/188

4.2.1 Technetium-99m Properties

Technetium-99m is studied heavily because of its nuclear properties and availability.[47,48,66] Technetium-99m has a short 6 hour half-life, which allows for a suitable amount of time for synthesis of the drug, delivery of the drug, and imaging a patient. Technetium-99m undergoes isomeric transition 100% of the time, releasing a 140.5 keV γ photon with an abundance of 89%.[67] The 140.5 keV γ energy is easily detected using SPECT cameras, which can be used to aid physicians in diagnostic medicine. Technetium-99m is provided using a $^{99}Mo/^{99m}Tc$ generator system that is available worldwide.

Since technetium can exist in oxidation states from -1 to 7, there are several opportunities to explore when designing a drug. Most of the drugs developed and studied now have Tc in the +1, +3, or +5 oxidation state. A common method used for developing pharmaceuticals with a radiometal, including technetium, is the bifunctional chelate approach (BFCA). The BFCA utilizes a chelator that both stabilizes the metal and allows for linking to a targeting moiety. Several researchers have looked into the best way to achieve a stable, targeted technetium imaging agent.

4.2.2 Rhenium-186 and Rhenium-188 Properties

Rhenium-186/188 have nuclear properties suitable for therapy purposes, therefore rhenium, as the third row congener of technetium, is often studied alongside technetium. Both ^{186}Re and ^{188}Re are beta emitters. ^{186}Re (β^-_{max} = 1.07 MeV) has a half-life of 3.7 days and ^{188}Re (β^-_{max} = 2.12 MeV) has a half-life of 17 hours.[68,69] Rhenium-188 can be obtained from a ^{188}W/^{188}Re generator system, which is set up similarly to the ^{99}Mo/^{99m}Tc generator.

Both technetium and rhenium form thermodynamic sinks in the +4 and +7 oxidation states, as MO_2 and MO_4^-, respectively. As perrhenate, rhenium is in the +7 oxidation state and is soluble in water, providing a stable starting material for drug development. Re^{5+} is the next most accessible oxidation state from Re^{7+}, and it can form the $Re^{V}O^{3+}$ or the $Re^{V}O_2^{+}$ core, which can be chelated by a suitable tetradentate ligand.

4.2.3 Technetium and Rhenium Schiff Base Chemistry

Tetradentate Schiff bases have been studied as potential chelators for technetium and rhenium for many years.[70–75] Both +3 and +5 metal complexes have been investigated for the purposes of nuclear medicine applications. Several Tc(III) Schiff

base complexes were developed with a set of ligands that were called the Q series. The Q series complexes were developed for the purpose of myocardial perfusion imaging. Figure 4-3A and 4-3B show structures of ^{99m}Tc-tetrofosmin and ^{99m}Tc-sestamibi, the imaging agents currently used today. The Q series complexes are monocationic complexes that have *trans* phosphine ligands to provide stability against *in vivo* reduction. ^{99m}Tc-Q12 (Figure 4-3C) provided good myocardial uptake and retention and cleared the blood and liver rapidly, which is a drawback with a current FDA approved drug, ^{99m}Tc-sestamibi (Figure 4-3B).[76]

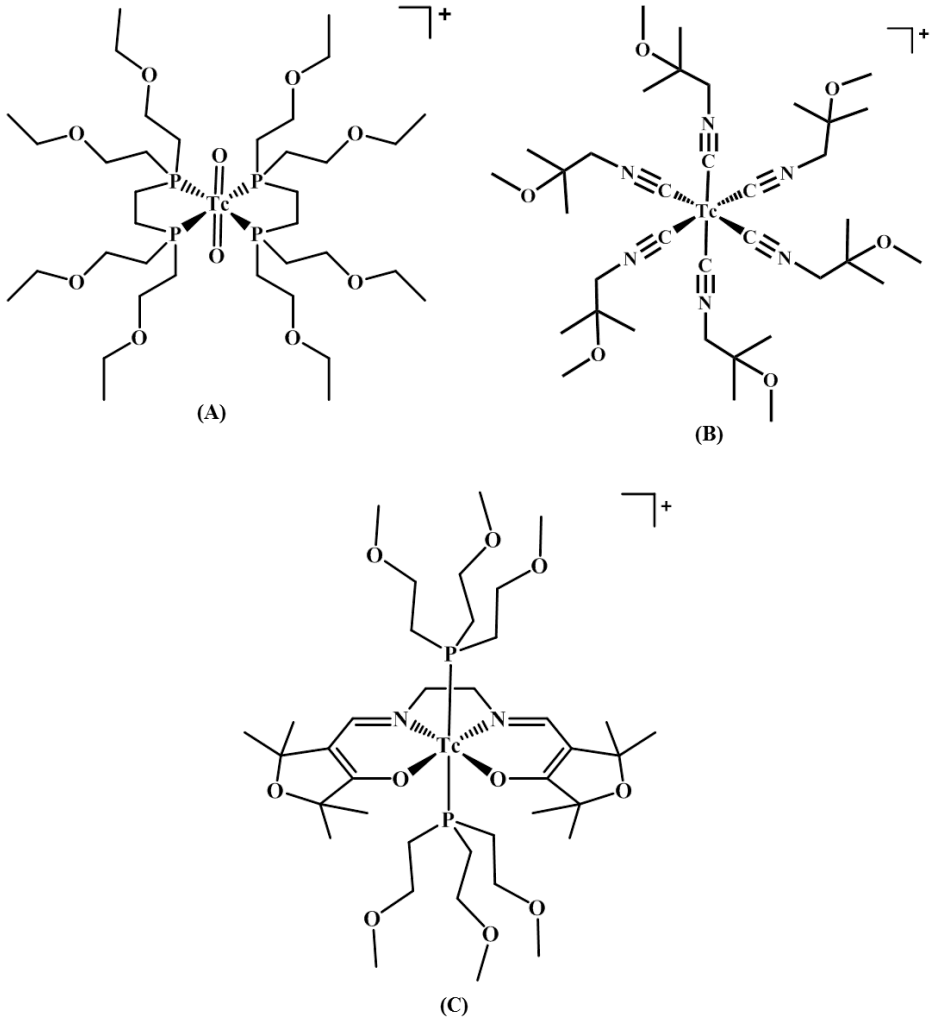

Figure 4-3. Structures of (A) ^{99m}Tc-tetrofosmin, (B) ^{99m}Tc-sestamibi, and (C) ^{99m}Tc-Q12.

The Q series is a set of Schiff bases that were extensively researched with ^{99m}Tc. Rhenium is more difficult to reduce than technetium, making the diphosphine rhenium(III) products more difficult to achieve.

Acetylacetone (acac-) and salicylaldehyde (sal-) based Schiff bases (Figure 4-4) have been studied as well.[70–72,77–79] These ligands and their metal complexes are easy to synthesize and lend structural information that is not easily attained on the radiotracer level. The backbone of these ligands will affect the isomers formed when reacted with the metal. Typically, the backbone is two to three carbons long, with the two carbon length forming more stable metal complexes due to ring size. Computationally and experimentally, it has been seen that both Tc and Re prefer to form 5-membered rings with ligands versus 6-membered rings.

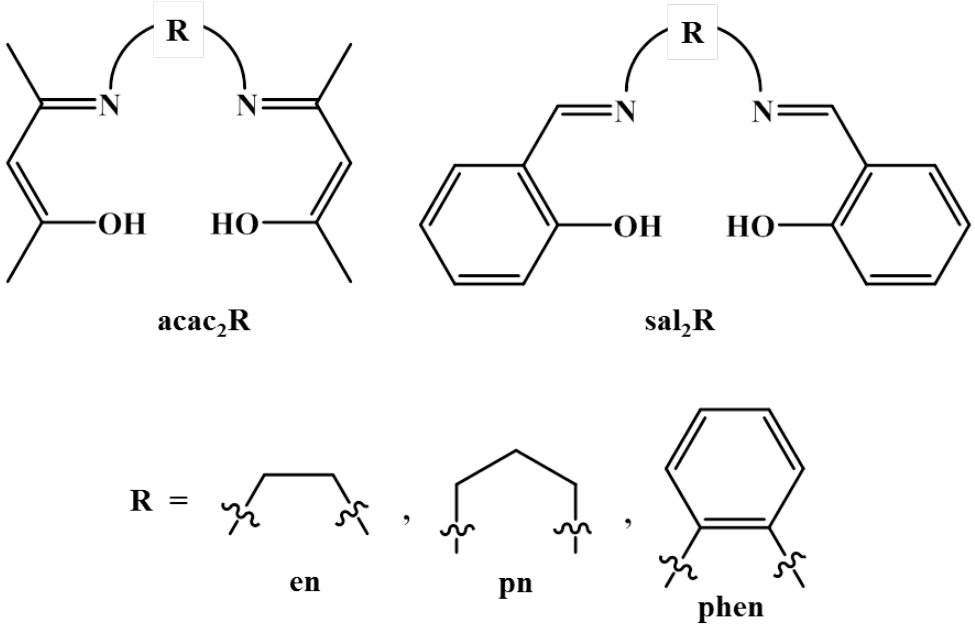

Figure 4-4. Structures of acac- and sal- based Schiff base ligands.

Previous work has shown that these tetradentate Schiff base ligands can form *cis* or *trans* mononuclear M(V) complexes. These complexes typically have octahedral geometries with an oxo ligand occupying one site and the Schiff base having four donor atoms (two amine nitrogens and two oxygens). The other coordination site can be one of several monodentate ligands: oxo, hydroxo, aquo, chloro, phosphine, cyano, isothiocyano. This monodentate ligand can bind either *cis* or *trans* with respect to the M=O bond. Stronger nucleophiles (e.g., CN^-, NCS^-) will bind *cis* to the oxo. This forces an oxygen from the Schiff base ligand to bind *trans* to the oxo group.

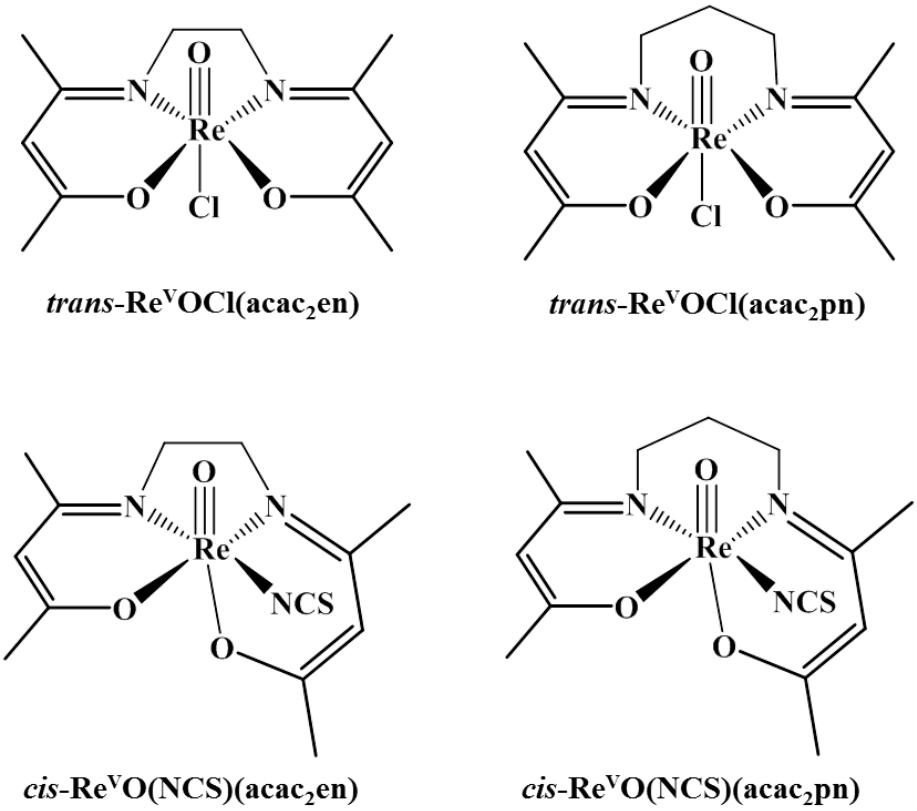

Figure 4-5. Structures of *trans*-$Re^{V}OCl(acac_2en)$, *cis*-$Re^{V}O(NCS)(acac_2en)$, *trans*-$Re^{V}OCl(acac_2pn)$, and *cis*-$Re^{V}O(NCS)(acac_2pn)$.

Studies have looked into the possibility of these nucleophilic ligands stabilizing the $[M^{V}O(N_2O_2)]^+$ complexes.[79] The monodentate ligands that are of particular interest

are thiocyanate (NCS^-) and cyanide (CN^-). Green et al. showed the complex transformed from a *trans*-ReOX($acac_2en$) to a *cis*-ReOX($acac_2en$) when NCS^- or CN^- was added. These Re(V) Schiff base complexes have been shown to be more stable with the addition of the CN^- or NCS^- ligand.

CHAPTER 5: RHENIUM SCHIFF BASE CHEMISTRY

5.1 Introduction

Technetium-99m remains the workhorse of diagnostic nuclear medicine despite the recent shortages and the increased availability of positron emission tomography (PET) imaging systems and radionuclides (e.g., ^{18}F).[51] Technetium is well-known for both its diagnostic imaging applications (^{99m}Tc; $t_{1/2}$ = 6.01 h; γ = 140 keV) and its environmental impact as a long-lived, mobile fission product (6.1% yield) produced during the nuclear fuel cycle (^{99}Tc; $t_{1/2} = 2.12 \times 10^5$ y; β^-_{max} = 0.292 MeV).[80] Rhenium has two radioisotopes (^{186}Re: $t_{1/2}$ = 90 h; β^-_{max} = 1.071 MeV; γ = 137 keV (9%) and ^{188}Re: $t_{1/2}$ = 17 h; β^-_{max} = 2.118 MeV; γ = 155 keV (15%)) suitable for theranostics, emitting both beta particles and gamma rays, and is often considered the radiotherapeutic "matched pair" for technetium in radiopharmaceutical development.[51,81,82]

In addition, rhenium, the third row congener of Tc, is often used as a non-radioactive analogue for developing Tc chemistry. Differences in their redox chemistry and substitution kinetics, however, may lead to "non-matched pair" behavior, requiring careful investigation of their fundamental inorganic chemistry. A major challenge for the development of potential Re radiopharmaceuticals is the kinetic and redox stability of the radiotracer complexes under the high dilution experienced *in vivo*. Instability leads to release of rhenium and oxidation to perrhenate.

The tetradentate N_2O_2 Schiff base ligands have shown very interesting chemistry with technetium, particularly in the field of nuclear medicine. The ^{99m}Tc "Q-series" (*trans*-[$^{99m}Tc^{III}(PR_3)_2(N_2O_2$-Schiff base)]$^+$), has been investigated for use as single photon emission computed tomography (SPECT) imaging agents.[83,84] Translation of the "Tc-Q"

chemistry to Re has highlighted some of the differences in chemistry between these two congeners, including redox chemistry and substitution kinetics.[70,71,78,79] Efforts have led to a variety of potential Re(III) and Re(V) Schiff base theranostic agents with and without coordinated phosphines and with very few examples of Re(III) analogues of the Tc-Q complexes.[71,78]

The chemistry of rhenium with Schiff base ligands has been extensively investigated.[85–89] Methyltrioxorhenium(VII) Schiff base complexes have been evaluated as potential catalysts for epoxidation reactions[86,87] while Re(V) salen complexes are being probed as potential oxidation and epoxidation catalysts.[85,88,89] Various rhenium Schiff base complexes have also been explored for potential applications to diagnostic and therapeutic nuclear medicine.[70,71,74,78,79,90–100]

Mononuclear, dinuclear, and trinuclear complexes of Re(V) with tetradentate Schiff base ligands were first reported by Middleton et al.[74] Mononuclear complexes ([ReOXL]) are generally isolated under dry, inert conditions using excess ligand as the proton scavenger. Dinuclear (μ-O[ReOL]$_2$) and trinuclear ((μ-O)$_2$O$_2$[ReL]$_3$) species are a result of reactions performed open to the atmosphere or in the presence of basic proton scavengers. They have also been isolated as conversion products from mononuclear species that have been left in solutions exposed to water and/or base.[70,74,93,94] Isolation of crystalline mononuclear species has proven difficult in past work since dinuclear and trinuclear species form under standard aerobic conditions from mononuclear species, likely due to the presence of water, and may preferentially crystallize.[71] Indeed, *trans*-[ReO(X)(aca$_2$en/pn)] (X = OH$_2$ or Cl$^-$) converted to the dinuclear complexes *trans*-[μ-O-(ReO(aca$_2$en/pn))$_2$] over time when left exposed to the atmosphere. The addition of base

(NaOH) to mononuclear complexes instantaneously converted them to the dinuclear complexes.[70] Conversion back to the mononuclear complexes has only been successful when dinuclear complexes are treated with two equivalents of $[Et_3Si]^+$. In these reactions, the bridging oxo ligand is successfully abstracted by the trialkylsilyl cation yielding $Et_3SiOSiEt_3$ and leaving the vacant coordination site of the resulting mononuclear complexes to be filled by solvent molecules.[99–101]

Many N_2O_2 Schiff base mononuclear complexes of the type *cis*/*trans*-[ReOX(L)], where L is an N_2O_2 Schiff base ligand, have a site *cis* or *trans* to the oxo group available for substitution. Reaction with pi-backbonding ligands may lead to complexes that are kinetically more inert. Addition of thiocyanate to *trans*-[ReO(X)(aca_2en/pn)] (X = OH_2 or Cl^-) led to the formation of *cis*-[ReO(NCS)$acac_2$en/pn]. A cyanide complex was also isolated for the $acac_2$en complex.[71,79] Interestingly, the dinuclear complex was not observed as in previous studies in the absence of NCS^- or CN^-, suggesting a method of trapping and stabilizing the mononuclear species.

Our efforts to understand and develop Re Schiff base chemistry suitable for translation to potential theranostic agents have led to the isolation of a novel Re(IV) Schiff base dimer complex and an unusually aqueous stable Re(V) Schiff base monomer complex. We previously reported on using a rigid Schiff base ligand (sal_2phen) to generate the Re analog of the "Q-compounds".[78] Now we report on using a sterically more hindered Schiff base to investigate the factors that might lead to *trans*-$[Re(PR_3)_2(\text{Schiff base})]^+$. The reaction of $(Bu_4N)[ReOCl_4]$ with a sal-based N_2O_2 Schiff base ligand derived from 1,2-diamino-2-methylpropane (α,α'-[(1,1-dimethylethylene)dinitrilo]di-*o*-cresol, sal_2ibnH_2) under various conditions led to several

products (Figure 5-1). Reaction of $ReOCl_4^-$ with the ligand gave the mononuclear Re(V) complex *cis*-[$Re^{V}OCl(sal_2ibn)$] and the dinuclear Re(V) complex *trans*-[μ-$O(Re^{V}O(sal_2ibn))_2$]. Addition of thiocyanate to the mononuclear chloro complex led to *cis*-[$Re^{V}O(NCS)(sal_2ibn)$], an unusually stable mononuclear Re(V) complex. Subsequent reduction of *cis*-[$Re^{V}O(NCS)(sal_2ibn)$] with triphenylphosphine generated the mononuclear *trans*-[$Re^{III}(NCS)(PPh_3)(sal_2ibn)$] and the novel dinuclear *trans*-[μ-$O(Re^{IV}(NCS)(sal_2ibn))_2$].

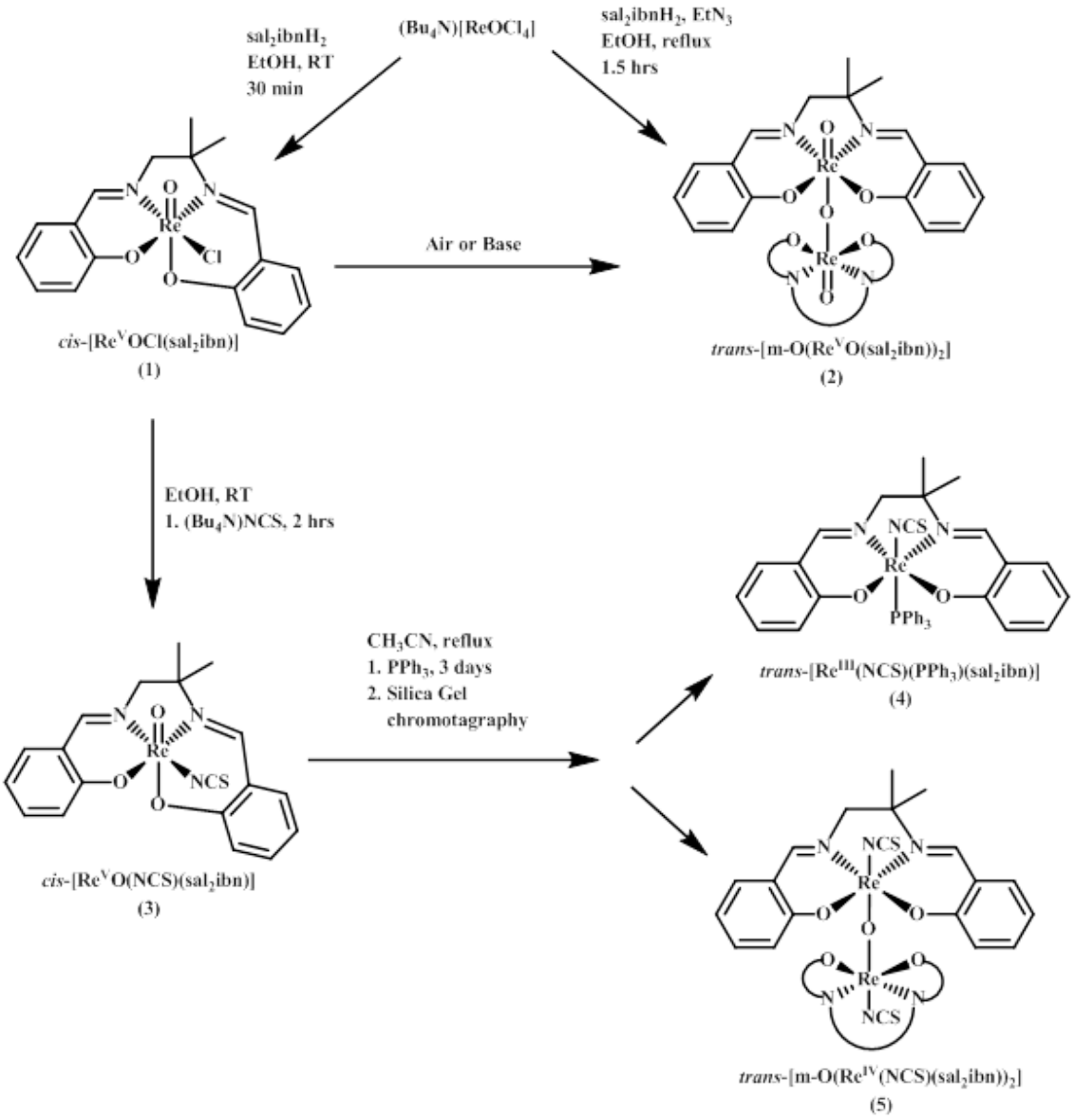

Figure 5-1. Complete reaction scheme of compounds 1-5.

5.2 Experimental Section

Unless noted, all common laboratory chemicals were of reagent grade or better. Absolute ethanol was degassed prior to use and experiments using ethanol were performed under an argon atmosphere, using standard Schlenk techniques for inert syntheses. ^{1}H and ^{13}C NMR spectra (including HMQC ^{1}H-^{13}C correlation) were recorded on a Brüker DRX300 WB or DRX500 at 25^{o}C in $CDCl_3$, CD_2Cl_2, CD_3CN, or DMSO-d_6 with TMS as an internal standard. Infrared spectra were obtained as KBr pellets on a Thermo Nicolet Nexus 670 FT-IR spectrometer. Electrospray Ionization Mass Spectroscopy (ESI-MS) was performed on a Thermo Finnigan TSQ7000 triple-quadrupole mass spectrometer. Elemental analysis was performed by Quantitative Technologies Inc. (QTI; Whitehouse, NJ).

5.2.1 Materials

Salicylaldehyde and 1,2-diamino-2-methylpropane were purchased from Sigma Aldrich and used as received. Triethylamine was purchased from Sigma Aldrich and distilled from $CuSO_4$ prior to use. Absolute ethanol, acetonitrile, toluene, dichloromethane, chloroform, and diethyl ether were used as purchased unless otherwise noted. $(Bu_4N)[ReOCl_4]$ was prepared by the literature method.[101] The ligand α,α'-[(1,1-dimethylethylene)dinitrilo]di-*o*-cresol (sal_2ibnH_2) was prepared as previously reported through condensation of two equivalents of salicylaldehyde with one equivalent of 1,2-diamino-2-methylpropane in absolute ethanol.[102] The purity of the starting materials was verified by ^{1}H NMR and FT-IR spectroscopies. The sal_2ibnH_2 was recrystallized from absolute ethanol prior to use.

5.2.2 Preparation of *cis*-[$Re^{V}OCl(sal_2ibn)$] · 3 $CHCl_3$ (1)

Sal_2ibnH_2 (0.1075 g, 0.363 mmol) and $(Bu_4N)[ReOCl_4]$ (0.213 g, 0.363 mmol) were combined in a Schlenk flask and the flask was evacuated and backfilled with argon three times. The solids were dissolved in absolute ethanol (20 mL), with a green solution forming quickly upon dissolution. The solution was stirred at room temperature under argon for 1 hour, after which the solution was brought to dryness *in vacuo*. The oily material was reconstituted in a minimal volume of $CHCl_3$ and filtered. X-ray quality crystals were obtained by allowing the solution to sit tightly capped at room temperature for several days. Yield 8.6 % (0.0278 g). ^{1}H NMR [500 MHz, CD_2Cl_2, r.t., δ (ppm)]: 8.60 (s, 1H, -C**H**=N-); 7.90 (s, 1H, -**H**C=N-); 6.89 – 7.65 (m, 8H, Ar**H**); 4.39 (d, *J* = 10 Hz, 1H, -NC$\mathbf{H_2}$-C(CH_3)); 4.28 (d, *J* = 10 Hz, 1H, -NC$\mathbf{H_2}$-C(CH_3)); 1.66 (s, 3H, C(C$\mathbf{H_3}$)); 1.01 (s, 3H, C(C$\mathbf{H_3}$)). ^{13}C NMR [500 MHz, CD_2Cl_2, r.t., δ (ppm)]: 175.94, 174.93 (-H**C**=N-); 174.81, 166.48 (**Ar**-O); 139.35, 138.40, 137.54, 134.60, 122.24, 121.70, 120.68, 119.71, 118.65, 118.60 (**Ar**); 80.22 (-N**C**H_2-C(CH_3)$_2$); 75.87 (-NCH_2-**C**(CH_3)$_2$); 27.01, 22.91 (C(**C**H_3)). FT-IR (KBr pellet, ν/cm^{-1}): 1601 (C=N st); 955 (Re=O st). ESI MS (m/z): 497.09 (497.09 calcd for $[C_{18}H_{18}O_3N_2Re]^+$ (M^+-Cl)). Elemental Anal. calcd (found) for $ReC_{18}H_{18}O_3N_2Cl$: C, 40.60 (39.95); H, 3.41 (3.11); N, 5.26 (5.07).

5.2.3 Preparation of *trans*-[μ-O($Re^{V}O(sal_2ibn)$)$_2$] · 4 $CHCl_3$ (2)

$(Bu_4N)[ReOCl_4]$ (1.0 g, 1.2 mmol), sal_2ibnH_2 (0.35 g, 1.2 mmol), and triethylamine (0.5 mL, 0.689 g, 6.81 mmol) were combined in 50 mL of ethanol in air. This solution was refluxed for 1.5 hours, and then taken to dryness on a rotary evaporator. The crude product was dissolved in 50 mL of chloroform and washed three times with an equal volume of water. The organic layer was collected and evaporated to

dryness with a rotary evaporator. The product was recrystallized from chloroform/hexanes. Crystals suitable for X-ray diffractometry were obtained by slow evaporation of a solution of **2** in $CHCl_3$. Yield 50% (0.43 g). ^{1}H NMR [500 MHz, CD_2Cl_2, r.t., δ (ppm)]: 8.20 (s, 2H, -**H**C=N-); 8.02 (s, 2H, -**H**C=N-); 6.52-7.54 (br m, 16H, Ar**H**); 4.57 (m, 2H, -NC**H$_2$**-C(CH_3)); 3.75 (m, 2H, -NC**H$_2$**-C(CH_3)); 2.04 (s, 4H, C(C**H$_3$**)); 1.95 (s, 2H, C(C**H$_3$**)); 1.31 (s, 6H, C(C**H$_3$**)). ^{13}C NMR [500 MHz, $CDCl_3$, r.t., δ (ppm)]: 177.0, 176.4 (-H**C**=N-); 172.88, 170.79 (Ar-O); 138.14, 138.04, 136.79, 136.66, 121.65, 120.68, 118.03, 117.33 (Ar); 77.58 (-N**C**H_2-C(CH_3)$_2$); 74.41 (-NCH_2-**C**(CH_3)$_2$); 29.39, 21.16 (C(**C**H_3)). FT-IR (KBr pellet, v/cm-1): 1597 (C=N st); 980 (Re=O st); 694 (Re-O-Re st). ESI MS (m/z): 1010.2 (1010.17 calcd for $[C_{36}H_{36}O_7N_4Re_2]^+$ (M^+)). Elemental Anal. Calcd (found) for $Re_2C_{36}H_{36}O_7N_4$: C, 42.76 (42.38); H, 3.59 (3.27); N, 5.55 (5.31).

5.2.4 Preparation of cis-[Re^{V}O(NCS)(sal$_2$ibn)] (3)

Sal_2ibnH_2 (0.051 g, 0.171 mmol) and (n-Bu_4N)[$ReOCl_4$] (0.100 g, 0.171 mmol) were combined in a Schlenk flask and the flask was evacuated and backfilled with argon three times. The solids were dissolved in degassed absolute ethanol (20 mL). A green solution formed quickly upon dissolution of the solids. After 30 minutes of reaction time, (n-Bu_4N)SCN (0.051 g, 0.171 mmol) was added to the flask using standard Schlenk techniques. The solution was allowed to stir for 2 hours or until the formation of green precipitate ceased. The kelly green solid was isolated on a medium porosity glass fritted funnel, washed with ethanol and then diethyl ether. X-ray quality crystals were obtained by slow evaporation of an acetonitrile solution of **3**. Yield 45.5 % (0.042 g). ^{1}H NMR [500 MHz, DMSO-d6, r.t., δ (ppm)]: 8.55 (s, 1H, -C**H**=N-); 7.92 (s, 1H, -**H**C=N-); 6.92 –

7.66 (m, 8H, Ar**H**); 4.33 (d, J = 11 Hz, 1H, -NC**H$_2$**-C(CH$_3$)); 4.27 (d, J = 11 Hz, 1H, -NC**H$_2$**-C(CH$_3$)); 1.66 (s, 3H, C(C**H$_3$**)); 1.00. (s, 3H, C(C**H$_3$**)). ^{13}C NMR [500 MHz, DMSO-d$_6$, r.t., δ (ppm)]: 175.71, 174.05 (-H**C**=N-); 172.55, 164.27 (Ar-O); 139.25, 138.09, 134.68, 121.03, 120.18, 119.81, 119.64, 119.49, 118.36 (Ar); 146.40 (N**C**S); 80.09 (-N**C**H$_2$-C(CH$_3$)$_2$); 77.00 (-NCH$_2$-**C**(CH$_3$)$_2$); 26.21, 22.71 (C(**C**H$_3$)). FT-IR (KBr pellet, ν/cm^{-1}): 2086 (NCS st as); 1603 (C=N st); 953 (Re=O st). ESI MS (m/z): 497.09 (497.09 calcd for [C$_{18}$H$_{18}$O$_3$N$_2$Re]$^+$ (M$^+$-NCS)). Elemental Anal. calcd (found) for ReC$_{19}$H$_{18}$O$_2$N$_3$S: C, 41.08 (40.74); H, 3.28 (3.37); N, 7.57 (5.45); S, 5.78 (5.83).

5.2.5 Preparation of *trans*-[Re^{III}(NCS)(PPh$_3$)(sal$_2$ibn)] (4)

Complex **3** (0.150 g, 0.270 mmol) was placed in a Schlenk flask and the flask evacuated and backfilled with argon three times. The solid was dissolved in 20 mL of dry degassed CH$_3$CN added via cannula. To this solution, triphenylphosphine (0.501 g, 1.90 mmol) was added following standard Schlenk techniques. The green solution was refluxed for 4 days under inert atmosphere, during which time the color changed to brownish yellow. The solution was then brought to dryness in vacuo, and the oily substance was reconstituted in CH$_2$Cl$_2$ and purified on a silica gel column pre-equilibrated with CH$_2$Cl$_2$. Compound **4** was the third visible band (red/orange in color) eluted with CH$_2$Cl$_2$. Slow evaporation of the solvent produced X-ray quality crystals of **4**. Yield 16.6 % (0.036 g). ^{1}H NMR [500 MHz, CD$_2$Cl$_2$, r.t., δ (ppm)]: 26.58 (d, J = 6.9, 1H, Ar**H**), 25.63 (d, J = 6.9, 1H, Ar**H**); 17.24 (t, J = 6.9, 1H, Ar**H**); 16.21 (t, J = 9.2, 1H, Ar**H**); 8.29 (br s, 3H, Ar**H**); 7.88 (br s, 9H, Ar**H**); 7.40-7.75 (m, 3H, Ar**H**); 2.36 (s, 1H, C(C**H$_3$**)); 1.27 (s, 2H, -NC**H$_2$**-C(CH$_3$)); -3.67 (s, 3H, C(C**H$_3$**)); -6.43 (dd; J = 6.9, 9.2; 1H; Ar**H**); -8.33 (dd; J = 6.9, 9.2; 1H; Ar**H**); -18.73 (d, J = 6.9 Hz, 1H, Ar**H**); -20.46 (d, J =

6.9 Hz, 1H, Ar**H**); -26.69 (s, 1H, -**H**C=N-); -40.74 (s, 1H, -**H**C=N-). ^{13}C NMR [500 MHz, $CDCl_3$, r.t., δ (ppm)]: 155.81, 46.19 (-H**C**=N-); 154.42, 138.80, 134.04, 126.26, 101.65, 68.43, 63.38, -1.88 (Ar); 138.01, 132.66, 129.82 (PPh_3); 30.38 (-N**C**H_2-C(CH_3)); 60.72, 21.01 (C(**C**H_3)). FT-IR (KBr pellet, ν/cm-1): 2072 (NCS st as); 2031 (NCS st sy); 1598 (C=N st). ESI MS (m/z): 800.96 (801.16 calcd for $[C_{37}H_{36}O_2N_3PSRe]^+$ (M^+)). Elemental Anal. calcd (found) for $ReC_{37}H_{36}O_2N_3PS{\cdot}CH_2Cl_2$: C, 51.55 (52.84); H, 4.08 (4.71); N, 4.78 (5.06); S, 3.6 (5.32).

5.2.6 Preparation of *trans*-[μ-O(Re^{IV}(NCS)(sal$_2$ibn))$_2$] · 2 CH_3CN (5)

This compound was prepared as described for compound **4** and isolated as a separate band from the silica gel column. Compound 5 remained at the top of the column until yellow band 5 was removed with CH_2Cl_2; purple compound **5** was then eluted with an CH_3CN:CH_2Cl_2 (1:9) solution. Slow evaporation of the solvent gave X-ray quality crystals of **5**. Yield 6.78 % (0.020 g). ^{1}H NMR (500 MHz, CD_3CN, r.t., δ /ppm): 13.49 (s, 1H, -C**H**=N-); 8.29 (s, 1H, -**H**C=N-); 10.29 (d, J = 8.0 Hz, 1H, Ar**H**); 10.23 (t, J = 8.0 Hz, 1H, Ar**H**); 8.99 (t, J = 7.5 Hz, 1H, Ar**H**); 8.55 (d, J = 7.5 Hz, 1H, Ar**H**); 7.29 (d, J = 7.5 Hz, 1H, Ar**H**); 7.24 (d, J = 7.5 Hz, 1H, Ar**H**); 6.50 (t, J = 7.5 Hz, 1H, Ar**H**); 3.00 (t, J = 7.5 Hz, 1H, Ar**H**); 4.85, -0.36 (d, J = 11 Hz, 1H, -NC**H$_2$**-C(CH_3)); 2.32 (s, 3H, C(C**H$_3$**)); -1.32 (s, 3H, C(C**H$_3$**)). ^{13}C NMR (500 MHz, CD_3CN, r.t., δ /ppm): 147.42, 145.44, 143.36, 141.58, 115.54, 113.75, 110.16, 104.56 (Ar); 123.72, 73.39 (-H**C**=N-); 93.63(-N**C**H_2-C(CH_3)); 22.91, 11.80 (C(**C**H_3)). FT-IR (KBr pellet, υ/cm-1): 2054 (SCN st as); 1597 (C=N st); 694 (Re-O-Re st). ESI MS (m/z): 1093.27 (1094.13 calcd for $[C_{38}H3_6O_5N_6S_2Re_2]^+$ (M+)). Elemental Anal. calcd (found) for $Re_2C_{38}H_{36}O_5N_6S_2$: C, 41.75 (41.83); H, 3.32 (3.42); N, 7.68 (7.05).

5.2.7 X-Ray Characterization

Intensity data were obtained at -100 ºC on a Brüker SMART CCD Area Detector system using the ω scan technique with Mo Kα radiation from a graphite monochromator. Intensities were corrected for Lorentz and polarization effects. Equivalent reflections were merged, and absorption corrections were made using the multi-scan method. The structures were solved by direct methods with full-matrix least-squares refinement, using the SHELX package.[103] All non-hydrogen atoms were refined with anisotropic thermal parameters. The hydrogen atoms were placed at calculated positions and included in the refinement using a riding model, with fixed isotropic U. The final difference maps contained no features of chemical significance.

5.3 Results and Discussion

5.3.1 Synthesis of Re(V) Mono- and Dinuclear Complexes 1, 2, and 3

Reaction of sal_2ibnH_2 with $(Bu_4N)[ReOCl_4]$ in ethanol in the presence of a proton scavenger gave the dinuclear complex *trans*-$[\mu\text{-}O(ReO(sal_2ibn))_2] \cdot 4\ CHCl_3$, **2**, as dark green cubic crystals. When sal_2ibnH_2 is reacted with $(Bu_4N)[ReOCl_4]$ in ethanol in the absence of a proton scavenger and under dry, inert conditions, the mononuclear complex *cis*-$[ReOCl(sal_2ibn)] \cdot 3\ CHCl_3$, **1**, was obtained as green cubic crystals. However, unless crystals rapidly form or crystallization is performed under inert conditions, dimerization occurs resulting in **2**. The conversion from mononuclear to dinuclear is so favorable that a pure sample of **1** will slowly convert to **2** while NMR spectroscopy is performed. This was confirmed by lack of any Re-O-Re stretch prior to sample dissolution for NMR measurements and subsequently observing the Re-O-Re stretch in the IR spectrum at 694 cm^{-1}. Several products were observed in the NMR spectrum of **1** (*vide infra*).

Interestingly, the mononuclear complex is readily isolated or "trapped" as *cis*-[ReO(NCS)(sal_2ibn)], **3**, by the addition of (Bu_4N)SCN. The SCN^- must be added after the mononuclear complex is formed but before the dinuclear complex forms. The yield of **3** decreases and the yield of **2** increases the longer sal_2ibnH_2 is allowed to react with (Bu_4N)[$ReOCl_4$]. Once SCN^- was added to the reaction mixture, a kelly green solid quickly formed and the green color of the solution faded. Recrystallization by slow evaporation of acetonitrile open to the atmosphere yielded **3** as the only product.

After confirmation of a single mononuclear species by IR and ^{1}H NMR analysis, the stability of compound **3** was investigated. Most Re(V) Schiff base complexes will undergo hydrolysis in the presence of water. Compound **3** was dissolved in a 1:1 CH_3CN:H_2O solution and left for over a week, after which time the sample was dried and analysed by IR and ^{1}H NMR. The complex was virtually unchanged demonstrating this compound's extraordinary water stability.

5.3.2 Synthesis of the Mononuclear Re(III) Complex 4 and Novel Dinuclear Re(IV) Complex 5

Complexes of technetium(III) and rhenium(III) are numerous, which can be attributed to the fact that the d^4 configurations are readily stabilized by ligands with pronounced donor and π-acceptor properties. However, Tc(IV) and Re(IV) are much rarer, owing to their tendency to hydrolyze to the thermodynamically favored MO_2.[104] The Tc(V) Schiff base complexes that were reduced with trialkyl phosphines to the corresponding *trans*-[$Tc^{III}(PR_3)_2$(Schiff base)]$^+$ (i.e., the Tc-Q series) were evaluated for radiopharmaceutical applications.[80,102] The use of hydrophilic substituents on the Schiff base or phosphine (e.g., ethers) can increase *in vivo* stability by reducing protein binding.

Translation of this chemistry to Re to form the analogous *trans*-$[Re^{III}(PR_3)_2(Schiff\ base)]^+$ has proven challenging.[74,95,97] The mononuclear Re(V) chloro complex (**1**) dimerizes readily to **2**, especially in the presence of water (or base); thus, the mononuclear Re(V) isothiocyanate complex (**3**) was reacted with triphenylphosphine. Unfortunately, disubstitution to yield *trans*-$[Re^{III}(PPh_3)_2(sal_2ibn)]^+$ did not occur most likely due to the steric requirements of the backbone gem-dimethyl groups, although the monosubstituted *trans*-$[Re^{III}(NCS)(PPh_3)(sal_2ibn)]$ (**4**) formed, along with a novel dimeric μ-oxo Re(IV) complex (**5**) in 16.6% and 6.78% yields, respectively.

Previously reported reactions of monooxorhenium(V) Schiff base complexes with phosphines yielded either the reduced *trans*-$[Re^{III}(PR_3)_2(Schiff\ base)]^+$ or the monosubstituted *cis*-$[Re^{V}O(PR_3)(Schiff\ base)]^+$ complex, depending on the particular Schiff base and phosphine used.[16,18] The Re(III) complex, **4**, represents a rare case in which a single tertiary phosphine coordinates and reduces the metal center with a simultaneous rearrangement of the sal_2ibn Schiff base ligand to purely equatorial coordination sites and with the phosphine and isothiocyanate groups positioned *trans* to each other.

The Re(IV) complex, **5**, containing a linear SCN-Re-O-Re-NCS moiety, is the first of its kind of which we are aware. Of the few non-Re(V) dinuclear complexes with a bridging oxo group, most contain additional bridging ligands, a terminal oxo, or are mixed-valent, but none have terminal NCS groups.[105–107] The mechanism for the formation of **5** is unclear. We postulated that complex **5** may have been a disproportionation product of **3** to ReO_4^- and complex **5**; however, refluxing complex **3** in CH_3CN for over a week showed no observable reaction. The IR spectrum of the dried

product from this reaction gave signals consistent with **3,** and no signals corresponding to **5** or any other dinuclear species were observed. Furthermore, ^{1}H NMR analysis of the refluxed sample gave signals corresponding only to compound **3**.

5.3.3 General Characterization

Electrospray ionization mass spectrometry (ESI-MS) of compounds **1 – 5** confirmed the identities of the products. The molecular ions with the expected rhenium isotope pattern were observed in the positive mode of ESI-MS for compounds **2** and **4**. Compounds **1** and **3** were observed as $[M - Cl]^{+}$ and $[M - NCS]^{+}$ in the positive mode, respectively. Compound **5** was observed as the radical cation $[M - e]^{+\cdot}$ in the positive mode and as the radical anion $[M - e]^{-\cdot}$ in the negative mode. Fragments of dimer **5** with m/z values corresponding to $[M - NCS - ReSC_{19}H_{18}N_3O_2]^{+}$ and $[M - ReOC_{18}H_{18}N_2O_2]^{+}$, where $[M] = [C_{38}H_{36}O_5N_6S_2Re_2]$, were also observed. The FT-IR spectra of all complexes showed the expected Schiff base C=N stretches between 1597 – 1603 cm^{-1}. The spectra of the monomeric oxo-rhenium(V) complexes showed the presence of the Re=O stretches near 950 cm^{-1}, and absence of the Re-O-Re stretch at 694 cm^{-1}. All dinuclear compounds exhibited the Re-O-Re stretch at 694 cm^{-1}. A signal at 980 cm^{-1} for the Re=O stretch, typical for multinuclear oxorhenium complexes,[70,71,74,78,91,108] was observed for compound **2** and was absent in compound **5**. The isothiocyanate-containing complexes exhibited SCN stretches from 2050 – 2090 cm^{-1}, consistent with literature values.[79,109] The elemental analyses of compounds **1 – 5** verified the chemical makeup of the dried complexes albeit compound **4** included an extraneous methylene chloride molecule. In addition, the sulfur content in compound **4** was higher than theoretically expected, possibly the result of free NCS^{-}.

5.3.3 NMR Analyses

The mononuclear and dinuclear complexes can be easily distinguished based on their ^{1}H NMR chemical shifts (Table 5-1). The asymmetry associated with the sal_2ibn ligand makes every carbon atom and virtually all protons unique. The ^{1}H and ^{13}C NMR spectra of the mononuclear compounds **1** and **3** are consistent with the coordination of the chloro and isothiocyanate *cis* to the Re(V) oxo group, respectively, and are very similar to one another. The proton NMR spectra of **1** and **3** showed two singlets for the ligand backbone geminal methyl groups, separate doublets for each methylene proton, and unique singlets for each imine proton. The aromatic protons were observed as expected between 6.8-7.6 ppm. The ^{1}H and ^{13}C NMR spectra of **1** also showed the presence of at least one other related species. We suspect that this may be $[ReO(X)sal_2ibn]$, where X = $OReO_3^-$, OH^-, OH_2, or solvent has replaced the chloro group.[70] The ^{1}H NMR spectra is almost unchanged with the exception of a new signal at 8.9 ppm for the imine proton. Rearrangement of the ligand from *cis* to *trans* occurs with the imine as the pivot point, which would account for the shift observed by NMR. The ^{13}C NMR spectrum showed double the signals expected for **1** with the chemical shifts very similar to those assigned to **1**; the additional chemical shifts are very similar to those for compound **2**.

Table 5-1. ^{1}H NMR Chemical Shifts.

	1	**2**	**3**	**4**	**5**
gem-dimethyl	1.01 (s, 3H) 1.66 (s, 3H)	1.31 (s, 4H) 1.95 (s, 2H) 2.04 (s, 6H)	1.00 (s, 3H) 1.66 (s, 3H)	2.36 (s, 3H) -3.67 (s, 3H)	2.32 (s, 3H) -3.67 (s, 3H)
methylene	4.28 (d, 1H) 4.39 (d, 1H)	3.75 (m, 2H) 4.57 (m, 2H)	4.27 (d, 1H) 4.33 (d, 1H)	1.27 (s, 2H)	4.85 (d, 1H) -0.36 (d, 1H)
imine	7.90 (s, 1H) 8.60 (s, 1H)	8.02 (s, 2H) 8.20 (s, 2H)	7.92 (s, 1H) 8.55 (s, 1H)	-26.69 (s, 1H) -40.74 (s, 1H)	8.29 (s, 1H) 13.49 (s, 1H)
aromatic	6.89-7.65 (m, 8H)	6.52-7.54 (m, 16H)	6.92-7.66 (m, 8H)	25.63 (d, 1 H) 25.58 (d, 1H) 17.24 (t, 1H) 16.21 (t, 1H) -6.43 (dd, 1H) -8.33 (dd, 1H) -18.73 (d, 1H) -20.46 (d, 1H)	10.29 (d, 1H) 10.23 (t, 1H) 8.99 (t, 1H) 8.55 (d, 1H) 7.29 (d, 1H) 7.24 (d, 1H) 6.50 (t, 1H) 3.00 (t, 1H)

The dinuclear complex **2** exhibited chemical shifts and splitting patterns similar to the monomeric complex **1**, with the exception of the methyl groups. Three different chemical shifts at 1.31, 1.95, and 2.04 ppm were observed for the geminal dimethyl protons. The resonance at 1.2 ppm integrates for six protons, and is likely indicative of the pseudo-equatorial methyl protons directed away from the coordination centers, corresponding to C17A (Figure 5-3), which is furthest from the influence of the rhenium. The two axially directed methyl groups are observed at two different chemical shifts, 2.0 and 1.9 ppm, integrating for 4 and 2 protons, respectively.

The ^{1}H NMR spectra for complexes **4** and **5** are much more complex due to the paramagnetic Re center. The ^{1}H NMR spectra exhibited sharp peaks with no evident peak broadening due to paramagnetism as observed in the literature, but each complex had distinctly different chemical shifts for the protons on the Schiff base ligand. For example, the aromatic protons from the ligand in complex **4** range from 3 to 11 ppm, whereas the same protons for complex **5** range from -21 to 27 ppm. As observed in the literature, ^{1}H NMR shifts for paramagnetic Re(III) complexes are unpredictable. Two dimensional NMR techniques were used to help assign the protons to the appropriate

chemical shifts. The ^{13}C NMR spectra displayed only minor shifts for compounds **4** and **5** relative to the diamagnetic complexes. Additionally, the NMR spectra of **5** demonstrates that some paramagnetic Re(IV) (d^3) complexes allow characterization by ^{1}H- and ^{13}C-NMR.

Initially, the NMR studies of compound **5** showed that the sample was not "clean" and another species was present. Purification on a second silica gel column pre-equilibrated with CH_2Cl_2 slowly eluted a faint green band, which was determined to be trans-[$Re^{IV}(NCS)_4(PPh_3)_2$], analogous to Re(IV) phosphine halogen complexes of the type trans-[$ReX_4(PR_3)_2$].[110–112] Compound **5** was then displaced with CH_3CN:CH_2Cl_2 (1:9) as a purple species and determined to be pure by NMR and ESI-MS studies.

5.3.4 X-Ray Crystal Structures

The Re(V) complexes *cis*-[ReOCl(sal_2ibn)] · 3 $CHCl_3$, **1**, *trans*-[μ-O(ReO(sal_2ibn))$_2$] · 4 $CHCl_3$, **2**, and *cis*-[ReO(NCS)(sal_2ibn)], **3**, the Re(III) complex *trans*-[Re(NCS)(PPh_3)sal_2ibn], **4**, and the Re(IV) complex *trans*-[μ-O(Re(NCS)sal_2ibn)$_2$] · 2 CH_3CN, **5**, were characterized by X-ray crystallography (Figures 5-2 to 5-6). All five complexes exhibit distorted octahedral geometry around the metal center. The ligand occupies the equatorial plane in the two dinuclear complexes (**2** and **5**), and this is also observed for the Re(III) complex, **4**. The mononuclear complexes **1** and **3** have a chloride and a isothiocyanate ligand, respectively, coordinated *cis* to the oxo, while the *trans* position is occupied by a phenolic oxygen from sal_2ibn. Space group, lattice parameters, and other relevant information are given in Table 5-2. Relevant bond lengths and angles are given in Table 5-3.

Table 5-2. X-ray crystal data, data collection parameters, and refinement parameters.

	1	**2**	**3**	**4**	**5**
CCDC #	933550	933551	933552	933553	933554
Formula	$C_{20}H_{20}Cl_7N_2O_3Re$	$C_{40}H_{40}Cl_{12}N_4O_7Re_2$	$C_{19}H_{18}N_3O_3SRe$	$C_{37}H_{33}N_3O_2SPRe$	$C_{42}H_{42}N_8O_5S_2Re_2$
FW	770.73	1481.83	554.62	800.89	1175.36
crystal system	monoclinic	monoclinic	triclinic	monoclinic	monoclinic
space group	$P2_1/c$	$P21/n$	*P-1*	*C2/c*	*P21/n*
a (Å)	11.1399(17)	9.602(2)	8.920(4)	39.067(8)	10.117(1)
b (Å)	9.4693(15)	17.819(3)	9.487(4)	8.746(2)	16.397(2)
c (Å)	24.716(4)	14.807(3)	11.657(5)	19.104(4)	13.168(2)
α (deg)	90	90	95.882(5)	90	90
β (deg)	95.913(2)	90.941(2)	96.864(5)	97.644(2)	95.155(2)
γ (deg)	90	90	103.701(4)	90	90
V (Å^3)	2593.4(7)	2533.1(7)	942.8(7)	6469(2)	2175.5(5)
Z	4	2	2	8	2
ρ_{calcd} (g/cm^3)	1.974	1.949	1.954	1.645	1.794
T, K	173(2)	173(2)	173(2)	173(2)	173(2)
μ, mm^{-1}	5.433	5.458	6.580	3.909	5.708
λ source (Å)	0.71073	0.71073	0.71073	0.71073	0.71073
[a]*R(F)*	0.0191	0.0345	0.0302	0.0583	0.0586
[a]$R_w(F)^2$	0.0422	0.0863	0.0713	0.1174	0.1282
GoF	1.119	1.096	1.058	1.174	1.157

[a] $R = (\Sigma||F_O| - |F_C||/\Sigma|F_O|)$. $R_W = [\Sigma\varpi(|F_O^2| - |F_C^2|)^2/\Sigma\varpi(|F_O^2|^2]^1$

Table 5-3. Selected bond lengths (Å) and angles (deg) for compounds 1-5.

	1	**2**	**3**	**4**	**5**
Re(1)-O(1)	2.009(2)	2.030(4)	1.992(3)	2.024(6)	2.004(7)
Re(1)-O(2)	1.999(2)	2.031(4)	2.014(3)	2.022(4)	2.008(7)
Re(1)-O(3) (Re=O)	1.693(2)	1.714(4)	1.689(4)	---	---
Re(1)-O(4) (Re-O-Re)	---	1.9236(3)	---	---	1.8385(4)[a]
Re(1)-N(1)	2.062(2)	2.067(4)	2.065(4)	2.025(8)	2.047(9)
Re(1)-N(2)	2.073(2)	2.057(5)	2.072(4)	2.038(7)	2.024(9)
Re(1)-Cl(1)	2.4401(6)	---	---	---	---
Re(1)-N(3) (Re-NCS)	---	---	2.087(4)	2.100(8)	2.13(1)
Re(1)-P(1)	---	---	---	2.429(2)	---
O(1)-Re(1)-O(2)	82.57(7)	88.7(2)	82.9(1)	99.0(2)	98.6(3)
O(1)-Re(1)-O(3) [O1-oxo]	169.97(8)	87.1(1)	104.1(2)	---	---
O(2)-Re(1)-O(3) [O2-oxo]	103.50(8)	89.5(1)	167.7(1)	---	---
O(1)-Re(1)-O(4) [O1-μ-O]	---	96.5(2)	---	---	91.0(2)
O(2)-Re(1)-O(4) [O2-μ-O]	---	95.8(2)	---	---	92.1(2)
O(3)-Re(1)-O(4) [oxo-μ-O]	---	173.6(2)	---	---	---
O(1)-Re(1)-N(1)	93.65(7)	95.0(2)	---	91.9(3)	91.2(4)
O(2)-Re(1)-N(1)	92.76(7)	170.8(2)	94.6(1)	167.9(3)	170.2(4)
O(3)-Re(1)-N(1) [oxo-N1]	94.01(8)	82.3(2)	95.2(2)	---	---
O(4)-Re(1)-N(1) [μ-O-N1]	92.1(2)	---	---	87.6(3)	
O(1)-Re(1)-N(2)	80.51(7)	169.8(2)	160.1(2)	172.2(3)	171.0(3)
O(2)-Re(1)-N(2)	160.21(7)	93.3(2)	80.4(1)	88.7(3)	89.4(3)
O(3)-Re(1)-N(2) [oxo-N2]	94.74(8)	82.9(1)	94.3(2)	---	---
O(4)-Re(1)-N(2) [μ-O-N2]	---	93.2(2)	---	---	93.0(3)
N(1)-Re(1)-N(2)	78.20(7)	81.7(2)	78.3(2)	80.3(3)	80.8(4)
N(1)-Re(1)-N(3) [N1-NCS]	---	---	174.9(1)	87.8(3)	92.8(4)
N(2)-Re(1)-N(3) [N2-NCS]	---	---	98.5(2)	91.3(3)	88.7(4)
O(1)-Re(1)-Cl(1)	82.43(5)	---	---	---	---
O(2)-Re(1)-Cl(1)	89.00(5)	---	---	---	---
O(3)-Re(1)-Cl(1) [oxo-Cl]	89.64(6)	---	---	---	---
N(1)-Re(1)-Cl(1)	175.46(5)	---	---	---	---
N(2)-Re(1)-Cl(1)	98.83(6)	---	---	---	---
O(1)-Re(1)-N(3) [O1-NCS]	---	---	89.4(2)	88.3(3)	87.4(3)
O(2)-Re(1)-N(3) [O2-NCS]	---	---	81.0(1)	87.2(3)	87.7(3)
O(3)-Re(1)-N(3) [oxo-NCS]	---	---	88.9(2)	---	---
O(4)-Re(1)-N(3) [μ-O-NCS]	---	---	---	---	178.3(3)
O(1)-Re(1)-P(1)	---	---	---	83.3(2)	---
O(2)-Re(1)-P(1)	---	---	---	91.7(2)	---
N(1)-Re(1)-P(1)	---	---	---	94.8(2)	---
N(2)-Re(1)-P(1)	---	---	---	97.4(2)	---
N(3)-Re(1)-P(1) [NCS-P]	---	---	---	171.2(2)	---
Re(1)-O(3)-Re(2)	---	179.9(1)	---	---	180

[a]This oxygen is labeled as O3 in Figure 5 and in the .cif file. It is labeled here as O4 to simplify the table. All μ-O are labeled in this table as O4.

5.3.4.1 *cis*-[ReOCl(sal$_2$ibn)] · 3 CHCl$_3$ (1)

The X-ray crystal structure of **1** shows a Re(V)-sal$_2$ibn complex with a chloride coordinated in the *cis* position relative to the oxo group (Figure 5-2). The complex displays distorted octahedral geometry with respect to the rhenium. Both nitrogen donors and one of the oxygen donors from the Schiff base ligand coordinate the rhenium in the equatorial plane along with the chloride, with the rhenium lying about 0.2 Å above the plane toward the oxo group. The second sal$_2$ibn phenolic oxygen donor is coordinated *trans* to the oxo group. No lengthening of the Re-O single bond *trans* to the oxo group is

observed compared to the Re-O bond *cis* to the oxo group. The two Re-O bond distances are similar, which is typical for these complexes, and fall within the range observed for similar Re(V) complexes (1.973-2.079 Å).[71,78,79,94,98] The Re=O bond distance of 1.693 Å also falls within the range observed for similar structures (1.679-1.697 Å).[71,78,79,94,98] The O=Re-O angle is close to linear at 169.97º, which is common for these complexes.[71,78,79,94,98] The bite angles made by the ligand and the Re atom (*i.e.*, the N-Re-N and O1-Re1-N1 angles) tend to vary from 78.5-91.9º,[71,78,79,94,98] with those here just outside of this range, most likely because of the constraints of the backbone, which reduced the N-Re-N angle and expanded the O2-Re-N5 angle.

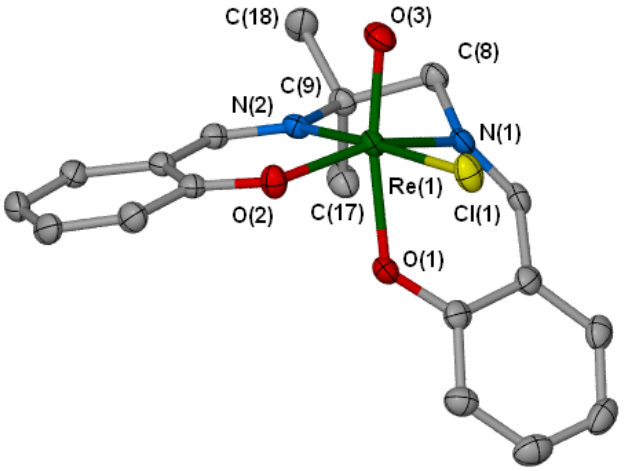

Figure 5-2. Thermal ellipsoid plot[70] of *cis*-[ReO(sal$_2$ibn)Cl] (**1**) with 50% probability ellipsoids (CCDC 933550). Hydrogens and solvent molecules are omitted for clarity.

5.3.4.2 *trans*-[μ-O(ReO(sal$_2$ibn))$_2$] · 4 CHCl$_3$ (2)

X-ray crystallography of **2** shows a neutral μ-oxo dimer, centrosymmetric about the bridging oxo group (Figure 5-3). The rhenium atoms are in an octahedral coordination environment, with the sal$_2$ibn ligand in the equatorial plane around the rhenium center and a capping oxo group *trans* to the bridging oxo. The two sal$_2$ibn ligands are oriented with the backbone methyl groups on opposite sides (*i.e.*, two N's of one ligand are situated above two O's of the other) to minimize steric crowding. The

ligand itself is chemically unchanged aside from deprotonation of the phenolic groups. The imine bonds are intact, with an average C=N bond length of 1.272(8), typical for a C=N double bond. Each of the Re atoms is situated above the plane of the ligand, toward their respective capping oxo group, by about 0.16 Å. The angles between bonds formed by the chelating ligand are within the range found for similar structures. The average O-Re-N angle is more obtuse at 93.5° and the N-Re-N angle is more acute at 81.6°. The oxo-rhenium multiple bond falls within the range of 1.665-1.711 Å.[70,71,78,91,98,113] As expected, the bridging oxo-rhenium single bond is slightly longer with a range of 1.9102-2.076 Å.[70,91,98,113] Lastly, the rhenium bonds to the ligand are within the range set by similar structures, with the Re-O bond having a range of 1.964-2.12 Å, and the Re-N bond having a range of 1.99-2.131 Å.[70,71,78,91,98,113] The bond lengths and angles of **2** are listed in Table 5-3.

The planes of the ligands are approximately 3.5 Å apart. The isobutylene backbone of the ligand is in a conformation placing the methyl group corresponding to C18A in a pseudo-axial position, parallel to the capping oxo, and the second methyl (C17A) in a pseudo-equatorial position, directed away from the complex. The complex is packed together in such a way that the axis of every other complex is offset by 50°, with pseudo-equatorial methyl and aryl hydrogen contacts of 2.9 Å.

Compound **2** was also isolated in the same space group with different unit cell dimensions due to different solvent molecules as *trans*-[μ-O(ReO(sal_2ibn))$_2$] · 3 $CHCl_3$ and *trans*-[μ-O(ReO(sal_2ibn))$_2$] · 2 CH_2Cl_2. Only minor differences were observed in bond lengths and angles.

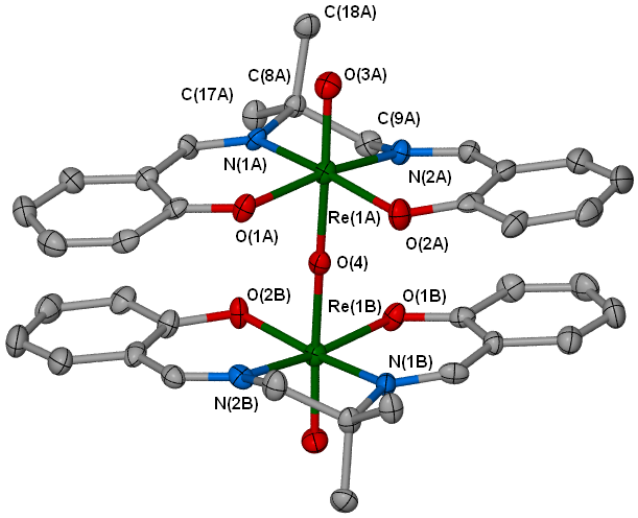

Figure 5-3. Thermal ellipsoid plot[70] of *trans*-[μ-O(ReO(sal$_2$ibn))$_2$] (**2**) with 50% probability ellipsoids (CCDC 933551). Hydrogens and solvent molecules are omitted for clarity.

5.3.4.3 *cis*-[ReO(NCS)(sal$_2$ibn)] (3)

X-ray crystallographic data of **3** shows a Re(V)-sal$_2$ibn complex with a isothiocyanate ligand coordinated *cis* relative to the oxo group (Figure 5-4). The geometry around the Re center is similar to that observed in **1**, where the nitrogen donors and one of the oxygen donors from the Schiff base ligand coordinate the rhenium in the equatorial plane along with the isothiocyanate. The rhenium is about 0.2 Å above the equatorial plane toward the oxo group. All bond lengths between the Re and the sal$_2$ibn ligand are similar to literature values. The Re=O bond distance is 1.698 Å, which falls within the range of literature values.[71,78,79,94,98] The thiocyanate ligand is close to linear, with an N-C-S bond angle of 179.9^o. The Re-C-N bond angle of the thiocyanate ligand is also close to linear (174.7^o), as typically observed for transition metals.[79] The Re-NCS (2.087 Å) bond is slightly longer than the Re-N bonds associated with the sal$_2$ibn ligand, but is typical for Re(V) complexes with a coordinated isothiocyanate.[79,114]

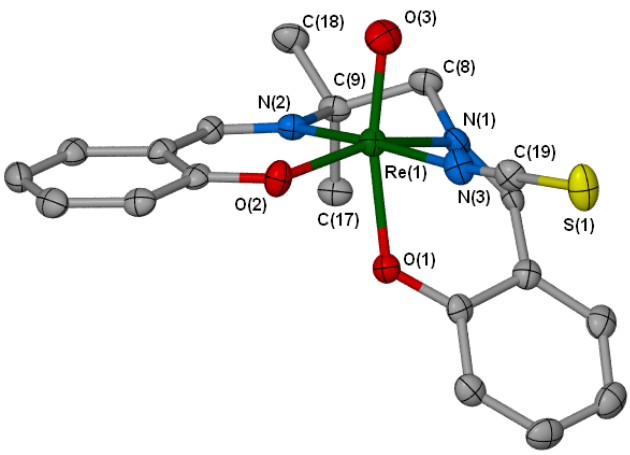

Figure 5-4. Thermal ellipsoid plot[70] of *cis*-[ReO(NCS)(sal_2ibn)] (**3**) with 50% probability ellipsoids (CCDC 933552). Hydrogens are omitted for clarity.

5.3.4.4 *trans*-[Re(NCS)(PPh_3)(sal_2ibn)] (4)

Complex **4** displays a distorted octahedral coordination environment with the triphenylphosphine coordinated *trans* to the thiocyanate (Figure 5-5). The bond angles about the Re(III) center are near expected values, with angles for the *cis* and *trans* ligands approximately 80-99 and 171°, respectively. The metal center itself is pulled slightly out of the equatorial plane towards the phosphine by 0.05 Å. The Re-O (2.011-2.012 Å) and the Re-N (2.030-2.042 Å) bond distances from the sal_2ibn are consistent with other Re(III) oxo Schiff base complexes.[71,78,79,94,98,115,116] The thiocyanate ligand is close to linear, with an N-C-S bond angle of 179.2°. The Re-N-C bond angle is further from linear (166.9°) and angles towards the pseudo-equatorial methyl group and is typical for similar Re and Tc systems reported in the literature. The Re-NCS (2.097 Å) bond is within typical ranges for Re(V) complexes with a coordinated thiocyanate and is on the long end of the reported Re-NCS and Tc-NCS bond distances for Re(III) complexes.[79,117–121] The Re-P (2.424 Å) bond distance is comparable to those observed in other Re(III) complexes.[71,78,122–125]

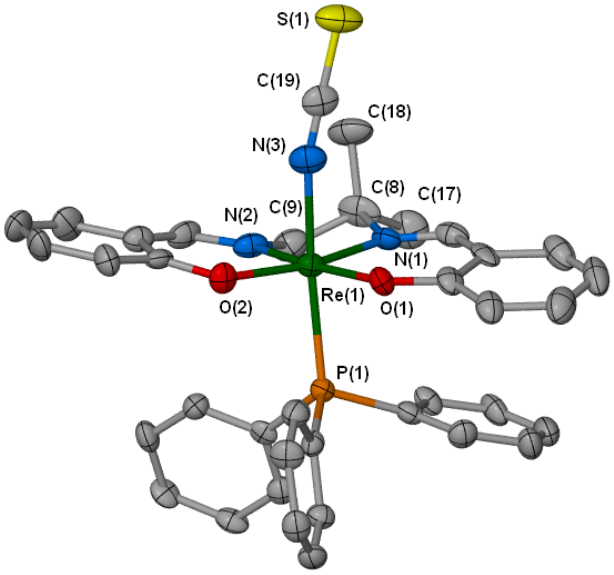

Figure 5-5. Thermal ellipsoid plot[70] of *trans*-[Re(NCS)(PPh_3)sal_2ibn] (**4**) with 50% probability ellipsoids (CCDC 933553). Hydrogens are omitted for clarity.

5.3.4.5 *trans*-[μ-O(Re(NCS)(sal_2ibn))$_2$] · 2 CH_3CN (5)

The structure of **5** (Figure 5-6) is of similar geometry to **2**, where two identical Re structures are bonded to a bridging oxo. Of the rare Re(IV) dinuclear complexes, this unusual compound is the first to not have terminal oxo groups, but rather thiocyanate ligands *trans* to the bridging oxo.[105,106,126] As in **4,** the thiocyanate ligands are near linear with N-C-S bond angles of 175.79° and the Re-NCS bond length (2.151 Å) is slightly longer than typically observed, and the Re-NCS bond angle (Re-N-C) deviates from linear (163.64°).[79,118,127,128] The two sal_2ibn ligands are positioned with the backbone methyl groups on opposite sides as in **2**. The planes of the ligands are on average 3.8 Å apart and are canted up or down on either side of the Re-O-Re bond. The Re metal center is pulled slightly out of the plane of the Schiff base ligands and toward the bridging oxo by 0.033 Å. The Re-μ-oxo (1.838 Å) bond distance is slightly longer than normal ranges for Re(V) complexes[70,78,91,98,113] and shorter than dinuclear Re(IV) complexes with bridging ligands other than an oxo moiety.[105,106,126] The Re-NCS bond distance of 2.13(1)

Å is longer than average literature values but still falls within the reported range, albeit literature values are from mixed metal complexes and NCS saturated Re coordination environments.[115,116,127–129]

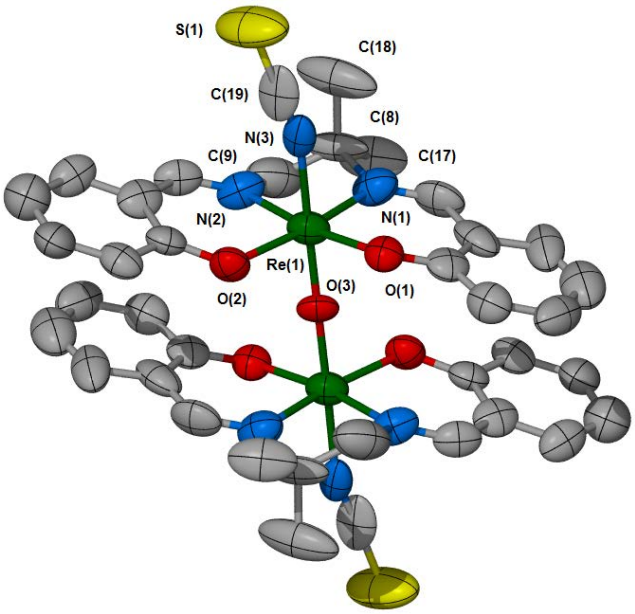

Figure 5-6. Thermal ellipsoid plot[70] of *trans*-[μ-O(Re(NCS)sal$_2$ibn)$_2$] (**5**) with 50% probability ellipsoids (CCDC 933554). Hydrogens are omitted for clarity. O3 is labeled as O4 in Table 4 to simplify the table.

5.4 Conclusions and Future Studies

Mononuclear rhenium Schiff base complexes convert to dinuclear species when water or base is present. The isolated mononuclear complex *cis*-[ReOCl(sal$_2$ibn)], **1**, readily dimerizes to form *trans*-[μ-O(ReO(sal$_2$ibn))$_2$], **2**, when exposed to the atmosphere. However, the mononuclear complex can be trapped and stabilized with thiocyanate as in **3**. Exposure of **3** to water for more than a week does not result in dimerization or decomposition as determined by ^{1}H-NMR. The thiocyanate coordination to the Re center in **3** is strong enough to resist displacement under refluxing acetonitrile and even upon reduction of the Re(V) center to Re(III) and Re(IV) by triphenylphosphine. However, the reduced Re-thiocyanate monophosphine complex

trans-[Re(NCS)(PPh_3)(sal_2ibn)], **4**, does not appear to be stable and undergoes conversion to several products. Complex **5**, *trans*-[μ-O(Re(NCS)(sal_2ibn))$_2$], is unique in that thiocyanates are in the terminal positions *trans* to the bridging oxo forming a linear X-Re-O-Re-X moiety, while other dinuclear Re(III) and Re(IV) complexes bridged by at least one oxo have the site that is *trans*/axial occupied by an oxo or a chelating ligand or form nonlinear moieties. These studies indicate that the chemistry of rhenium with Schiff base ligands can be very complex and have implications for potential nuclear medicine applications. The aqueous stability observed for *cis*-[ReO(NCS)(sal_2ibn)], **3**, makes this Re(V) complex useful for translation to the radiotracer level for potential radiotherapy using $^{186/188}$Re.

CHAPTER 6: TECHNETIUM SCHIFF BASE CHEMISTRY

6.1 Introduction

The majority of technetium research performed is with ^{99m}Tc, primarily because of the utility of ^{99m}Tc radiopharmaceutical imaging agents.[47–49,51,66] However, ^{99}Tc, with its 2.1 x 10^5 year half-life is of major concern as the daughter of ^{99m}Tc and as a significant fission product of nuclear reactors. The long-lived isotope can lend structural information that cannot be achieved on the tracer level, which is useful for both environmental concerns and pharmaceutical applications. There was a great deal of radioactive waste deposited into the environment from the nuclear arms race, and in order to sequester many of the radioactive elements, chelators, reducing agents, and other chemicals were introduced into the holding tanks along with the radioactive material.

Chelating agents such as N_2O_2 Schiff bases are of interest for two reasons. They can represent possible chelating agents used when attempts were made to cleanup nuclear waste and for complexing ^{99m}Tc in the field of nuclear medicine. ^{99m}Tc-Schiff base complexes, more commonly known as the "Q-series", have been investigated for use as single photon emission computed tomography (SPECT) imaging agents.[83,84]

The current work involves the synthesis and characterization of the first dinuclear Tc(IV) complex with a single bridging oxo group of which we are aware. Complexes of Tc(IV) are relatively limited in number when compared to the neighboring oxidation states. Many of the Tc(IV) compounds exhibit structural features with the $[Tc(\mu\text{-}O)_2Tc]^{4+}$ core. The chemistry of Tc(IV) compounds in water is very limited as many hydrolyze and form TcO_2, which is one of the thermodynamically stable forms of Tc(IV).

6.2 Experimental Section

6.2.1 Materials

Unless noted, all common laboratory chemicals were of reagent grade or better. NMR spectra were recorded on a Brüker DRX500 or DRX600 at 25^{o}C in CD_2Cl_2 or CD_3CN with TMS as an internal standard. Infrared spectra were obtained as KBr pellets on a Thermo Nicolet Nexus 670 FT-IR spectrometer.

Caution! Technetium-99m emits a 140 keV γ-ray with a half-life of 6.0 hours and ^{99}Tc emits a 0.294 MeV β^-_{max} with a half-life of $2.1x10^5$ years. All operations were carried out in radiochemical laboratories equipped and approved for handling these radionuclides.

Technetium-99m was eluted as sodium pertechnetate from a ^{99}Mo/^{99m}Tc generator (Covidien) using saline. Technetium-99 was obtained from Oak Ridge National Laboratory as ammonium pertechnetate. The material was black due to the formation of TcO_2. Prior to use, the material was refluxed in hydrogen peroxide for 1 hour to regenerate pertechnetate and then to destroy excess H_2O_2. The peroxide level was checked with Quantofix peroxide indicator strips.

Salicylaldehyde and 1,2-diamino-2-methylpropane were purchased from Sigma Aldrich and used as received. Absolute ethanol was used as purchased unless otherwise noted. TLC saturation pads were purchased from Aldrich Chemical Co. (*n*-$Bu_4N)[TcOCl_4]$ was prepared by the literature method.[130] The ligand α,α'-[(1,1-dimethylethylene)dinitrilo]di-*o*-cresol (sal_2ibnH_2) (Figure 6-1) was prepared as previously reported through condensation of two equivalents of salicylaldehyde with one equivalent of 1,2-diamino-2-methylpropane in absolute ethanol.[131] The purity of the

starting materials was verified by ^{1}H NMR and FT-IR spectroscopies. Sal_2ibnH_2 was recrystallized from absolute ethanol prior to use. 4,4'-((1*E*,1'*E*)-(ethane-1,2-diylbis(azanylylidene))bis(methanylylidene))bis(2,2,5,5-tetramethyl-2,5-dihydrofuran-3-ol) (tmf_2enH_2) (Figure 6-1) was gifted by Mallinckrodt Medical (St. Louis).

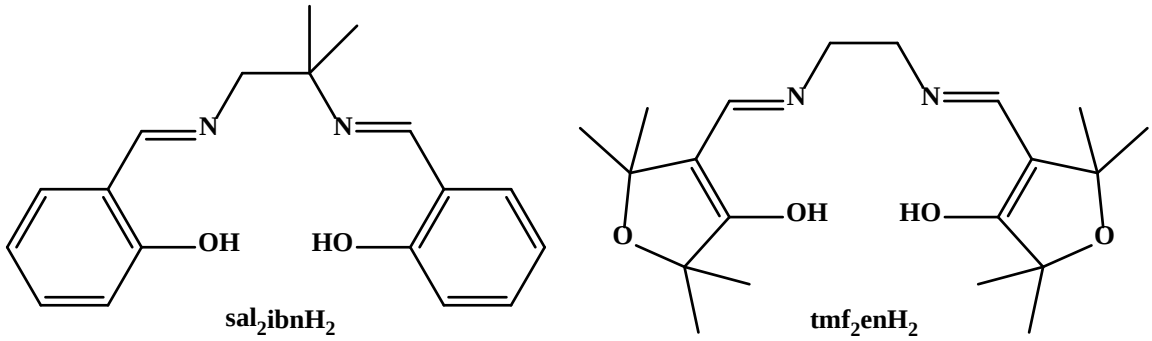

sal_2ibnH_2 **tmf_2enH_2**

Figure 6-1. Structures of sal_2ibnH_2 and tmf_2enH_2.

6.2.2 Preparation of [*trans*-(μ-O($Tc^{IV}Cl(sal_2ibn)$)$_2$)] · 3 $(CH_3)_2CO$ (1)

(*n*-Bu_4N)[$TcOCl_4$] (0.045 g, 0.0905 mmol) was dissolved in absolute ethanol (10 mL) in a 20 mL vial open to the atmosphere. Sal_2ibnH_2 (0.0339 g, 0.1145 mmol) was dissolved separately in absolute ethanol (5 mL) and then added to the $TcOCl_4^-$ solution to give a maroon solution. The solution was stirred while capped at room temperature for several hours. The solvent was evaporated and the solid dissolved in acetone. X-ray quality crystals were obtained by allowing the solution to stand at room temperature loosely capped for several days. Yield 54.9 % (0.026 g). ^{1}H NMR [500 MHz, CD_2Cl_2, r.t., δ (ppm)]: 19.63 (s, 2H, -**H**C=N-), 19.49 (s, 2H, -**H**C=N-) 7.56 (t, 2H, Ar**H**), 7.33 (d, 2H, Ar**H**), 7.06 (t, 4H, Ar**H**), 5.87 (d, 2H, Ar**H**), 5.74 (d, 2H, Ar**H**), 5.63 (t, 2H, Ar**H**); 5.19 (t, 2H, Ar**H**); 2.72 (m, 2H, C**H**$_2$), 2.21 (m, 2H, C**H**$_2$), 1.20 (s, 6H, C(C**H**$_3$)); 1.06. (s, 6H, C(C**H**$_3$)). FT-IR (KBr pellet, ν/cm^{-1}): 1597 (C=N); 751 (Tc-O-Tc).

6.2.3 Preparation of [*cis*-(TcO(NCS)sal$_2$ibn)] (2)

(n-Bu$_4$N)[TcOCl$_4$] (0.031 g, 0.0623 mmol) and sal$_2$ibnH$_2$ (0.0271 g, 0.0781 mmol) were dissolved separately in absolute ethanol (10 and 5 mL, respectively) in air at room temperature. The ligand solution was added slowly to the $TcOCl_4^-$ solution to give a maroon solution. After 15 minutes, (Bu$_4$N)NCS (0.041 g, 0.0781 mmole) was added as a 3 mL solution in absolute ethanol. There was no immediate observable reaction. The maroon solution was allowed to stir overnight. Black solid lined the walls and floor of the vessel. The mixture was filtered through Celite to give a dark fuchsia filtrate (which was saved for later use) and a dark solid on the Celite. The solid was washed three times with diethyl ether (3 mL aliquots) and finally dissolved from the Celite with CH_3CN (10 mL). X-ray quality crystals were obtained from the dissolved sample by allowing the solution to stand at room temperature loosely capped for several days. Yield 71.0 % (0.022 g). ^{1}H NMR [500 MHz, CD_2Cl_2, r.t., δ (ppm)]: 8.98 (s, 1H, -C**H**=N-); 8.85 (s, 1H, -**H**C=N-); 6.87 – 7.83 (m, 8H, Ar**H**); 4.35 (s, 2H, -NC**H$_2$**-C(CH$_3$)); 2.09 (s, 3H, C(C**H$_3$**)); 1.956. (s, 3H, C(C**H$_3$**)). ^{13}C NMR [500 MHz, CD_2Cl_2, r.t., δ (ppm)]: 179.02, 172.87 (**Ar**-O); 170.09, 169.43 (-H**C**=N-); 136.53, 120.71, 120.12, 119.53, 118.95, 116.31, 114.26, 113.38, 112.79 (**Ar**); 76.25 (-N**C**H$_2$-C(CH$_3$)$_2$); 72.94 (-NCH$_2$-**C**(CH$_3$)$_2$); 25.15, 23.51 (C(**C**H$_3$)). FT-IR (KBr pellet, ν/cm^{-1}): 2052 (NCS); 1599 (C=N); 949 (Tc≡O)

6.2.4 Preparation of (*n*-Bu$_4$N)$_2$[*trans*-((TcClsal$_2$ibn)μ-O(Tc(NCS)$_5$))] · (CH$_3$)$_2$CO (3)

This compound was a second product isolated from the reaction that formed compound **2**. The dark fuchsia filtrate from the aforementioned reaction was collected and taken to dryness. The resulting solid was dissolved in acetone and allowed to stand at room temperature loosely capped. X-ray quality crystals were obtained within several

days. Yield 22.8 % (0.008 g). FT-IR (KBr pellet, ν/cm^{-1}): 2106 and 2059 (NCS); 1600 (C=N); 754 (Tc-O-Tc).

6.2.5 Preparation of [^{99m}TcOX(sal_2ibn)]

100 μL of sal_2ibnH_2 stock solution (1 mg/mL in DI H_2O), 100 μL of sodium tartrate (1 mg/mL in DI H_2O), 100 μL DI H_2O, and 400 μL of acetonitrile were added to a reaction vial. 30 μL of a saturated stannous tartrate solution were added to the reaction vial. Finally, 300 μL of sodium [^{99m}Tc]pertechnetate (1.3 mCi) in saline solution was added to the vial. The reaction was heated to 70º for 30 minutes.

The reactions that were prepared with NCS proceeded as follows. After 30 minutes, 100 μL of *n*-Bu_4N(NCS) (1 mg/mL solution in acetonitrile) was added. The reaction was heated for another 20 minutes.

HPLC was used to verify and purify the complex. The column used was a Betabasic-18 column with a length of 150 mm, diameter of 4.6 mm, and a particle size of 5 μm (Thermo Scientific, Waltham, MA). The gradient used was 5-50 % acetonitrile in H_2O acid over 35 minutes.

The desired complex was purified by HPLC by collecting the fraction from 27-30 minutes and drying under a stream of nitrogen gas. This eliminated any reaction components that were in excess during the reaction. The product was then dissolved in 50% acetonitrile in water. HPLC was used to track the stability of the complex with time points at 1, 4, and 24 hours. Studies were done to investigate the stability of the complex over time comparing reactions with and without NCS^-.

6.2.6 Preparation of *trans*-TcOX(tmf_2en)

Tmf_2enH_2 (0.015 g, 0.04 mmol) was dissolved in 2 mL of ethanol. In a separate vial, (n-Bu_4N)[$TcOCl_4$] (0.02 g, 0.04 mmol) was dissolved in 2 mL of ethanol. The $[TcOCl_4]^-$ solution was added to the tmf_2enH_2 solution. A deep purple solution resulted. The reaction mixture was dried in a centrifan under N_2. The residue was re-dissolved in EtOH and loaded onto a silica gel column equilibrated in CH_2Cl_2. The column was first flushed with CH_2Cl_2. The product was then eluted with 30% ACN in CH_2Cl_2 as a purple solution. Radiochemical yield 53% (determined by Radio-TLC performed in 20% ACN in CH_2Cl_2). ^{1}H NMR [600 MHz, CD_2Cl_2, r.t., δ (ppm)]: 7.54 (s, 2H, -C**H**=N-); 4.53 (s, 2H, -C**H$_2$**-); 4.22 (s, 2H, -C**H$_2$**-); 1.53 (s, 6H, -C**H$_3$**); 1.49 (s, 6H, -C**H$_3$**); 1.43 (s, 6H, C**H$_3$**); 1.37 (s, 6H, -C**H$_3$**). ^{13}C NMR [600 MHz, CD_2Cl_2, r.t., δ (ppm)]: 199.06, 198.85 (**C**-O); 158.11 (-H**C**=N-); 118.14, 117.81 (**C**(CH=N); 83.10, 80.45 (**C**H_2); 32.03, 31.51, 27.28, 27.15 (**C**H_3). FT-IR (KBr pellet, ν/cm^{-1}): 1597 (C=N); 951 (Tc≡O).

6.2.7 X-Ray Characterization

Intensity data were obtained at -100 ^{0}C on a Brüker APEX II CCD Area Detector system using the ω scan technique with Mo Kα radiation from a graphite monochromator. Intensities were corrected for Lorentz and polarization effects. Equivalent reflections were merged, and absorption corrections were made using the multi-scan method. Space group, lattice parameters, and other relevant information are given in Table 6-1. The structures were solved by direct methods with full-matrix least-squares refinement, using the SHELX package.[103] All non-hydrogen atoms were refined with anisotropic thermal parameters. The hydrogen atoms were placed at calculated

positions and included in the refinement using a riding model, with fixed isotropic *U*. The final difference maps contained no features of chemical significance.

6.3 Results and Discussion

6.3.1 Synthesis of Tc(IV) dinuclear complex

The formation of *trans*-[μ-O(Tc^{IV}Cl(sal_2ibn))$_2$], compound **1**, from the reaction of (Bu_4N)[$TcOCl_4$] and sal_2ibnH_2 was unexpected as this complex has been reduced from Tc(V) to Tc(IV) without the addition of a reducing agent. We postulate that the mononuclear complex [TcOCl(sal_2ibn)] was first synthesized and then disproportionated to form TcO_4^- and [*trans*-(μ-O(Tc^{IV}Cl(sal_2ibn))$_2$)]. This hypothesis is corroborated by the 50% yield of **1** and the formation of black insoluble precipitate, TcO_2. It is well established that Tc(V) complexes will undergo disproportionation upon standing in solution.[33,132–134] Another possibility for the formation of the reduced species could stem from the Tc starting material. The starting material may have contained some $TcCl_6^{2-}$ as this complex is the thermodynamic end product in the reaction of concentrated HCl with TcO_4^-, the reagents used to prepare (Bu_4N)[$TcOCl_4$].[132,135–139]

6.3.2 Synthesis of Tc(V) mononuclear and dinuclear Tc complexes with thiocyanate

Addition of thiocyanate to the ^{99}Tc-sal_2ibn reaction produced both the *cis*-[Tc^{V}O(NCS)sal_2ibn], **2**, and a unique dinuclear species, (Bu_4N)[*trans*-(($TcClsal_2ibn$)μ-O(Tc($NCS)_5$))], **3**. The two products were separated by silica gel chromotography and characterized. The yield of **2** increased the longer $[TcOCl_4]^-$ was allowed to react with sal_2ibnH_2, suggesting that [TcOCl(sal_2ibn)] was initially formed and the labile chloride was displaced with the thiocyanate. The formation of **2** is similar to chemistry that was explored between NCS^- and Re Schiff base complexes in Chapter 5. Aqueous stability of

the mononuclear $Tc^{V}O(NCS)sal_2ibn$ was performed in a 50/50 mix of acetonitrile in DI H_2O. The acetonitrile was used to keep the complex in solution. No degradation was evident by ^1H NMR after 24 hours.

The formation of the asymmetric dinuclear Tc complex, **3**, was unexpected. The yield of **3** increases when NCS^- is added directly after sal_2ibnH_2, suggesting that the Tc did not have adequate time to react with sal_2ibnH_2. The complex could be Tc(IV)/Tc(IV) or a mixed valent Tc(V)/Tc(III) complex. The majority of Tc(V) complexes have multiply bonded groups to Tc (i.e., Tc≡O or Tc≡N). The bond lengths, discussed in the crystallographic section, do not help with the oxidation state assignment as there are very few Schiff base complexes of technetium with thiocyanate groups and many of the Tc-NCS complexes reported are mixed valent.[121,140,141]

6.3.3 Synthesis of Tc-tmf_2en product

Addition of tmf_2enH_2 to $TcOCl_4^-$ yielded *trans*-$TcOX(tmf_2en)$. This product was supported by NMR and IR data. The ^1H NMR showed a nearly symmetrical complex, with each of the peaks shifting downfield with respect to the ligand starting material, indicating the ligand is coordinating in the equatorial plane of the Tc metal center. The complex remained dark purple when in non-coordinating solvents, such as CH_2Cl_2. When dissolved in H_2O the complex turns deep red, indicating a ligand exchange (e.g., Cl^- exchanged with H_2O). No degradation was detected by ^1H NMR, indicating the complex remained stable in aqueous solutions.

6.3.4 General Characterization

The FT-IR spectra of all complexes showed the expected Schiff base C=N stretches between 1597 – 1600 cm^{-1}. The spectrum of the dinuclear μ-oxo-technetium

complexes showed the presence of the Tc-O-Tc stretching frequency near 750 cm^{-1}, consistent with literature values.[92,142–146] The monomeric oxo-technetium(V) complexes showed the presence of the Tc≡O stretches near 935 cm^{-1}, and absence of the Tc-O-Tc.[77,142] The thiocyanate-containing complexes exhibited NCS stretches from 2050 – 2110 cm^{-1}, consistent with literature values.[140,141,147]

6.3.5 X-Ray Crystal Structures

X-ray quality crystals were obtained for [*trans*-(μ-O(Tc^{IV}Cl(sal_2ibn))$_2$)] · 3 $(CH_3)_2CO$ (**1**), [*cis*-(TcO(NCS)sal_2ibn)] (**2**), and (n-$Bu_4N)_2$[*trans*-((TcClsal$_2$ibn)μ-O(Tc$(NCS)_5$))] · $(CH_3)_2CO$ (**3**) (Figures 6-2 to 6-4). Each complex exhibited distorted octahedral geometry around the Tc center. The ligand occupies the equatorial plane in the two dinuclear complexes (**1** and **3**). The mononuclear complex (**2**) has an isothiocyanate ligand bound *cis* to the Tc≡O bond; this forces one of the oxygen donors of the Schiff base to coordinate *trans* to the Tc≡O bond. Space group, lattice parameters, and other relevant information are given in Table 6-1. Relevant bond lengths and angles are given in Table 6-2.

6.3.5.1 *trans*-[μ-O(Tc^{IV}Cl(sal_2ibn))$_2$] · 3 $(CH_3)_2CO$ (1)

The X-ray crystal structure of **1** shows a neutral dinuclear, μ-oxo, Tc(IV)-sal_2ibn complex centrosymmetric about the bridging oxo group (Figure 6-2). A recurrent structural feature of Tc(IV) complexes is the $[Tc(\mu\text{-}O)_2Tc]^{4+}$ core, making complex **1** a rare example of a single μ-oxo dinuclear Tc(IV) complex.[104,143,144,148,149] The structure of **1** is nearly identical to the dinuclear Re(IV) complex from Chapter 5, *trans*-[μ-O(Re(NCS)(sal_2ibn))$_2$], with the exception of the axial ligands, in which chlorides replace the thiocyanate groups. In brief, the technetium atoms are in octahedral coordination

environments, where the sal_2ibn ligand is in the equatorial plane oriented with the backbone methyl groups on opposite sides, and a capping chlorides lies *trans* to the μ-oxo group. The Tc-Cl bond lengths average to 2.399 Å and are similar to those reported for other Tc(IV) complexes.[121,150] The Tc-N (sal_2ibn) bond lengths are shorter than dinuclear Tc(V)-N complexes and longer than mononuclear Tc(III)-N complexes.[77,142,143] The Tc-O (bridging) bond length of 1.838(3) Å is comparable to other Tc(IV) mono-oxo bridged complexes.[150] Tc(1) and Tc(2) are pulled out of the planes of the ligands towards the bridging oxo by 0.014 and 0.046 Å, respectively. The Tc(1)-O(5)-Tc(2) arrangement is nearly linear with an angle of 176.2° and is consistent with most mono-oxo bridging dinuclear Tc complexes.[151,152]

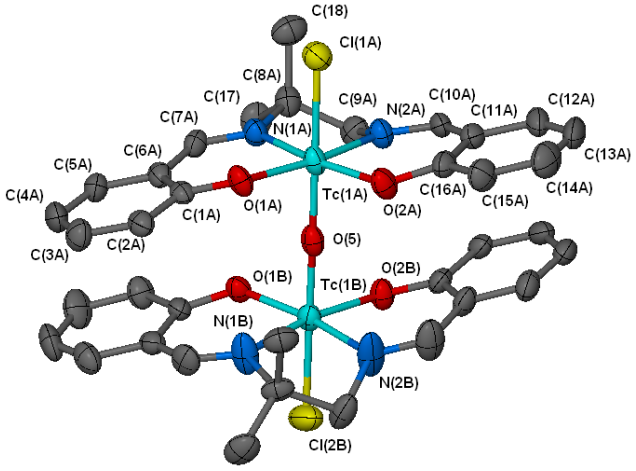

Figure 6-2. ORTEP representation of trans-[μ-O($TcCl(sal_2ibn)$)$_2$] (**1**). Thermal ellipsoids are shown with 50% probability. Hydrogens have been removed for clarity.

6.3.5.2 *cis*-[TcO(NCS)sal_2ibn] (2)

The coordination environment of **2** is similar to the previously discussed *cis*-[ReO(NCS)(sal_2ibn)] (Chapter 5). Complex **2** shows a Tc(V)-sal_2ibn complex with a thiocyanate ligand coordinated *cis* relative to the oxo group. Two nitrogen donors and one phenolic oxygen from the sal_2ibn ligand occupy the equatorial plane of the

technetium, and the second phenolic oxygen coordinated *trans* to the oxo group. The final equatorial coordination site is occupied by a thiocyanate moiety. The bond lengths between the metal center and the two phenolic oxygens are similar, with the axial position slightly longer, and are representative of Tc(V) mononuclear complexes.[121,143] The thiocyanate ligand is close to linear with an angle of 179.3° and the Tc-N-C bond angle is slightly distorted from linear with an angle of 175.1°, consistent with similar structures reported.[79,121,140] The Tc-NCS bond length (2.121 Å) is longer than those reported for Tc(III)-NCS complexes.[121,140,141] We were unable to find any bond lengths reported for Tc(V)-NCS complexes. Tc(1) is 0.186 Å out of the plane of the ligand towards the oxo, consistent with other Tc≡O complexes.

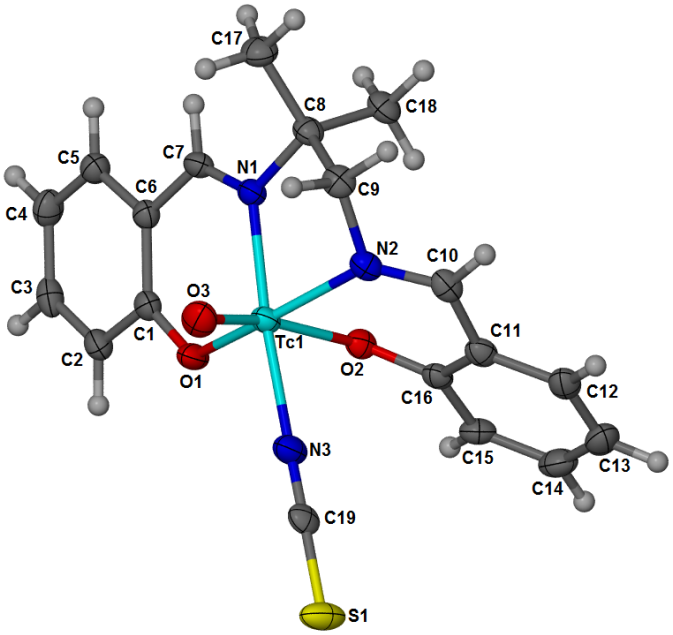

Figure 6-3. ORTEP representation of cis-[(TcO(NCS)sal$_2$ibn)] (**2**). Thermal ellipsoids are shown with 50% probability. Hydrogens have been removed.

6.3.5.3 (Bu$_4$N)$_2$[*trans*-((TcCl(sal$_2$ibn))μ-O(Tc(NCS)$_5$))] · (CH$_3$)$_2$CO (3)

Crystallographic data for **3** shows an asymmetric μ-oxo dinuclear complex. Both technetium atoms are arranged in an octahedral coordination environment. One

technetium has the equatorial plane coordinated by the sal_2ibn ligand and a chloro *trans* to the bridging oxo, whereas the second technetium is coordinated with five isothiocyanates. The Tc-Cl bond length (2.441 Å) is longer than those reported for Tc(IV)-Cl (average 2.338 Å) complexes and shorter than for Tc(V)-Cl (2.527) complexes, most likely as an effect from the chloride being *trans* to the bridging oxo group.[121,144,150] The bond lengths associated with sal_2ibn are within the range observed for mono- and dinuclear Tc(V) Schiff base complexes.[77,142,143] The bridging oxo is shared almost evenly between the two Tc centers but is slightly shorter towards Tc(1), consistent with a dinuclear system.[105–107] The second technetium has the equatorial plane occupied by four isothiocyanate ligands with an average Tc-N bond length of 2.04 Å, which is similar to literature Tc(II)-NCS (2.035(9) – 2.052(6) Å) and Tc(III)-NCS bond lengths (2.04(2) – 2.06(2) Å), as opposed to Tc(IV)-NCS (1.991(6) - 2.003(6) Å) and Tc(V)-NCS (2.045(4) – 2.162(9) Å) bond lengths. They are also very similar to those reported for Tc(II/III)-NCS complexes (2.042 Å), suggesting that the complex could potentially be Tc(V)/Tc(III).[77,121,140,141,144,150] The axial NCS, *trans* to an oxo, has a bond length of 2.093 Å, which is longer than those reported for Tc(II)-NCS, Tc(III)-NCS, and Tc(IV)-NCS complexes but falls within the range of Tc(V)-NCS complexes.

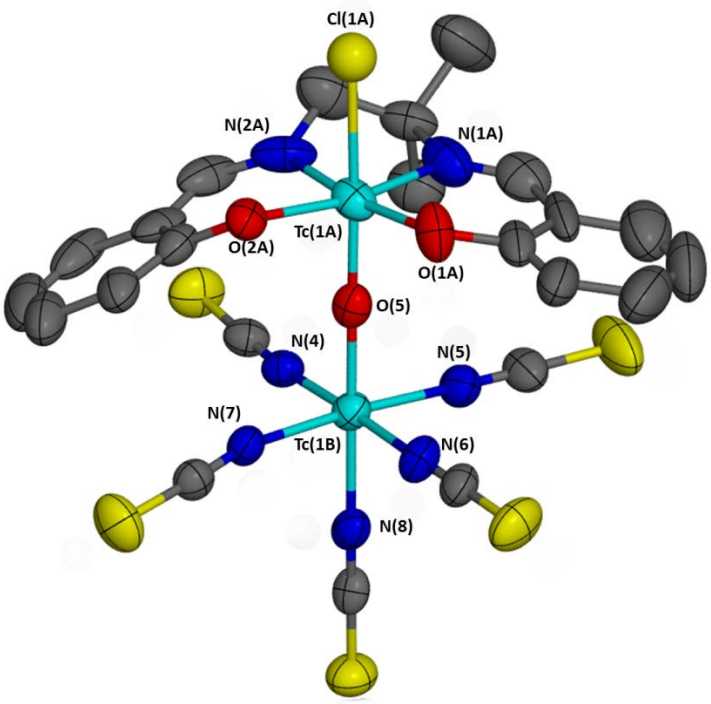

Figure 6-4. ORTEP representation of *trans*-[(TcClsal$_2$ibn)μ-O(Tc(NCS)$_5$)] (**3**). Thermal ellipsoids are shown with 50% probability. Hydrogens have been removed for clarity.

Table 6-1. X-ray Crystal Data, Data Collection Parameters, and Refinement parameters.

	1	**2**	**3**
Formula	$C_{45}H_{54}Cl_2N_4O_8Tc_2$	$C_{19}H_{18}N_3O_3STc$	$C_{20}H_{105}ClN_9O_{5.5}S_5Tc_2$
Fw	1045.82	466.43	1432.28
cryst syst	monoclinic	triclinic	monoclinic
space group	$P2_1/c$	*P-1*	$P2_1$/n
***a* (Å)**	14.418(1)	8.866(3)	13.2124(4)
***b* (Å)**	13.299(1)	9.496(3)	13.5231(5)
***c* (Å)**	23.792(2)	11.711(4)	39.5734(16)
α (deg)	90	95.214(4)	90
β (deg)	92.777(1)	97.199(4)	98.209(2)
γ (deg)	90	103.669(4)	90
V (Å^3)	4556.6(6)	943.1(6)	6998.3(4)
Z	4	2	4
ρ_{calcd} (g/cm^3)	1.524	1.642	1.359
***T*, K**	173(2)	173(2)	173(2)
μ, mm^{-1}	0.780	0.899	0.634
λ source (Å)	0.71073	0.71073	0.71073
***R(F)*^{a}**	0.0509	0.0292	0.0811
***R*$_w$*(F)*^{a}**	0.1275	0.0627	0.2133
GoF	1.026	1.045	1.035

Table 6-2. Selected bond lengths (Å) and angles (deg) for compounds **1**-**3**.

	1	**2**	**3**
Tc(1A)-O(1A)	2.000(3)	1.992(2)	1.983(5)
Tc(1A)-O(2A)	1.989(3)	2.006(2)	1.977(4)
Tc(1)-O(3)	---	1.666(2)	---
Tc(1A)-N(1A)	2.065(3)	2.060(2)	2.039(7)
Tc(1A)-N(2A)	2.053(3)	2.071(2)	2.084(6)
Tc(1)-N(3) (NCS)	---	2.121(2)	---
Tc(1A)-O(5) (Tc-O-Tc)	1.838(3)	---	1.829(4)
Tc(1A)-Cl(1A)	2.3996(12)	---	2.442(2)
Tc(1B)-O(1B)	1.979(3)	---	---
Tc(1B)-O(2B)	2.000(3)	---	---
Tc(1B)-N(1B)	2.071(4)	---	---
Tc(1B)-N(2B)	2.065(4)	---	---
Tc(1B)-O(5) (Tc-O-Tc)	1.829(3)	---	---
Tc(1B)-Cl(1B)	2.399(1)	---	---
Tc(1A)-O(5)-Tc(1B)	176.2(2)	---	178.7(3)
O(1A)-Tc(1A)-O(2A)	99.18(1)	83.04(7)	100.87(18)
O(1A)-Tc(1A)-O(5)	90.68(1)	---	92.2(2)
O(2A)-Tc(1A)-O(5)	92.52(1)	---	90.79(17)
O(1A)-Tc(1A)-N(1A)	90.75(1)	92.39(8)	92.2(3)
O(1A)-Tc(1A)-N(2A)	171.29(1)	160.33(8)	171.1(2)
O(1A)-Tc(1A)-Cl(1A)	88.89(9)	---	89.30(17)
O(2)-Tc-O(3)	---	104.49(9)	---
O(2A)-Tc(1A)-N(1A)	170.07(1)	96.36(7)	166.2(3)
O(2A)-Tc(1A)-N(2A)	89.14(1)	80.69(8)	87.3(2)
O(2A)-Tc(1A)-Cl(1A)	87.55(9)	---	87.81(13)
O(2)-Tc-O(3)	---	164.95(8)	---
O(5)-Tc(1A)-N(1A)	87.59(1)	---	93.1(2)
O(5)-Tc(1A)-N(2A)	90.38(1)	---	91.3(2)
O(5)-Tc(1A)-Cl(1A)	179.66(9)	---	178.12
N(1A)-Tc(1A)-N(2A)	80.66(1)	78.56(8)	79.4(3)
N(1)-Tc-N(3) (NCS)	---	175.55(8)	---
N(2)-Tc-N(3) (NCS)	---	98.00(8)	---
N(1A)-Tc(1A)-Cl(1A)	92.41(1)	---	87.94(19)
N(1)-Tc-O(3)	---	96.33(9)	---
N(2A)-Tc(1A)-Cl(1A)	89.95(1)	---	87.43(16)
N(2)-Tc-O(3)	---	93.94(9)	---
Cl(1A)-Tc(1A)-O(5)	179.66(9)	---	
O(1)-Tc-N3 (NCS)	---	90.02(8)	---
O(2)-Tc-N3 (NCS)	---	80.23(8)	---
O(3)-Tc-N3 (NCS)	---	86.67(9)	---
O(1B)-Tc(1B)-O(2B)	100.09(1)	---	---

O(1B)-Tc(1B)-O(5)	91.38(1)	---	---
O(2B)-Tc(1B)-O(5)	90.99(1)	---	---
O(1B)-Tc(1B)-N(1B)	89.66(1)	---	---
O(1B)-Tc(1B)-N(2B)	169.84(1)	---	---
O(1B)-Tc(1B)-Cl(2B)	88.62(9)	---	---
O(2B)-Tc(1B)-N(1B)	169.40(1)	---	---
O(2B)-Tc(1B)-N(2B)	89.95(1)	---	---
O(2B)-Tc(1B)-Cl(2B)	88.25(9)	---	---
O(5)-Tc(1B)-N(1B)	92.94(1)	---	---
O(5)-Tc(1B)-N(2B)	89.95(2)	---	---
O(5)-Tc(1B)-Cl(2B)	87.55(9)	---	---
N(1B)-Tc(1B)-N(2B)	80.22(1)	---	---
N(1B)-Tc(1B)-Cl(2B)	87.83(1)	---	---
N(2B)-Tc(1B)-Cl(2B)	90.19(2)	---	---
Cl(1B)-Tc(1B)-O(5)	179.23(9)	---	---
N(8)-Tc(1B)-N(4)	---	---	97.74(19)
N(8)-Tc(1B)-N(5)	---	---	88.1(2)
N(8)-Tc(1B)-N(6)	---	---	89.3(2)
N(8)-Tc(1B)-N(7)	---	---	88.2(2)
O(5)-Tc(1B)-N(8)	---	---	177.64(19)

6.3.6 Translation to tracer level

Several different tracer-level reactions to form the ^{99m}Tc-sal$_2$ibn complex were evaluated. When synthesizing the ^{99m}Tc-sal$_2$ibn complex on the tracer level, several conditions were attempted. Parameters that were varied include pH, reducing agent, solvent system, transchelating agent, time, and temperature. The best method involved using excess sodium tartrate with the stannous tartrate as well as keeping the pH around 5.5 in a solution of water and acetonitrile. The complex was purified by HPLC. Figure 6-5 shows the comparison of the HPLC chromatograms of TcOsal$_2$ibn reaction with NCS^- and ReO(NCS)sal$_2$ibn (Chapter 5). The product peaks have similar retention times, but they do not co-elute. This could be due to a different conformation (i.e., *cis* versus *trans* complexation) that takes place with technetium on the tracer level. Studies were done on the isolated ^{99m}TcOsal$_2$ibn complex to investigate the stability of the complex

over time comparing reactions with and without NCS^-. The reactions with NCS^- showed better stability after 4 hours, even maintaining some product out to 24 hours. The reactions with no NCS^- present showed much more degradation after 4 hours and no detectable product after 24 hours. Chromatograms are shown in Figure 6-6.

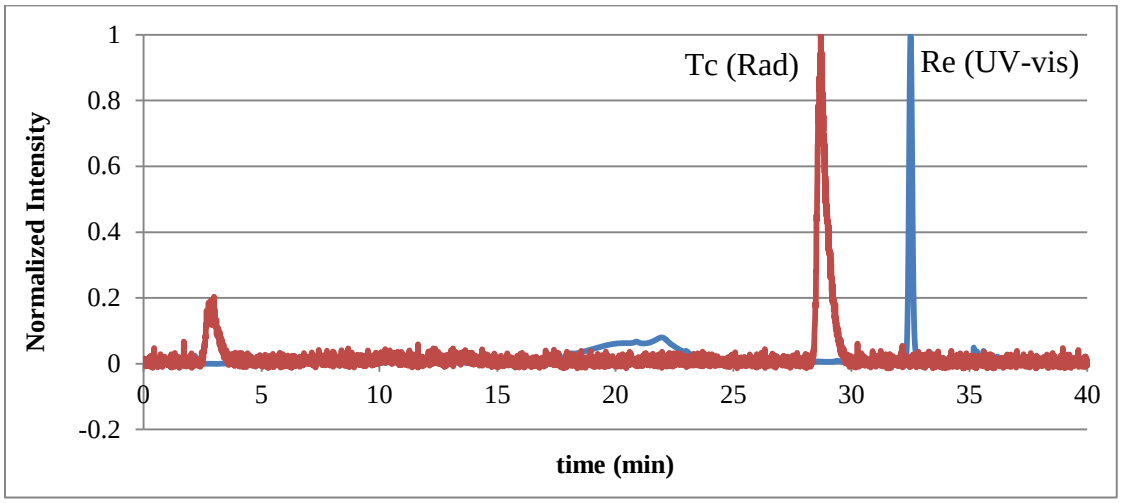

Figure 6-5. Overlaying HPLC chromatograms of ReO(sal2ibn)(NCS) (red line) and TcO(sal2ibn) with NCS-(blue line).

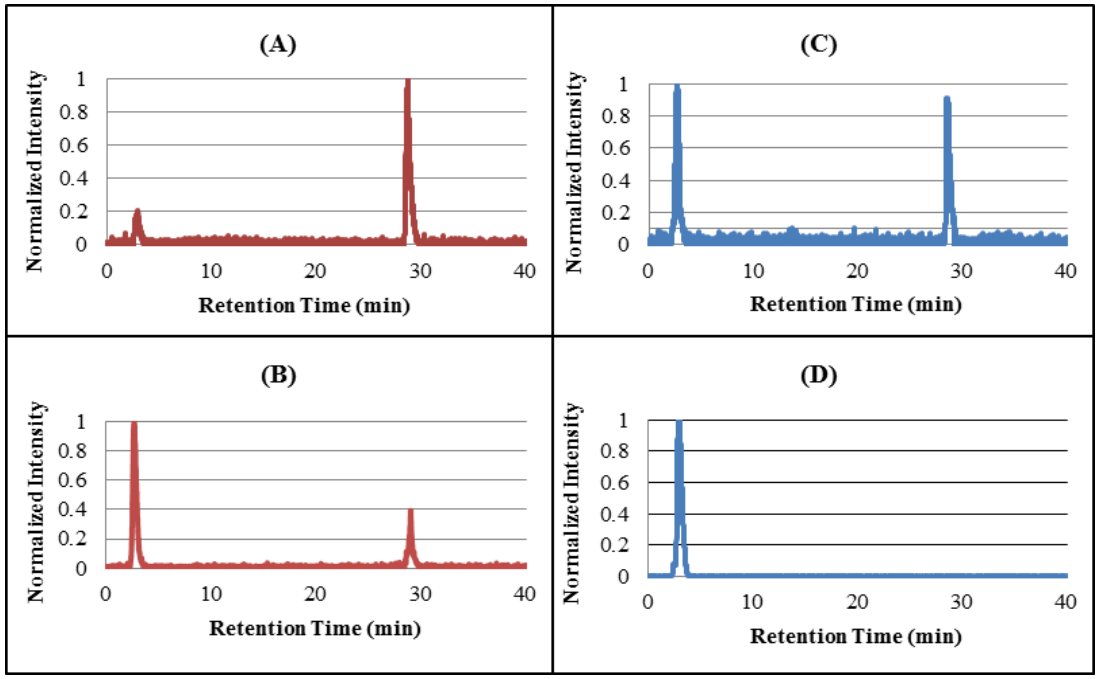

Figure 6-6. HPLC chromatograms of NCS^- stability studies. (A) Rad-HPLC of $TcO(sal_2ibn)$ w/ NCS^- at 4 hours; (B) Rad-HPLC of $TcO(sal_2ibn)$ w/ NCS^- at 24 hours; (C) Rad-HPLC of $TcO(sal_2ibn)$ w/o NCS^-- at 4 hours; (D) Rad-HPLC of $TcO(sal_2ibn)$ w/o NCS^- at 24 hours.

6.4 Conclusion and Future Studies

Experimentally, we have shown that ^{99}Tc forms a dinuclear species when reacted with sal_2ibnH_2 and NCS^-, but the mononuclear species can be isolated. Also, we can form the Tc-sal_2ibn complex on the tracer-level with ^{99m}Tc, which is more stable with the addition of NCS^-. Overall, like the $Re^{V}O(NCS)$ Schiff base complexes, the $Tc^{V}O(NCS)$ Schiff base complexes are shown to be more aqueous stable and seem to be less susceptible to degradation.

In the future, these reactions should be more thoroughly explored with the tmf_2enH_2. Tmf_2enH_2 is soluble in a wider variety of solvents, including water. Also, it would be interesting to investigate the reducing ability of HCl during the reaction by varying the concentration of HCl and comparing the yield of Tc(IV) complexes. This study would provide more understanding into the mechanism that led to the dinuclear complex with capping Cl^-.

COMBINED REFERENCES

(1) Shi, K.; Hou, X.; Roos, P.; Wu, W. Determination of Technetium-99 in Environmental Samples: A Review. *Anal. Chim. Acta* **2012**, *709*, 1–20.

(2) Curtis, D.; Fabryka-Martin, J.; Dixon, P.; Cramer, J. Nature's Uncommon Elements: Plutonium and Technetium. *Geochim. Cosmochim. Acta* **1999**, *63* (2), 275–285.

(3) Wildung, R. E.; McFadden, K. M.; Garland, T. R. Technetium Sources and Behavior in the Environment1. *J. Environ. Qual.* **1979**, *8* (2), 156.

(4) Boyd, G. E. Technetium and Promethium. *J. Chem. Educ.* **1959**, *36* (1), 3.

(5) Kotegov, K.; Pavlov, O.; Shvedov, V. *Advances in Inorganic Chemistry and Radiochemistry, Vol. 2*; Academic Press, New York, 1968.

(6) Luykx, F. Technetium Discharges into the Environment. In *Technetium in the Environment*; Desmet, G., Myttenaere, C., Eds.; Springer Netherlands, 1986; pp 21–27.

(7) Agency, F. S. *Radioactivity in Food and the Environment (RIFE) 2009 | Food Standards Agency*.

(8) Agency, F. S. *Radioactivity in Food and the Environment (RIFE) 2012 | Food Standards Agency*.

(9) Uchida, S.; Tagami, K.; Rühm, W.; Steiner, M.; Wirth, E. Separation of Tc-99 in Soil and Plant Samples Collected around the Chernobyl Reactor Using a Tc-Selective Chromatographic Resin and Determination of the Nuclide by ICP-MS. *Appl. Radiat. Isot.* **2000**, *53* (1–2), 69–73.

(10) Dahlgaard, H.; Chen, Q.; Herrmann, J.; Nies, H.; Ibbett, R. D.; Kershaw, P. J. On the Background Level of 99Tc, 90Sr and 137Cs in the North Atlantic. *J. Mar. Syst.* **1995**, *6* (5–6), 571–578.

(11) Attrep, M.; Enochs, J. A.; Broz, L. D. Atmospheric Technetium-99. *Environ. Sci. Technol.* **1971**, *5* (4), 344–345.

(12) García-León, M. 99Tc in the Environment: Sources, Distribution and Methods. *J. Nucl. Radiochem. Sci.* **2005**, *6* (3), 253–259.

(13) Tagami, K.; Uchida, S. Global Fallout Technetium-99 Distribution and Behavior in Japanese Soils. *J. Nucl. Radiochem. Sci.* **2002**, *3* (2), 1–5.

(14) Krijger, G. C.; Harms, A. V.; Leen, R.; Verburg, T. G.; Wolterbeek, B. Chemical Forms of Technetium in Tomato Plants; $TcO4^{-}$, Tc–cysteine, Tc–glutathione and Tc–proteins. *Environ. Exp. Bot.* **1999**, *42* (1), 69–81.

(15) Lembrechts, J.; Desmet, G. Reaction Mechanisms Responsible for Transformation of Pertechnetate in Photoautotrophic Organisms. *Health Phys.* **1989**, *57* (2), 255–262.

(16) Sheppard, S.; Evenden, W. Can Aquatic Macrophytes Mobilize Technetium by Oxidizing Their Rhizosphere? *J. Environ. Qual.* **1991**, *20* (4), 738–744.

(17) Manjón, G.; García-León, M.; Ballestra, S.; López, J. J. The Presence of Man-Made Radionuclides in the Marine Environment in the South of Spain. *J. Environ. Radioact.* **1995**, *28* (2), 171–189.

(18) Roh, C.; Kang, C.; Lloyd, J. R. Microbial Bioremediation Processes for Radioactive Waste. *Korean J. Chem. Eng.* **2015**, 1–7.

(19) McBeth, J. M.; Lear, G.; Lloyd, J. R.; Livens, F. R.; Morris, K.; Burke, I. T. Technetium Reduction and Reoxidation in Aquifer Sediments. *Geomicrobiol. J.* **2007**, *24* (3-4), 189–197.
(20) Fan, D.; Anitori, R. P.; Tebo, B. M.; Tratnyek, P. G.; Lezama Pacheco, J. S.; Kukkadapu, R. K.; Engelhard, M. H.; Bowden, M. E.; Kovarik, L.; Arey, B. W. Reductive Sequestration of Pertechnetate (99TcO4–) by Nano Zerovalent Iron (nZVI) Transformed by Abiotic Sulfide. *Environ. Sci. Technol.* **2013**, *47* (10), 5302–5310.
(21) Korte, N. E.; Muck, M. T.; Zutman, J. L.; Schlosser, R. M.; Liang, L.; Gu, B.; Siegrist, R. L.; Houk, T. C.; Fernando, Q. *In Situ Treatment of Mixed Contaminants in Groundwater: Application of Zero-Valence Iron and Palladized Iron for Treatment of Groundwater Contaminated with Trichloroethene and Technetium-99*; ORNL/TM--13530; Oak Ridge National Lab., Grand Junction, CO (United States), 1997.
(22) Cantrell, K. J.; Kaplan, D. I.; Wietsma, T. W. Zero-Valent Iron for the in Situ Remediation of Selected Metals in Groundwater. *J. Hazard. Mater.* **1995**, *42* (2), 201–212.
(23) Um, W.; Chang, H.-S.; Icenhower, J. P.; Lukens, W. W.; Serne, R. J.; Qafoku, N. P.; Westsik, J. H.; Buck, E. C.; Smith, S. C. Immobilization of 99-Technetium (VII) by Fe(II)-Goethite and Limited Reoxidation. *Environ. Sci. Technol.* **2011**, *45* (11), 4904–4913.
(24) Liu, Y.; Terry, J.; Jurisson, S. S. Pertechnetate Immobilization in Aqueous Media with Hydrogen Sulfide under Anaerobic and Aerobic Environments. *Radiochim. Acta* **2007**, *95* (12), 717–725.
(25) Thornton, E. .; Gilmore, T. j.; Olsen, K. b.; Giblin, J. t.; Phelan, J. m. Treatment of a Chromate-Contaminated Soil Site by in Situ Gaseous Reduction. *Ground Water Monit. Remediat.* **2007**, *27* (1), 56–64.
(26) Thornton, E. C.; Amonette, J. E. Hydrogen Sulfide Gas Treatment of Cr(VI)-Contaminated Sediment Samples from a Plating-Waste Disposal SiteImplications for in-Situ Remediation. *Environ. Sci. Technol.* **1999**, *33* (22), 4096–4101.
(27) Liu, Y.; Terry, J.; Jurisson, S. S. Potential Interferences on the Pertechnetate-Sulfide Immobilization Reaction. *Radiochim. Acta Int. J. Chem. Asp. Nucl. Sci. Technol.* **2009**, *97* (1), 33–41.
(28) Szecsody, J. E.; Truex, M. J.; Zhong, L.; McKinley, J. P.; Qafoku, N. P.; Lee, B. D.; Saurey, S. D. Remediation of Technetium in Vadose Zone Sediments Using Ammonia and Hydrogen Sulfide Gases. *Vadose Zone J.* **2015**.
(29) Blower, P. J.; Singh, J.; Clarke, S. E. The Chemical Identity of Pentavalent Technetium-99m-Dimercaptosuccinic Acid. *J. Nucl. Med. Off. Publ. Soc. Nucl. Med.* **1991**, *32* (5), 845–849.
(30) Frisch, M. J.; Trucks, G. W.; Schlegel, H. B.; Scuseria, G. E.; Robb, M. A.; Cheeseman, J. R.; Scalmani, G.; Barone, V.; Mennucci, B.; Petersson, G. A.; et al. *Gaussian~09 Revision D.01*.
(31) Leszczynski, J. *Handbook of Computational Chemistry*; Springer Science & Business Media, 2012.

(32) Gu, B.; Dong, W.; Liang, L.; Wall, N. A. Dissolution of Technetium(IV) Oxide by Natural and Synthetic Organic Ligands under Both Reducing and Oxidizing Conditions. *Environ. Sci. Technol.* **2011**, *45* (11), 4771–4777.
(33) Icenhower, J. P.; Qafoku, N. P.; Zachara, J. M.; Martin, W. J. The Biogeochemistry of Technetium: A Review of the Behavior of an Artificial Element in the Natural Environment. *Am. J. Sci.* **2010**, *310* (8), 721–752.
(34) Spies, H.; Scheller, D. Chemical and 1 H NMR Spectroscopic Investigations of Stereoisomeric Tc (V) DMSA Complexes. *Inorganica Chim. Acta* **1986**, *116* (1), 1–4.
(35) Demoin, D. W. Utilizing an Experimental and Computational Approach to Ligand Design for Chelating Oxorhenium(V) and Oxotechnetium(V), University of Missouri: Columbia, MO.
(36) Demoin, D. W.; Li, Y.; Jurisson, S. S.; Deakyne, C. A. Method and Basis Set Analysis of oxorhenium(V) Complexes for Theoretical Calculations. *Comput. Theor. Chem.* **2012**, *997*, 34–41.
(37) Li, Y.; Kreuer, J. A.; Demoin, D. W.; Jurisson, S. S.; Deakyne, C. A. Using Potential Energy Surface Scans to Examine the Bond Dissociation Energies of Trans-ReOS2N2 and [ReOS3N]1− Model Complexes. *Comput. Theor. Chem.* **2014**, *1048*, 25–34.
(38) Humphrey, W.; Dalke, A.; Schulten, K. VMD – Visual Molecular Dynamics. *J. Mol. Graph.* **1996**, *14*, 33–38.
(39) Smith, M. B.; March, J. Addition to Carbon–Carbon Multiple Bonds. In *March's Advanced Organic Chemistry*; John Wiley & Sons, Inc., 2006; pp 999–1250.
(40) Foster, R. F. HISTORY OF HANFORD AND ITS CONTRIBUTION OF RADIONUCLIDES TO THE COLUMBIA RIVER. *Pp 3-18 Columbia River Estuary Adjac. Ocean Waters Pruter T Ed Seattle Univ Wash. Press 1972* **1972**.
(41) Gephart, R. E.; others. *Hanford: A Conversation about Nuclear Waste and Cleanup.*; Battelle Press, 2003.
(42) Hua, B.; Deng, B. Reductive Immobilization of Uranium(VI) by Amorphous Iron Sulfide. *Environ. Sci. Technol.* **2008**, *42* (23), 8703–8708.
(43) Liu, Y.; Terry, J.; Jurisson, S. S. Pertechnetate Immobilization with Amorphous Iron Sulfide. *Radiochim. Acta Int. J. Chem. Asp. Nucl. Sci. Technol.* **2008**, *96* (12), 823–833.
(44) Fan, D.; Anitori, R. P.; Tebo, B. M.; Tratnyek, P. G.; Lezama Pacheco, J. S.; Kukkadapu, R. K.; Kovarik, L.; Engelhard, M. H.; Bowden, M. E. Oxidative Remobilization of Technetium Sequestered by Sulfide-Transformed Nano Zerovalent Iron. *Environ. Sci. Technol.* **2014**, *48* (13), 7409–7417.
(45) Banerjee, S.; Ambikalmajan Pillai, M. R.; Ramamoorthy, N. Evolution of Tc-99m in Diagnostic Radiopharmaceuticals. *Semin. Nucl. Med.* **2001**, *31* (4), 260–277.
(46) Drozdovitch, V.; Brill, A. B.; Callahan, R. J.; Clanton, J. A.; DePietro, A.; Goldsmith, S. J.; Greenspan, B. S.; Gross, M. D.; Hays, M. T.; Moore, S. C.; et al. Use of Radiopharmaceuticals in Diagnostic Nuclear Medicine in the United States: 1960–2010. *Health Phys.* **2015**, *108* (5), 520–537.
(47) Jurisson, S. S.; Lydon, J. D. Potential Technetium Small Molecule Radiopharmaceuticals. *Chem. Rev.* **1999**, *99* (9), 2205–2218.

(48) Schwochau, K. Technetium Radiopharmaceuticals—Fundamentals, Synthesis, Structure, and Development. *Angew. Chem. Int. Ed. Engl.* **1994**, *33* (22), 2258–2267.
(49) Jürgens, S.; Herrmann, W. A.; Kühn, F. E. Rhenium and Technetium Based Radiopharmaceuticals: Development and Recent Advances. *J. Organomet. Chem.* **2014**, *751*, 83–89.
(50) Jurisson, S.; Berning, D.; Jia, W.; Ma, D. Coordination Compounds in Nuclear Medicine. *Chem. Rev.* **1993**, *93* (3), 1137–1156.
(51) Carroll, V.; Demoin, D. W.; Hoffman, T. J.; Jurisson, S. S. Inorganic Chemistry in Nuclear Imaging and Radiotherapy: Current and Future Directions. *Radiochim. Acta* **2012**, *100* (8-9), 653–667.
(52) *The Chemistry of Molecular Imaging*; Long, N. J., Wong, W.-T., ebrary, Inc, Eds.; Wiley: Hoboken, New Jersey, 2015.
(53) Zeglis, B. M.; Houghton, J. L.; Evans, M. J.; Viola-Villegas, N.; Lewis, J. S. Underscoring the Influence of Inorganic Chemistry on Nuclear Imaging with Radiometals. *Inorg. Chem.* **2014**, *53* (4), 1880–1899.
(54) Wu, A. M.; Senter, P. D. Arming Antibodies: Prospects and Challenges for Immunoconjugates. *Nat. Biotechnol.* **2005**, *23* (9), 1137–1146.
(55) R. Dilworth, J.; J. Parrott, S. The Biomedical Chemistry of Technetium and Rhenium. *Chem. Soc. Rev.* **1998**, *27* (1), 43.
(56) Prekeges, J.; others. *Nuclear Medicine Instrumentation*; Jones & Bartlett Publishers, 2012.
(57) Friedlander, G.; Macias, E. S.; Kennedy, J. W. Radiochemical Applications. In *Nuclear and Radiochemistry*; John Wiley & Sons, 1981; pp 442–448.
(58) Choppin, G. R.; Liljenzin, J.-O.; Rydberg, J. *Radiochemistry and Nuclear Chemistry*; Butterworth-Heinemann, 2002.
(59) Baidoo, K. E.; Yong, K.; Brechbiel, M. W. Molecular Pathways: Targeted α-Particle Radiation Therapy. *Clin. Cancer Res. Off. J. Am. Assoc. Cancer Res.* **2013**, *19* (3), 530–537.
(60) Friedberg, E. C. DNA Damage and Repair. *Nature* **2003**, *421* (6921), 436–440.
(61) Kowalsky, R. J.; Falen, S. W. *Radiopharmaceuticals in Nuclear Pharmacy and Nuclear Medicine*; APhA, American Pharmacists Association, 2004.
(62) Kim, Y.-S.; Brechbiel, M. W. An Overview of Targeted Alpha Therapy. *Tumour Biol. J. Int. Soc. Oncodevelopmental Biol. Med.* **2012**, *33* (3), 573–590.
(63) Friedlander, G.; Macias, E. S.; Kennedy, J. W. Interactions of Radiation with Matter. In *Nuclear and Radiochemistry*; John Wiley & Sons, 1981; pp 206–242.
(64) Kassis, A. I.; Adelstein, S. J. Considerations in the Selection of Radionuclides for Cancer Therapy. In *Handbook of Radiopharmaceuticals*; Welch, M. J., Redvanly, C. S., Eds.; John Wiley & Sons, Ltd, 2002; pp 767–793.
(65) Richards, P. The Technetium-99m Generator. *BNL-9601*, 1–16.
(66) Mahmood, A.; Jones, A. G. Technetium Radiopharmaceuticals. In *Handbook of Radiopharmaceuticals*; Welch, M. J., Redvanly, C. S., Eds.; John Wiley & Sons, Ltd, 2002; pp 323–362.
(67) Browne, E.; Tuli, T. *Nuclear Data Sheets 112*; National Nuclear Database, 2011; p 275.
(68) Singh, B. *Nuclear Data Sheets 95*; National Nuclear Database, 2002; p 387.

(69) Baglin, C. *Nuclear Data Sheets 99*; National Nuclear Database, 2003; p 1.
(70) Benny, P. D.; Barnes, C. L.; Piekarski, P. M.; Lydon, J. D.; Jurisson, S. S. Synthesis and Characterization of Novel Rhenium(V) Tetradentate N2O2 Schiff Base Monomer and Dimer Complexes. *Inorg. Chem.* **2003**, *42* (20), 6519–6527.
(71) Benny, P. D.; Green, J. L.; Engelbrecht, H. P.; Barnes, C. L.; Jurisson, S. S. Reactivity of Rhenium(V) Oxo Schiff Base Complexes with Phosphine Ligands: Rearrangement and Reduction Reactions. *Inorg. Chem.* **2005**, *44* (7), 2381–2390.
(72) Jurisson, S. S.; Dancey, K.; McPartlin, M.; Tasker, P. A.; Deutsch, E. Synthesis, Characterization, and Electrochemical Properties of Technetium Complexes Containing Both Tetradentate Schiff Base and Monodentate Tertiary Phosphine Ligands: Single-Crystal Structure of Trans-(N,N'-Ethylenebis(acetylacetone Iminato))bis-(triphenylphosphine) technetium(III) Hexafluorophosphate. *Inorg. Chem.* **1984**, *23* (26), 4743–4749.
(73) Mazzi, U.; Refosco, F.; Tisato, F.; Bandoli, G.; Nicolini, M. Synthesis and Characterization of technetium(III) Complexes with Schiff-Base and Phosphine Ligands. Molecular Structure of (diethylphenylphosphine)[N-(2-Oxidophenyl)salicylideneiminato-NOO′](quinolin-8-Olato-NO)technetium(III). *J. Chem. Soc. Dalton Trans.* **1988**, No. 4, 847–850.
(74) Middleton, A. R.; Masters, A. F.; Wilkinson, G. Schiff Base Complexes of rhenium(IV) and rhenium(V). *J. Chem. Soc. Dalton Trans.* **1979**, No. 3, 542–546.
(75) Refosco, F.; Tisato, F.; Mazzi, U.; Bandoli, G.; Nicolini, M. Technetium(V) and rhenium(V) Complexes with Schiff-Base Ligands Containing the ONNNO Donor Atom Set. Crystal Structure of [N,N′-3-Azapentane-1,5-diylbis(salicylideneiminato)(3–)-O,O′,N,N′,N″]-oxotechnetium(V). *J. Chem. Soc. Dalton Trans.* **1988**, No. 3, 611–615.
(76) Matsunari, I.; Haas, F.; Nguyen, N. T. B.; Reidel, G.; Wolf, I.; Senekowitsch-Schmidtke, R.; Stöcklin, G.; Schwaiger, M. Comparison of Sestamibi, Tetrofosmin, and Q12 Retention in Porcine Myocardium. *J. Nucl. Med.* **2001**, *42* (5), 818–823.
(77) Jurisson, S.; Lindoy, L. F.; Dancey, K. P.; McPartlin, M.; Tasker, P. A.; Uppal, D. K.; Deutsch, E. New oxotechnetium(V) Complexes of N,N'-Ethylenebis(acetylacetone Imine), N,N'-Ethylenebis(salicylideneamine), and O-Phenylenebis(salicylideneamine). X-Ray Structures of the Complexes of N,N'-Ethylenebis(acetylacetone Imine) and N,N'-Ethylenebis(salicylideneamine). *Inorg. Chem.* **1984**, *23* (2), 227–231.
(78) Lane, S. R.; Sisay, N.; Carney, B.; Dannoon, S.; Williams, S.; Engelbrecht, H. P.; Barnes, C. L.; Jurisson, S. S. Re(V) and Re(III) Complexes with Sal2phen and Triphenylphosphine: Rearrangement, Oxidation and Reduction. *Dalton Trans. Camb. Engl. 2003* **2011**, *40* (1), 269–276.
(79) Green, J. L.; Benny, P. D.; Engelbrecht, H. P.; Barnes, C. L.; Jurisson, P. S. S. Substitution and Intramolecular Rearrangement of trans-[ReO(X)(acac2en/pn)]0/+ (X = OH2 or Cl−) to Yield Asymmetric cis-[ReO(Y)(acac2en/pn)] Complexes with Cyanide and Thiocyanate. *Synth. React. Inorg. Met.-Org. Nano-Met. Chem.* **2005**, *35* (1), 53–59.
(80) Yoshihara, K.; 1929-; Ōmori, T. *Technetium and Rhenium*; Springer, 1996.

(81) Volkert, W. A.; Hoffman, T. J. Therapeutic Radiopharmaceuticals. *Chem. Rev.* **1999**, *99* (9), 2269–2292.
(82) Heeg, M. J.; Jurisson, S. S. The Role of Inorganic Chemistry in the Development of Radiometal Agents for Cancer Therapy. *Acc. Chem. Res.* **1999**, *32* (12), 1053–1060.
(83) Deutsch, E.; Vanderheyden, J. L.; Gerundini, P.; Libson, K.; Hirth, W.; Colombo, F.; Zecca, L.; Savi, A.; Fazio, F. Development of Nonreducible Technetium-99m(III) Cations as Myocardial Perfusion Imaging Agents: Initial Experience in Humans. *J. Nucl. Med. Off. Publ. Soc. Nucl. Med.* **1987**, *28* (12), 1870–1880.
(84) Rossetti, C.; Vanoli, G.; Paganelli, G.; Kwiatkowski, M.; Zito, F.; Colombo, F.; Bonino, C.; Carpinelli, A.; Casati, R.; Deutsch, K. Human Biodistribution, Dosimetry and Clinical Use of technetium(III)-99m-Q12. *J. Nucl. Med. Off. Publ. Soc. Nucl. Med.* **1994**, *35* (10), 1571–1580.
(85) Sachse, A.; Mösch-Zanetti, N. C.; Lyashenko, G.; Wielandt, J. W.; Most, K.; Magull, J.; Dall'Antonia, F.; Pal, A.; Herbst-Irmer, R. Rhenium (V) Oxo Complexes with Acetylacetone Derived Schiff Bases: Structure and Catalytic Epoxidation. *Inorg. Chem.* **2007**, *46* (17), 7129–7135.
(86) Xu, Z.; Zhou, M.-D.; Drees, M.; Chaffey-Millar, H.; Herdtweck, E.; Herrmann, W. A.; Kühn, F. E. Mono-and Bis-Methyltrioxorhenium (VII) Complexes with Salen Ligands: Synthesis, Properties, Applications. *Inorg. Chem.* **2009**, *48* (14), 6812–6822.
(87) Altmann, P.; Cokoja, M.; Kühn, F. E. Halide Substituted Schiff-Bases: Different Activities in methyltrioxorhenium(VII) Catalyzed Epoxidation via Different Substitution Patterns. *J. Organomet. Chem.* **2012**, *701*, 51–55.
(88) Gerber, T. I. A.; Yumata, N. C.; Betz, R. The Reaction of Salicylhydrazide with [ReOX3(PPh3)2]. Influence of X on Product Formation. *Inorg. Chem. Commun.* **2012**, *15*, 69–72.
(89) Grünwald, K. R.; Saischek, G.; Volpe, M.; Mösch-Zanetti, N. C. Mechanistic Insight into Olefin Epoxidation Catalyzed by Rhenium(V) Oxo Complexes That Contain Pyridazine-Based Ligands. *Inorg. Chem.* **2011**, *50* (15), 7162–7171.
(90) Banbery, H. J.; McQuillan, F.; Hamor, T. A.; Jones, C. J.; McCleverty, J. A. Synthesis and X-Ray Crystal Structure of [ReO(Cl){(2-OC6H4CH?NCH2CH2OCH2)2}], an Example of Four-Co-Ordination by a Potentially Sexidentate Ligand. *J. Chem. Soc. Dalton Trans.* **1989**, No. 7, 1405.
(91) Banbery, H. J.; McQuillan, F. S.; Hamor, T. A.; Jones, C. J.; McCleverty, J. A. The Synthesis and X-Ray Crystal Structure of the Trinuclear Complex [{ORe(OC6H4-2-CMeNCH2-)2(-μ-O)} 2Re(OC6H4-2-CMeNCH2-)2]Cl· H2O·0.5CH2Cl2]. *Inorganica Chim. Acta* **1990**, *170* (1), 23–26.
(92) Tisato, F.; Refosco, F.; Mazzi, U.; Bandoli, G.; Dolmella, A. Synthesis, Characterization and Electrochemical Studies on technetium(V) and rhenium(V) Oxo-Complexes with N,N′-2-Hydroxypropane-1,3-Bis(salicylideneimine). *Inorganica Chim. Acta* **1989**, *164* (2), 127–135.
(93) Tisato, F.; Refosco, F.; Mazzi, U.; Bandoli, G.; Nicolini, M. Rhenium(V) Oxo Complexes with Schiff Base Ligands Containing Four or Five Coordination Sites. X-Ray Molecular Structure of [N,N′-3-Azapentane-1,5-

diylbis(salicylideneiminato)(3-)-O,O′,N,N′,N″]oxorhenium(V). *Inorganica Chim. Acta* **1991**, *189* (1), 97–103.
(94) Herrmann, W. A.; Rauch, M. U.; Artus, G. R. J. Multiple Bonds between Main Group Elements and Transition Metals. 153.1 Rhenium(V) Oxo Complexes with Tetradentate Schiff Bases: Structural Considerations. *Inorg. Chem.* **1996**, *35* (7), 1988–1991.
(95) Bottomley, L. A.; E. Wojciechowski, P.; Holder, G. N. Voltammetry of Monomeric and Dimeric oxorhenium(V) Complexes of Schiff Base Ligands N,N′-Ethylenebis(acetylacetone)diimine, N,N′-Ethylene(salicylidene)diimine and N,N′-Phenylenebis(salicylidene)diimine. *Inorganica Chim. Acta* **1997**, *255* (1), 149–155.
(96) van Bommel, K. J. C.; Verboom, W.; Kooijman, H.; Spek, A. L.; Reinhoudt, D. N. Rhenium(V)−Salen Complexes: Configurational Control and Ligand Exchange. *Inorg. Chem.* **1998**, *37* (17), 4197–4203.
(97) Béreau, V. M.; Khan, S. I.; Abu-Omar, M. M. Synthesis of Enantiopure Oxorhenium(V) and Arylimidorhenium(V) "3 + 2" Schiff Base Complexes. X-Ray Diffraction, Cyclic Voltammetry, UV−Vis, and Circular Dichroism Characterizations. *Inorg. Chem.* **2001**, *40* (26), 6767–6773.
(98) Gerber, T. I. A.; Luzipo, D.; Mayer, P. Different Coordination Modes of Tetradentate Schiff Bases in Monomeric and Dimeric oxorhenium(V) Complexes. *J. Coord. Chem.* **2005**, *58* (16), 1505–1512.
(99) Du, G.; Abu-Omar, M. M. Catalytic Hydrosilylation of Carbonyl Compounds with Cationic Oxorhenium(V) Salen. *Organometallics* **2006**, *25* (20), 4920–4923.
(100) Ison, E. A.; Cessarich, J. E.; Du, G.; Fanwick, P. E.; Abu-Omar, M. M. Synthesis of Cationic Oxorhenium Salen Complexes via μ-Oxo Abstraction and Their Activity in Catalytic Reductions. *Inorg. Chem.* **2006**, *45* (6), 2385–2387.
(101) Du, G.; Fanwick, P. E.; Abu-Omar, M. M. Cationic Oxorhenium Chiral Salen Complexes for Asymmetric Hydrosilylation and Kinetic Resolution of Alcohols. *Inorganica Chim. Acta* **2008**, *361* (11), 3184–3192.
(102) Marmion, M. E.; Woulfe, S. R.; Neumann, W. L.; Nosco, D. L.; Deutsch, E. Preparation and Characterization of Technetium Complexes with Schiff Base and Phosphine Coordination. 1. Complexes of Technetium-99g and -99m with Substituted acac2en and Trialkyl Phosphines (where acac2en = N,N′-Ethylenebis[acetylacetone Iminato]). *Nucl. Med. Biol.* **1999**, *26* (7), 755–770.
(103) Sheldrick, G. SHELX-97, Program for the Solution and Refinement of Crystal Structures. *Univ. Gött. Ger.* **1997**.
(104) Endicott, J. *In Comprehensive Coordination Chemistry II, ; McCleverty, J. and Meyer, TJ, Eds*; Pergamon: Oxford, UK, 2003.
(105) Bartley, S. L.; Dunbar, K. R.; Shih, K. Y.; Fanwick, P. E.; Walton, R. A. Reactions of the Electron-Rich Triply Bonded dirhenium(II) Complexes Re2X4(.mu.-dppm)2 (X = Cl, Br) with Dioxygen. 1. Multielectron Redox Chemistry with Preservation of the Re2X4(dppm)2 Unit. *Inorg. Chem.* **1993**, *32* (8), 1341–1349.
(106) Shih, K. Y.; Fanwick, P. E.; Walton, R. A. Use of Dirhenium Complexes as Templates for the Reductive Coupling of Carbon Monoxide with Alkynes through Carbon-Oxygen Bond Formation. Synthesis and Characterization of 3-Metallafuran Complexes. *J. Am. Chem. Soc.* **1993**, *115* (20), 9319–9320.

(107) Bartley, S. L.; Dunbar, K. R.; Shih, K.-Y.; Fanwick, P. E.; Walton, R. A. The Oxygenation of the Electron-Rich Triple Bond in the Complexes [Re2X4(mu-dppm)2][X = Cl or Br; Dppm = Bis(diphenylphosphino)methane]. Multielectron Redox Behaviour Involving Retention of the Re2X4P4 Unit. *J. Chem. Soc. Chem. Commun.* **1993**, No. 1, 98.
(108) Grove, D. E.; Wilkinson, G. Oxo-Complexes of rhenium(V). *J. Chem. Soc. Inorg. Phys. Theor.* **1966**, 1224.
(109) Cotton, F. A.; Robinson, W. R.; Walton, R. A.; Whyman, R. Some Reactions of the octahalodirhenate(III) Ions. IV. Reactions with Sodium Thiocyanate and the Preparation of Isothiocyanate Complexes of rhenium(III) and rhenium(IV). *Inorg. Chem.* **1967**, *6* (5), 929–935.
(110) Colton, R.; Wilkinson, G. *Halide Compounds of Rhenium*; SOC CHEMICAL INDUSTRY 14 BELGRAVE SQUARE, LONDON SW1X 8PS, ENGLAND, 1959.
(111) Cariati, F.; Sgamellotti, A.; Morazzoni, F.; Valenti, V. Electronic Spectra and Magnetic Properties of Some rhenium(IV) and rhenium(III) Complexes. *Inorganica Chim. Acta* **1971**, *5*, 531–535.
(112) Johnson, N. P.; Lock, C. J. L.; Wilkinson, G. 204. Amine, Phosphine, Arsine, and Stibine Complexes of Rhenium-(III), -(IV), and -(V). *J. Chem. Soc. Resumed* **1964**, No. 0, 1054–1066.
(113) de CT Carrondo, M. A.; Middleton, A. R.; Skapski, A. C.; West, A. P.; Wilkinson, G. A Novel Linear O-Re-O-Re-O-Re-O System: The Synthesis and X-Ray Structure of Di-μ-Oxo-Bi {[NN′ Ethylenebis (acetylacetiminatol)] Oxorhenium (V)}[NN′ Ethylenebis (acetylacetiminato)] Rhenium (V) Perrhenate. *Inorganica Chim. Acta* **1980**, *44*, L7–L8.
(114) Battistuzzi, R.; Saladini, M. Structure of Trans-Diisothiocyanato(ethoxo)oxo-bis(triphenylphosphine)rhenium(V) Complex. *Inorganica Chim. Acta* **2000**, *304* (1), 114–117.
(115) Sugimoto, H.; Kamei, M.; Umakoshi, K.; Sasaki, Y.; Suzuki, M. Preparation, Structure, and Properties of Bis(μ-oxo)dirhenium(III,IV) and -dirhenium(IV) Complexes of Tris(2-Pyridylmethyl)amine and Its (6-Methyl-2-Pyridyl)methyl Derivatives. *Inorg. Chem.* **1996**, *35* (24), 7082–7088.
(116) Sugimoto, H.; Takahira, T.; Yoshimura, T.; Shiro, M.; Yamasaki, M.; Miyake, H.; Umakoshi, K.; Sasaki, Y. Preparation, Spectroscopic Properties, and Dynamic Behavior of a μ-Oxo dirhenium(III) Complex [Re2(μ-O)Cl2(tpa)2](PF6)2 (tpa=tris(2-Pyridylmethyl)amine). *Inorganica Chim. Acta* **2002**, *337*, 203–211.
(117) Rall, J.; Weingart, F.; Ho, D. M.; Heeg, M. J.; Tisato, F.; Deutsch, E. Heptacoordinate Rhenium(III)-Bis(terpyridine) Complexes: Syntheses, Characterizations, and Crystal Structures of[Re(terpyridine)2X]2+ (X = OH, Cl, NCS). Substitution Kinetics of [Re(terpyridine)2OH]2+. *Inorg. Chem.* **1994**, *33* (16), 3442–3451.
(118) Dinda, S.; Hazra, D. K.; RoyChowdhury, S.; Helliwell, M.; Abdul Malik, K. M.; Mukherjee, M.; Bhattacharyya, R. Reductive Thiocyanolysis of Tetraoxorhenate (VII): Synthesis, Crystal Structure, Catalytic Oxidation and Kinetic Studies of (PPh4)2[Re(NCS)6] and (PPh4)2[ReO(NCS)5]. *Inorganica Chim. Acta* **2009**, *362* (7), 2108–2116.

(119) Cotton, F. A.; Matusz, M. Structural and Spectroscopic Characterization of the Dirhenium Octakis(isothiocyanato) Salt (Ph4As)2Re2(NCS)8.2L (L = (CH3)2 CO, C5H5N). *Inorg. Chem.* **1987**, *26* (21), 3468–3472.
(120) Yoshimura, T.; Chen, Z.-N.; Itasaka, A.; Abe, M.; Sasaki, Y.; Ishizaka, S.; Kitamura, N.; Yarovoi, S. S.; Solodovnikov, S. F.; Fedorov, V. E. Preparation, Structures, and Redox and Emission Characteristics of the Isothiocyanate Complexes of Hexarhenium(III) Clusters [Re6(μ3-E)8(NCS)6]4- (E = S, Se). *Inorg. Chem.* **2003**, *42* (16), 4857–4863.
(121) Jurisson, S.; Halihan, M. M.; Lydon, J. D.; Barnes, C. L.; Nowotnik, D. P.; Nunn, A. D. Linkage Isomerization of MSCN(CDOH)2(CDO)BMe to MNCS(CDOH)2(CDO)BMe (M = Tc, Re). Crystal Structures of TcNCS(CDOH)2(CDO)BMe, ReNCS(CDOH)2(CDO)BMe, and ReSCN(CDOH)2(CDO)BMe. *Inorg. Chem.* **1998**, *37* (8), 1922–1928.
(122) Pearson, C.; Beauchamp, A. 1H NMR Study of Monomeric Chloro-rhenium(III) Complexes with Triarylphosphines and Nitriles. *Inorganica Chim. Acta* **1995**, *237* (1–2), 13–18.
(123) Mitsopoulou, C. A.; Mahieu, N.; Motevalli, M.; Randall, E. W. Second-Order Paramagnetic rhenium(III) Complexes: Solid-State Structure and Assignment of the Carbon-13 Magnetic Resonance Spectra in Solution. *J. Chem. Soc. Dalton Trans.* **1996**, No. 24, 4563.
(124) Bhattacharyya, S.; Banerjee, S.; Dirghangi, B. K.; Menon, M.; Chakravorty, A. Synthesis, Structure and Redox Behaviour of Facial [ReIIIL(PPh3)Cl3] and Its Stereoretentive Conversion to [ReIVL′(PPh3)Cl3] via Metal Promoted Aldimine → Amide Oxidation (L = Pyridine-2-Aldimine; L′ = Pyridine-2-Carboxamide). *J. Chem. Soc. Dalton Trans.* **1999**, No. 2, 155–160.
(125) Rossi, R.; Duatti, A.; Magon, L.; Casellato, U.; Graziani, R.; Toniolo, L. Synthesis and Characterization of Paramagnetic Triazenido-Complexes of rhenium(III). The Crystal Structure of [ReCl2(p-MeC6H4NNNC6H4Me-p)(PPh3)2]. *J. Chem. Soc. Dalton Trans.* **1982**, No. 10, 1949–1952.
(126) Sokolov, M. N.; Fedorova, N. E.; Pervukhina, N. V.; Peresypkina, E. V.; Virovets, A. V.; Pätow, R.; Fedorov, V. E.; Fenske, D. Rhenium(IV) and rhenium(V) Complexes with 3,5-Dimethylpyrazole. *Russ. Chem. Bull.* **2006**, *55* (1), 53–61.
(127) González, R.; Barboza, N.; Chiozzone, R.; Kremer, C.; Armentano, D.; De Munno, G.; Faus, J. Linkage Isomerism in the Metal Complex hexa(thiocyanato)rhenate(IV): Synthesis and Crystal Structure of (NBu4)2[Re(NCS)6] and [Zn(NO3)(Me2phen)2]2[Re(NCS)5(SCN)]. *Inorganica Chim. Acta* **2008**, *361* (9–10), 2715–2720.
(128) González, R.; Acosta, A.; Chiozzone, R.; Kremer, C.; Armentano, D.; De Munno, G.; Julve, M.; Lloret, F.; Faus, J. New Family of Thiocyanate-Bridged Re(IV)-SCN-M(II) (M = Ni, Co, Fe, and Mn) Heterobimetallic Compounds: Synthesis, Crystal Structure, and Magnetic Properties. *Inorg. Chem.* **2012**, *51* (10), 5737–5747.
(129) Homolya, L.; Preetz, W. Kristallstrukturen, Schwingungsspektren Und Normalkoordinatenanalyse von Cis-(n-Bu4N)2[ReBr4(NCS)(SCN)], Trans-(n-Bu4N)2[ReBr4(NCS)(SCN)] Und Trans-(n-Bu4N)2[ReBr4(NCSe)(SeCN)]. *Z. Für Naturforschung B* **2014**, *54* (8), 1009–1014.

(130) Davison, A.; Trop, H. S.; Depamphilis, B. V.; Jones, A. G.; Thomas, R. W.; Jurisson, S. S. 34. Tetrabutylammonium Tetrachlorooxo-Technetate(V). In *Inorganic Syntheses*; Jr, J. P. F., Ed.; John Wiley & Sons, Inc., 1982; pp 160–162.
(131) Patel, K. S.; Bailar Jr., J. C. The Stereochemistry of the nickel(II), cobalt(II), copper(II) and palladium(II) Complexes of the Tetradentate Schiff Base Derived from Salicylaldehyde and Isobutylenediamine. *J. Inorg. Nucl. Chem.* **1971**, *33* (5), 1399–1406.
(132) Alberto, R. Technetium. In *Comprehensive Coordination Chemistry II*; Meyer, J. A. M. J., Ed.; Pergamon: Oxford, 2003; pp 127–270.
(133) Rulfs, C. L.; Pacer, R. A.; Hirsch, R. F. Technetium Chemistry, Oxidation States and Species. *J. Inorg. Nucl. Chem.* **1967**, *29* (3), 681–691.
(134) Kowalsky, R. J.; Pharm, D. *Technetium Radiopharmaceutical Chemistry*; Volume, 2006.
(135) Fergusson, J. E.; Hickford, J. H. Complexes of Quadrivalent Technetium. *J. Inorg. Nucl. Chem.* **1966**, *28* (10), 2293–2296.
(136) Preetz, W.; Peters, G. Darstellung Und Charakterisierung Der Tetrabutylammoniumsalze von [Tc2Cl8]2-, [Tc2Cl8]3- Und [Tc2Br8]2- Preparation and Characterization of the Tetrabutylammonium Salts of [Tc2Cl8]2-, [Tc2Cl8]3- Und [Tc2Br8]2-. *Z. Für Naturforschung B* **2014**, *35* (7), 797–801.
(137) Davison, A.; Jones, A. G. The Chemistry of Technetium (V). *Int. J. Appl. Radiat. Isot.* **1982**, *33* (10), 875–881.
(138) Fergusson, J. E.; Greenaway, A. M.; Penfold, B. R. Preparative and Structural Studies of Pentahalogeno-oxometallate(V) Salts of the Transition Metals Cr, Mo, W, Tc, Re. *Inorganica Chim. Acta* **1983**, *71*, 29–34.
(139) Thomas, R. W.; Davison, A.; Trop, H. S.; Deutsch, E. Technetium Radiopharmaceutical Development. 2. Preparation, Characterization, and Synthetic Utility of the oxotetrahalotechnetate(V) Species TcOX4- (X = Chloro, Bromo, Iodo). *Inorg. Chem.* **1980**, *19* (9), 2840–2842.
(140) Trop, H. S.; Davison, A.; Jones, A. G.; Davis, M. A.; Szalda, D. J.; Lippard, S. J. Synthesis and Physical Properties of hexakis(isothiocyanato)technetate(III) and -(IV) Complexes. Structure of the [Tc(NCS)6]3- Ion. *Inorg. Chem.* **1980**, *19* (5), 1105–1110.
(141) Rochon, F. D.; Melanson, R.; Kong, P.-C. Synthesis of New Mixed-Ligands Tc Complexes Containing Monodentate Phosphine and Isothiocyanato Ligands: Crystal Structures of Complexes Tc(P(C3H7)3)2(NCS)4, Tc(P(CH3)2Ph)4(NCS)2 and Tc(P(OCH3)Ph2)4(NCS)2·1/2CH2Cl2. *Inorganica Chim. Acta* **2000**, *300–302*, 43–48.
(142) Bandoli, G.; Nicolini, M.; Mazzi, U.; Refosco, F. Synthesis and Characterization of technetium(V) Oxo-Complexes with Quadridentate Schiff-Base Ligands: X-Ray Structures of Mu-Oxo-Bis-{oxo[N,N-Propane-1,3-diylbis(salicylideneiminato)]technetium(V)} and Chloro-oxo[N,N-Propane-1,3-Diylbis(salicylideneiminato)]-technetium(V). *J. Chem. Soc. Dalton Trans.* **1984**, No. 11, 2505.
(143) Pillai, M. R. A.; John, C. S.; Lo, J. M.; Schlemper, E. O.; Troutner, D. E. .mu.-Oxo-Bis(oxo) Dinuclear Complexes of technetium(V) with Amine Phenol

Ligands: Syntheses, Characterization, and X-Ray Crystal Structures. *Inorg. Chem.* **1990**, *29* (10), 1850–1856.
(144) Clarke, M. J.; Kastner, M. E.; Podbielski, L. A.; Fackler, P. H.; Schreifels, J.; Meinken, G.; Srivastava, S. C. Low-Symmetry, Mixed-Valent, .mu.-Oxo Technetium Complexes with Pyridine and Halide Ligands. *J. Am. Chem. Soc.* **1988**, *110* (6), 1818–1827.
(145) Barrera, J.; Bryan, J. C. Synthesis, Electronic Properties, and Solid-State Structure of {[(tpy)(Me2bpy)Tc]2(μ-O)}4+/2+. *Inorg. Chem.* **1996**, *35* (7), 1825–1830.
(146) Baldas, J. S. F. Colmanet and MF Mackay. *J Chem Soc Dalton Trans* **1988**, *1725*.
(147) Roodt, A.; Leipoldt, J.; Deutsch, E.; Sullivan, J. Core: Protonation and Ligation of Dioxotetracyanotechnetate (V) Ions and Crystal Structure of 2, 2-Bipyridinium Trans-Oxothiocyanatotetracyanotechnetate (V),". *Inorg. Chem.* **1992**, *31*, 1080–1085.
(148) Anderegg, G.; Müller, E.; Zollinger, K.; Bürgi, H.-B. Preparation, Characterization, Crystal and Molecular Structure of Na2[N(CH2COO)399Tc(IV)(μ-O)299Tc(IV)N(CH2COO)3] · 6H2O. *Helv. Chim. Acta* **1983**, *66* (5), 1593–1598.
(149) Linder, K. E.; Dewan, J. C.; Davison, A. Technetium Bis(.mu.-Oxo) Dimers of 1,4,7-Triazacyclonane-N,N',N''-Triacetate (TCTA). Synthesis and Characterization of [(TCTA)Tc(.mu.-O)2Tc(TCTA)]n- (n = 2, 3) and the Crystal Structure of Ba2[(TCTA)Tc(.mu.-O)2Tc(TCTA)](ClO4).9H2O. *Inorg. Chem.* **1989**, *28* (20), 3820–3825.
(150) Lu, J.; Clarke, M. J.; Hiller, C. D. Synthesis and Electrochemistry of (.mu.-Oxo)technetium Complexes with Bipyridine and Halide Ligands. Crystal Structures of (.mu.-O)[X(bpy)2Tc]2X2.cntdot.bpy (X = Cl, Br) and (.mu.-O)[Cl(phen)2Tc]2Cl2. *Inorg. Chem.* **1993**, *32* (8), 1417–1423.
(151) Abram, U.; Abram, S.; Mäcke, H. R.; Koch, P. μ-Oxoverbrückte, Dimere Technetium- Und Rheniumkomplexe Mit Funktionalisierten Aminophenolato-Liganden. Darstellung Und Strukturen von [O □TcL1□O□L1T
[O -Bis(2-Hydroxybenzyl)-(1,2-Diamino-2-(4-Nitrobenzyl)propan). *Z. Für Anorg. Allg. Chem.* **1995**, *621* (5), 854–860.
(152) Pietzsch, H.-J.; Spies, H.; Leibnitz, P.; Reck, G.; Beger, J.; Jacobi, R. Technetium Complexes with Thioether Ligands—ii. Synthesis and Structural Characterization of Neutral Oxotechnetium(v) Complexes with Dithioethers. X-Ray Structure Analysis of μ-Oxo-bis(5,8-Dithiadodecane)dichlorooxotechnetium(v) and (8-Hydroxy-3,6-Dithiaoctan-1-Olato)dichlorooxotechnetium(v). *Polyhedron* **1993**, *12* (2), 187–193.

VITA

Kimberly Marie Mason Reinig was born in Belleville, Illinois. In January of 2006, she graduated from O'Fallon Township High School, and went to Southeast Missouri State University in Cape Girardeau, MO. In fall of 2007, she transferred to the University of Missouri-Columbia to finish her undergraduate degree. She received a Bachelor of Science with a major in chemistry in 2010. In August 2010, she began graduate school with the University of Missouri Department of Chemistry.